Theory and Design of Tunable and Reconfigurable Microwave Passive Components on Partially Magnetized Ferrite Substrate

Dissertation by

Farhan Abdul Ghaffar

In Partial Fulfillment of the Requirements

For the degree of

Doctor of Philosophy

King Abdullah University of Science and Technology

Thuwal, Kingdom of Saudi Arabia

November, 2016

EXAMINATION COMMITTEE PAGE

The dissertation/thesis of Farhan Abdul Ghaffar is approved by the examination committee.

Committee Chairperson: Atif Shamim
Committee Members: Madhavan Swaminathan, Hakan Bagci, Ying Wu

ABSTRACT

Theory and Design of Tunable and Reconfigurable Microwave Passive Components on Partially Magnetized Ferrite LTCC Substrate

Farhan Abdul Ghaffar

Typical microwave components such as antennas are large in size and occupy considerable space. Since multiple standards are utilized in modern day systems and thus multiple antennas are required, it is best if a single component can be reconfigured or tuned to various bands. Similarly phase shifters to provide beam scanning and polarization reconfigurable antennas are important for modern day congested wireless systems.

Tunability of antennas or phase shifting between antenna elements has been demonstrated using various techniques which include magnetically tunable components on ferrite based substrates. Although this method has shown promising results it also has several issues due to the use of large external electromagnets and operation in the magnetically saturated state. These issues include the device being bulky, inefficient, non-integrable and expensive. In this thesis, we have tried to resolve the above mentioned issues of large size and large power requirement by replacing the large electromagnets with embedded bias windings and also by operating the ferrites in the partially magnetized state.

New theoretical models and simulation methodology have been used to evaluate the performance of the microwave passive components in the partially magnetized state. A multilayer ferrite Low Temperature Cofired Ceramic (LTCC) tape system has been used to verify the performance experimentally. There exists a good agreement between the theoretical, simulation and measurement results. Tunable antennas with tuning range of almost 10 % and phase shifter with an FoM of 83.2°/dB have been demonstrated in this work, however the major

contribution is that this has been achieved with bias fields that are 90 % less than the typically reported values in the literature. Finally, polarization reconfigurability has also been demonstrated for a circular patch antenna using a low cost additive manufacturing technique.

The results are promising and indicate that highly integrated ferrite based tunable components are feasible in small form factor, without the need of the large electromagnets and coils, and thus can be operated at very low bias levels as compared to the ones which are operated in the saturated state with external bias mechanisms.

ACKNOWLEDGEMENTS

It has been a long but a very pleasant journey. To start with, I would like to thank Almighty Allah for all the blessings He has showered upon me. Without His guidance this work would not have been possible. I pray to Allah to shower peace and blessings on Prophet Muhammad (peace be upon him) and his family. I want to express my deepest gratitude to my thesis supervisor, Professor Atif Shamim, for all his help, guidance and support throughout the course of my degree. It has been a great time working under his supervision. He is an exceptional adviser who always encourages his students towards positive thinking. This thesis would not have been possible without his technical and professional expertise. Along with the thesis research, I would also like to acknowledge his support in building my professional career.

I really appreciate the efforts of my thesis committee members which include Professor Madhavan Swaminathan, Professor Hakan Bagci and Professor Ying Wu. Their feedback was quite encouraging with very positive critic towards the work. I wish to thank Professor Langis Roy and Professor Joey Bray for welcoming me in their research groups during my graduate studies and for giving me great scientific insights about the topic.

I would like to thank my colleagues at KAUST, Eyad Arabi, Ahmed Ali Nafe, Mohammed Vaseem, Muhammad Fahad Farooqui, Mahmoud Nafe, Rana Muhammad Bilal, Mina Gadalla, Garret McKerricher, Loic Marnat, Hammad Mehmood Cheema, Adnan Ahmed Khan, Muhammad Akram Karimi, Gaurav Jayeswal, Aftab Hussain and Shahid Hussain.

Finally, I would like to acknowledge the help and support of my family members. I was able to produce my best because of the love and prayers of my parents, Muhammad Abdul Ghaffar and Shaheena Ghaffar and the support of my sisters, Faiza Imran and Nausheen Irfan.

TABLE OF CONTENTS

LIST OF FIGURES

LIST OF TABLES

Chapter 1

Introduction

The increasing number of applications and the versatility of modern communication systems require radio frequency (RF) and microwave components that are tunable and reconfigurable. Applications such as satellite communications, automotive radars and microwave imaging systems all require components that can be reconfigured for specific performance parameters [1], [2]. One method of incorporating reconfigurability in microwave components is by using magnetic materials such as ferrites. It is well known that the magnetostatic properties of a ferrite material can be varied dynamically by the application of a bias field across it [3], [4]. Previously, ferrites have been used for the realization of reconfigurable microwave designs using large external electromagnets/magnets to bias the ferrite substrates, as shown in Fig. 1.1 [5-7]. Most of this work was conducted in the era of the 1970s and 1980s where military applications were targeted.

Although this concept showed promising results, there are several issues with regards to its implementation. The first problem was that the designs that were implemented on the bulk ferrite substrates were widely inefficient due the demagnetization effect at the air-to-ferrite boundary [3-7]. In addition, these designs relied on the saturation of the substrate, thus requiring very high bias fields, in the order of 1000 Oe (80 kA/m). Finally integration of such designs in modern communication systems is not feasible due to their bulky and non-portable nature. As a result, research in ferrite based tunable and reconfigurable components has gradually decreased, particularly in the last three decades. However, with the advent of the multilayer magnetic

substrates such as ferrite low temperature Cofired ceramic (LTCC), the downsides of the conventional ferrite substrates can be alleviated by a system on package (SoP) approach which can ensure their seamless integration with the present communication systems [8]. The aim of this work is to demonstrate highly integrated microwave passive components on multilayer ferrite technologies that can cope with the challenges of size, efficiency and cost while maintaining the desired impedance and radiation performance.

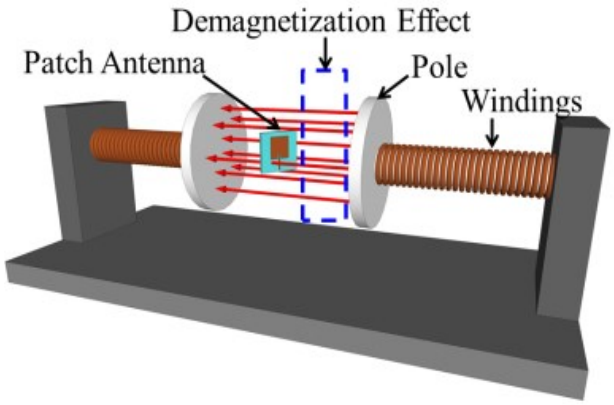

Fig. 1.1 Providing magnetostatic biasing to antenna on ferrite substrate through external electromagnet

The multilayer technology enables the vertical integration of the components as opposed to the horizontal integration used in the traditional Printed Circuit Board (PCB) technology. Using this 3D integration, magnetostatic bias windings can be embedded inside the substrate to provide the required magnetization hence replacing the external electromagnets. The magnetic field generated by these windings can be used to control the radio frequency (RF) performance of the passive microwave elements. This approach will not only reduce the size of the system but will also permit tunability using low intensity magnetostatic fields. Using this concept, J. Bray and L. Roy presented a ferrite LTCC substrate integrated waveguide (SIW) based phase shifter

employing embedded windings [9]. Although the concept was encouraging, there were several drawbacks and unresolved issues such as, operation in the saturated state, unoptimized bias windings, and the placement of the windings inside the waveguide which can affect the high frequency performance of the device. Addressing the problems discussed above, designs of tunable antennas and phase shifters using ferrite LTCC technology will be covered in this thesis. The microwave components will be operated in the partially magnetized state thus requiring low intensity magnetostatic bias. Mathematical models will be studied and electromagnetic simulators will be used to model the microwave devices and their respective bias windings. Finally, using the multilayer ferrite SoP approach the designs will be fabricated and characterized for their impedance and radiation properties to validate the proposed mathematical models.

1.1 Objectives

As discussed above, the traditional ferrite mediums are not suitable for modern communication systems due to their large size, bulky nature, and use of an external magnetostatic source. The aim of this thesis is to demonstrate highly integrated and efficient tunable/reconfigurable microwave passive components. This can be accomplished by the use embedded bias windings as opposed to external magnetic source and using vertical integration techniques. The specific goals of this work are:

- To study the microwave characteristics of a ferrite LTCC tape system, ESL40012, and a multilayer magnetic ink based substrate for their utilization in the design of the reconfigurable microwave components.

- To use embedded bias windings as a magnetic source instead of the external electromagnets, thus reducing the overall size of the system and making it efficient with the use of low intensity bias magnetic fields.
- The use of the low intensity magnetostatic fields means that the substrate will be operated in the partially magnetized state as opposed to the traditional saturated case. Therefore, one of the goals is to understand the operation of the microwave components in the unsaturated state.
- To develop simulation set ups to ensure the modeling of the bias windings using the magnetostatic solver which will, in turn, be used to model the RF components designed on the magnetized substrates in the high frequency simulator.
- To achieve tunability and reconfigurability of the microwave components by exploiting the magnetic nature of the material and the use of the embedded bias windings.

1.2 Challenges

The realization of the RF components using the multilayer ferrite technology is quite novel and has many challenges associated with it. Some of the challenges that are expected in this area of research are:

- When saturated, a ferrite medium is modeled by the well-known Polder's equations [10]. However, these equations are not applicable to a partially magnetized ferrite substrate. To address this, a new set of equations have been presented by Schlomann, Rado, Green, and Sandy [11] which defines the characteristics of the magnetic material in the partially magnetized state. These equations have not been used for the modeling of RF components such as antennas and phase shifters. Therefore, it is important that the

theoretical model presented in [11] is considered while studying the wave propagation in a microwave component on a partially magnetized ferrite substrate.

- For saturated state at higher frequencies, Polder's equations are considered to be standard [10]. In Polder's equations initial relative permeability is considered to be 1. However, Schlomann demonstrated in his work [11], that this assumption is not true for all cases. According to Schloman, for frequencies close to f_m the initial relative permeability is less than 1. Thus if Polders' assumption of initial relative permeability being 1 is used in a design operating in the partially magnetized state, the performance of the prototype will vary considerably from the expected performance. Thus, the actual initial relative permeability of the material should be taken into account when designing a microwave component.
- The presence of the magnetostatic bias windings in the same substrate as the antenna will provide miniaturization and enhanced efficiency. At the same time, however, it can affect the impedance and radiation performance of the microwave structures, which is undesirable. To address this concern, the placement of these windings is optimized such that they do not affect the RF performance.
- A co-simulation environment, using magnetostatic simulation and microwave simulation, is necessary to predict and understand the microwave behavior under magnetic bias. At the same time, these simulation models should have some correlation with the theoretical models studied in this work.
- Bias windings are to be optimized so that they can produce required magnetostatic field strength with minimum power consumption keeping in view the available space for their design.

- In the last chapter of this thesis an iron oxide based magnetic ink is used for realization of the substrate. The use of a novel magnetic ink means that its fabrication process needs to be optimized. The magnetic ink is printed using manual screen printing/squeegee technique. Since the fabrication is completely new, there will be challenges involved in the fabrication of devices using this ink.

1.3 Contributions

- A reliable simulation environment has been developed through CST EM Studio and CST Microwave Studio to predict the performance of the antenna and other microwave components. This has been verified both analytically as well as through prototyping.
- A linearly polarized patch antenna is designed on a partially magnetized substrate with embedded bias windings. The design is analytically and practically studied on a partially magnetized substrate for both extraordinary (E) and ordinary (O) modes of operation. The antenna shows a maximum tuning range of 10 % for the E mode of operation.
- A dual-purpose tunable helical antenna is presented, that was developed using the ferrite LTCC technology where a single element provides the bias and works as an antenna. This design is a step further from the tunable patch antenna design.
- Using the same strategy as followed for the patch antenna design, a half mode substrate integrated waveguide (SIW) based phase shifter is implemented using the ferrite LTCC substrate. The phase shifter provides a phase shift if 83.2 ° with an insertion loss of 1 dB.
- A patch antenna array is realized using the half mode SIW phase shifter to demonstrate its utilization in beam steering applications. This is the first time that a monolithically integrated ferrite LTCC based phased antenna array is demonstrated.

- As a final step, a polarization reconfigurable antenna is implemented using the printing technology in conjunction with the in-house prepared magnetic ink. The antenna has been studied for its theory and simulated using low and high frequency simulators. A prototype has been developed which validates the phenomenon of frequency splitting as observed in the proposed theory and simulations.

1.4 Thesis Organization

Chapter 2-Background and Literature Review: Chapter 2 of this thesis discusses the fundamental theory of the ferrite and ferromagnetic materials. With ferrite-based designs, it is important to understand the material behavior of magnetic mediums for high-frequency components. Therefore, some basic concepts pertaining to ferrite are discussed in this chapter. Furthermore, an extensive literature review of the ferrite based tunable and reconfigurable components is also summarized to highlight the work that has been conducted in this field.

Chapter 3-Ferrite LTCC Based Tunable Antennas: Theory, simulations and measurements of a linear polarized patch antenna operating in the partially magnetized state are presented as the first contribution of this work. Complete magnetostatic simulations and microwave simulations using two different softwares are outlined here. The fabricated prototype is characterized for its impedance and radiation performance in the biased and unbiased states to show its viability in tunable applications. As the second contribution of this thesis, a dual-purpose helical antenna design is demonstrated. The helical structure is used as bias solenoid windings and as an antenna. Complete monolithic integration of the RF chokes and DC block capacitor in one package is achieved by the virtue of using the vertical integration technique.

Chapter 4-Ferrite LTCC Based Half Mode SIW Phase Shifter for Phased Array Applications: The theory of the half mode SIW phase shifter is derived using the first principles of the electromagnetic theory while using the anisotropic nature of the ferrite material, similar to the patch antenna. The fundamental difference between the two cases is in the mode of the operation and the boundary conditions. A closed-form equation is derived as the final solution of the theoretical model, which can predict the phase shift of the waveguide for uniform biasing. The theory is compared with the simulations and measurements in the biased state of the phase shifter. Finally, the phase shifter design is integrated into a patch antenna array to show its viability in beam-steering applications.

Chapter 5- Polarization Reconfigurable Patch Antenna Realized through Low Cost Additive Manufacturing Process: The last contribution of this thesis introduces a new iron oxide nano-particle based magnetic ink for realization of tunable microwave devices. At first, the fabrication process of the ink is studied which is followed by its magnetostatic and microwave characterization. Using these characterization steps a polarization diverse and frequency tunable circular patch antenna is demonstrated. Like the last two chapters, a theoretical model for this design has been studied in the partially magnetized state of operation. Using the simulations and fabrication of a prototype the proposed theory has been validated. This design shows that on a normally biased ferrite a circular patch antenna can show circular polarization with opposite sense at two different frequencies. The center frequencies of these polarizations can be controlled by changing the bias across the substrate.

Chapter 6-Conclusion and Future Work: This chapter concludes the work presented in this thesis and highlights the area where this work can be implemented in future.

1.5 Publications

Journals:

1. F. A. Ghaffar and A. Shamim, “A Partially Magnetized Ferrite LTCC Based SIW Phase Shifter for Phased Array Applications”, *IEEE Transactions on Magnetics*, vol.51, no.6, pp.1-8, June 2015.
2. F. A. Ghaffar and A. Shamim, "A Ferrite LTCC Based Dual Purpose Helical Antenna Providing Bias for Tunability," *IEEE Antennas and Wireless Propagation Letters*, vol. 14, pp. 831-834, 2015.
3. F. A. Ghaffar, J. R. Bray and A. Shamim, "Theory and Design of a Tunable Antenna on a Partially Magnetized Ferrite LTCC Substrate," *IEEE Transactions on Antennas & Propagation*, vol.62, no.3, pp.1238-1245, March 2014.
4. E. Arabi, F. A. Ghaffar and A. Shamim, "Tunable Bandpass Filter Based on Partially Magnetized Ferrite LTCC with Embedded Windings for SoP Applications," *IEEE Microwave and Wireless Components Letters,* vol. 25, no.1, pp.16-18, January 2015.
5. A. Nafe, F. A. Ghaffar, M. F. Farooqui and A. Shamim, “A Ferrite LTCC-Based Monolithic SIW Phased Antenna Array”, *IEEE Transactions on Antennas and Propagation* (accepted with minor revisions).
6. F. A. Ghaffar, M. Vaseem and A. Shamim, “Polarization reconfigurable patch antenna realized through low cost additive manufacturing”, *IEEE Transactions on Antennas and Propagation* (submitted)
7. F. A. Ghaffar, A. Nafe and A. Shamim, “Remanent characteristics of ferrite LTCC multilayer tape system”, IEEE Transactions on Components, Packaging and Manufacturing Technology, (under submission).

Conference Proceedings:

1. F. A. Ghaffar, M. Vaseem, M. F. Farooqui and A. Shamim, "A Fully Printed Ferrite Nano-particle Ink Based Tunable Antenna", *IEEE International Symposium on Antennas and Propagation*, AP-S/URSI, 2016.
2. F. A. Ghaffar, M. Vaseem and A. Shamim, "A Ferrite Nano-particle based Printing Process for Tunable Microwave Components", *IEEE MTT-S International Microwave Symposium (IMS)*, May 2016.
3. F. A. Ghaffar, A. Nafe and A. Shamim “Ferrite LTCC based Phased Array Antennas”, *IEEE International Symposium on Antennas and Propagation* (*AP-S/URSI),* 2016. (Accepted)
4. F. A. Ghaffar and A. Shamim, "A Self-biased 3D Tunable Helical Antenna in Ferrite LTCC Substrate", *IEEE International Symposium on Antennas and Propagation* (*AP-S/URSI)*, pp. 2291-2292, 2015.
5. F. A. Ghaffar and A. Shamim, "Theory and Design of a Half-Mode SIW Ferrite LTCC Phase Shifter ", *IEEE MTT-S International Microwave Symposium (IMS)*, pp. 1-3, 2015.
6. F. A. Ghaffar, A. Shamim and J. R. Bray, "Design strategy for a tunable antenna on a partially magnetized ferrite LTCC substrate," *IEEE International Symposium of Antennas and Propagation Society (APS/URSI),* pp.779-780, 2014.

Chapter 2

Background and Literature Review

The thesis covers the theory, design, and characterization of magnetically tunable and reconfigurable microwave components. Therefore, before discussing the details of the work, it is important to discuss propagation of RF waves in biased ferrite mediums. This chapter first covers the propagation of waves in ferrites with different direction of bias, after which a comprehensive literature review of the work that has been done on tunable and reconfigurable ferrite based microwave components is presented. The merits of the work that has been done are discussed along with the short comings to explain why further exploration of this area is necessary.

2.1 Microwave Characteristics of Ferrite Medium

Ferrite materials are composed of magnetic dipoles due to the uncompensated spin of electrons [12]. When a magnetostatic/magnetic field is applied across a ferrite, it causes the electrons to precess around the field with a frequency known as Larmor's frequency, f_0 or ω_0, given by Eq. 2.1 [10], [12], [13]:

$$f_0 = \mu_0 \gamma H_i \tag{2.1}$$

where γ is the gyromagnetic ratio, H_i is the magnetostatic field inside the material. Gyromagnetic ratio is the ratio between the spin magnetic moment and the angular momentum of the electron.

For most of the ferrite/ferromagnetic materials this quantity is equal to 2.8 MHz/Oe. The motion of the electron under the influence of the magnetic field is shown in Fig. 2.1.

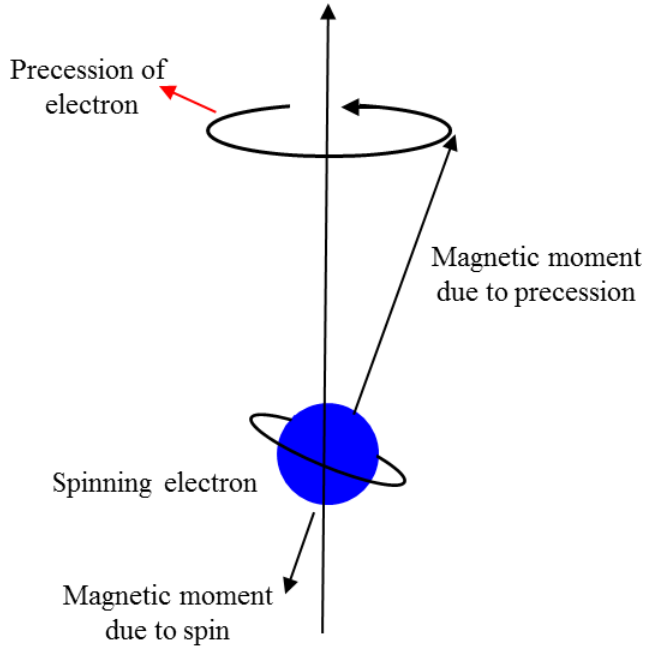

Fig. 2.1. Precession of electron due to the presence of an external magnetic field [10]

In a lossless medium, the electrons will continue to precess without any hindrance, but for practical materials, these electrons will align themselves with the applied magnetic field and achieve equilibrium. This phenomenon is known as the damping of electronic precession and is quantified by the damping factor, α. In a saturated ferrite material, all of the electrons have reached equilibrium. As a result, the dipole moments inside the medium are aligned with the applied magnetic field.

Now let us consider that an alternating magnetic field such as an RF signal is applied to a ferrite medium which has a DC magnetic bias around it. The magnitude of the RF signal will be small compared to the DC magnetic field. However, the electrons will tend to precess under the

influence of the applied RF magnetic field. Thus, the interaction of the RF field in a biased ferrite medium is complex. It has been observed that the behavior of the ferrite medium in the presence of both the RF and DC magnetic field is heavily dependent on the direction of these applied magnetic fields. It has been explained in detail in [19] that a ferrite medium behaves like an anisotropic medium when a bias is applied across it. For this purpose, the permeability tensor given by Eq. 2.2 is used to explain the characteristics of a biased magnetic medium [10], [14].

$$\boldsymbol{\mu} = \mu_0 \begin{bmatrix} \mu_x & 0 & 0 \\ 0 & \mu & -j\kappa \\ 0 & j\kappa & \mu \end{bmatrix} \tag{2.2}$$

where μ_0 is the free space permeability, $\mu_x = 1$ for saturated state, μ and κ are the elements of the permeability tensor and are given by Polder's Equation,

$$\mu = \mu_0 \left(1 + \frac{f_0 f_m}{{f_0}^2 - f^2}\right) \tag{2.3}$$

$$\kappa = \mu_0 \left(\frac{f f_m}{{f_0}^2 - f^2}\right) \tag{2.4}$$

where f_m is the magnetization frequency and depends on the saturation magnetization ($4\pi M_s$) of the medium while f is the operating frequency which could take different values,

$$f_m = \mu_0 \gamma M_s \tag{2.5}$$

It is important to clarify it here that the permeability tensor of Eq. 2.2 is for the X direction of bias. Using Eq. 2.2, the permeability tensor for the other two bias conditions i.e. Y and Z can be evaluated. The equations outlined above are only valid for the case when the material is completely saturated. For this thesis, most of the work will be done using the partially magnetized state of ferrite i.e. the region where the magnetization, M is increasing with the applied, H and has not reached M_s. For the partially magnetized state, Schlomann, Rado and Green and Sandy proposed a different set of equations for the same permeability tensor [11], [15], [16]:

$$\mu = \mu'_o + (1 - \mu'_o)\left(\frac{M}{M_S}\right)^{\frac{3}{2}} \tag{2.6}$$

$$\kappa = n\frac{\gamma 4\pi M}{f_{res.}} \tag{2.7}$$

$$\mu_x = \mu'^{\left(1-\left(\frac{M}{M_S}\right)^{\frac{5}{2}}\right)}_o \tag{2.8}$$

where μ'_o is the initial relative permeability of the substrate in the demagnetized state, the relative μ and κ values replace the standard elements of the Polder permeability tensor, M and M_s are the partial and saturation magnetization, $f_{res.}$ is the frequency of operation, and n is the coefficient expressing the deviation of κ from Rado's model [17]. In saturated state μ_x, is always taken to be 1; however in the partially magnetized state it has to be computed using Eq. 2.8. The initial relative permeability of a magnetic substrate in the demagnetized state was given by Schlomann [15]:

$$\mu'_o = \frac{2}{3}\left[1 - \left(\frac{\gamma 4\pi M_S}{f_{res.}}\right)^2\right]^{\frac{1}{2}} + \frac{1}{3} \tag{2.9}$$

The theoretical models developed in this work will be based on Eq. 2.6 to Eq. 2.9. All of the equations that are discussed in this section consider ferrite as a lossless medium. Considering the medium as lossless greatly simplifies the theoretical models while providing the right prediction of tunability or reconfigurability. It is still important to discuss the losses that are experienced by RF waves in the ferrites. Therefore, they are discussed in the next section.

2.1.1 Loss in Ferrites

Like all dielectrics, ferrites also suffer from losses within the material. Conventional dielectric mediums suffer from losses due to the electric dipoles and the conductive current. The conductive current and loss due to the electric dipoles are common between ferrites and other dielectric mediums. Here, we would like to ignore the loss due to the conductive current for simplicity purposes. The electric dipoles do not show any losses at lower frequencies. However, after a certain band of operation, it is observed that the losses from these dipoles increases significantly and therefore the material is not usable above that band of frequency. As a result, it is observed that dielectrics always have an upper limit to the band of operation where they can be used. Above this frequency band RF components will suffer from the material losses due to the electric dipoles. The dielectric losses are usually defined by the dielectric loss tangent which is the ratio between the imaginary part (ε'') and real part (ε') of the dielectric constant (ε) [19]. Ferrites also suffer from dielectric losses and therefore they have a dielectric loss tangent. However the loss tangent in the case of ferrites is not only due to the electric dipoles but also because of the magnetic dipoles. Interestingly magnetic dipoles are lossy at lower frequencies and loss due to them becomes less at higher frequencies. This limit of frequency is known as magnetization frequency (f_m). After f_m, the frequency of the signal is high enough that the loss

due to magnetic dipoles is insignificantly [12]. Therefore when the ferrite material is not saturated, the magnetic dipoles are free to absorb energy causing loss in the transmission of the signal. These losses are termed as low field losses. Once the medium is saturated the dipoles are strongly held by the applied DC magnetic field in a particular direction and do not affect/absorb the incoming RF waves. Therefore it can be said that the dipoles are transparent to the waves in the saturated state. Due to the presence of the low field losses it is recommended to use the ferrite material either in saturation or at a frequency which is above the magnetization frequency, f_m [10]. Because once the ferrite is saturated it will not suffer from any low field losses due to the alignment of all the magnetic dipoles, however in the partially magnetized state or in the absence of any bias, a ferrite material will always suffer from this type of loss if the operation is at a frequency below f_m.

The magnetic dipoles can absorb power at all frequencies till the magnetization frequency. However for a particular strength of the magnetic field inside the ferrite medium, H_i, there is one frequency where the loss is maximum. This frequency is termed as Larmor's frequency (f_0) as introduced previously. We know that the magnetic loss in the medium is due to the resonance of the magnetic dipoles by the incoming RF energy. The frequency at which the resonance is maximum is known as Larmor's frequency and this phenomenon of resonance is known as gyromagnetic resonance. To characterize the loss of ferrites due to the resonance of magnetic dipoles a term known as Linewidth (ΔH) of the ferrite medium is used. To define linewidth let us consider that the loss in ferrite medium is given by quantity, X and a signal of fixed frequency (ω) is excited through the biased ferrite medium. The loss incurred by the signal is measured for different strengths of bias fields, H. This will generate a response as shown in Fig. 2.2. The maximum loss (X_{max}) occurs at a particular bias strength which in the figure is referred to as

H_{max}. Moving away from H_{max} in either direction shows a reduction in the loss value. There will be two strengths of magnetic field, H, where the value of the loss will be half of the maximum value $\left(\frac{X_{max}}{2}\right)$. These two magnetic field values are referred to as H_1 and H_2. The difference between H_1 and H_2 is known as the linewidth of the material represented by ΔH. The linewidth is the characteristic value of a material and it will not change if the applied RF frequency is varied. The maximum loss value will be changing with the change in the frequency, for example, at Larmor's frequency the loss value will be maximum as compared to at any other frequency. However the value of linewidth will remain constant independent of the frequency band. Therefore the loss of a ferrite is usually characterized by its linewidth. Lower the linewidth of a ferrite medium, better it is in terms of loss.

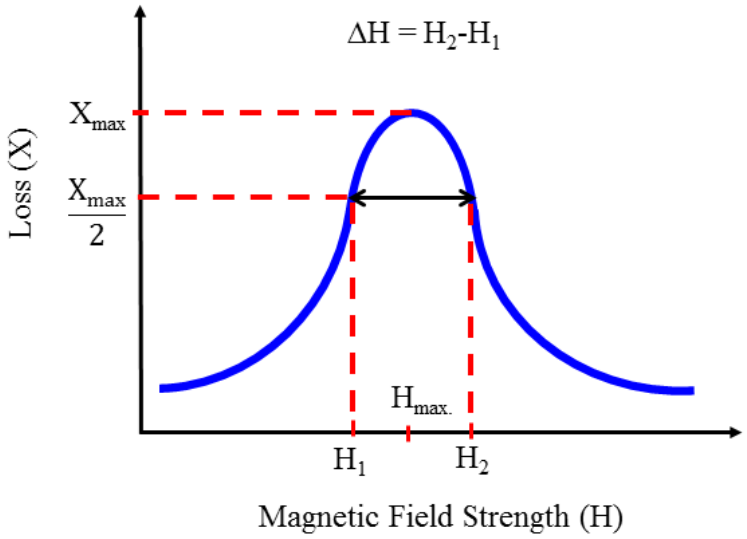

Fig. 2.2. Definition of linewidth (ΔH) [10]

Similar to the dielectric loss tangent, there is a magnetic loss tangent which is the ratio of the imaginary part of the permeability (μ'') to its real part (μ'). From the explanation above, it can be concluded that the loss of the magnetic medium is mainly due to the magnetic dipoles at low frequencies. If these dipoles are saturated they will not incur any loss to the propagating waves. Therefore, most of the ferrite work done until now has been in saturated state. However, this work concentrates on the partially magnetized state of the ferrite medium. Therefore, to avoid all the losses due to ferrite, one can operate above the magnetization frequency. This property of ferrites will be exploited in this work.

2.1.2 Wave Propagation in Ferrites

At this point, the microwave behavior of a ferrite is well defined by the equations given above and the loss mechanism discussed in the last section. Using these equations, the wave propagation in a biased ferrite medium can be studied. Given that ferrites are anisotropic in nature, three different cases for wave propagation are discussed here:

i. When the direction of the magnetic bias inside the substrate is parallel or anti-parallel to the direction of the propagation of the wave. This case is known as Faraday rotation.

ii. When the direction of the magnetic bias inside the substrate is perpendicular to the direction of the propagation of the wave and to the RF magnetic fields. This case is known as extraordinary (E) mode.

iii. When the direction of the magnetic bias inside the substrate is perpendicular to the direction of the propagation of the wave and is parallel to the RF magnetic fields. This case is known as ordinary (O) mode.

i. Faraday Rotation: Consider an infinite ferrite-filled medium that is biased by a DC source in the Z direction. If a linearly polarized wave propagating in the Z direction enters this medium then the right hand circularly polarized (RHCP) and left hand circularly polarized (LHCP) components propagate with different propagation constants (i.e. β; assuming the medium to be lossless, $\alpha = 0$). This is because the effective permeability experienced by the two waves is different. RHCP waves will experience $\mu+\kappa$ while LHCP waves experience μ-κ, indicating that the two components propagate in the same direction but with different phase constants (in lossless ferrite). Therefore, when looking in the direction of the propagation, the wave is observed as rotating when it is travelling through the medium. However, it is important to clarify that the wave is still linearly polarized because the rotation of the wave is not in time but in space [10].

It is well known that for a circularly polarized wave the electric and magnetic field vector keep rotating with time even if we consider a single point in space, whereas here the wave is rotating in space (i.e. the field vectors are rotating when the wave moves from one point to the next in space but the position of the vector at a point in space will always be same irrespective of the time coordinate). This type of wave rotation is known as Faraday rotation, after the name of the discoverer Michael Faraday. This is one case of wave propagation in biased ferrite medium.

ii. Propagation Transverse to Bias (E and O mode): Assuming again that the ferrite region is infinite in space and is biased in the Z-direction and considering that the wave is propagating transverse to the Z direction (i.e. in XY plane), such a scenario can have two possibilities: the RF magnetic field is in the direction of the bias or they are perpendicular to each other. The former case is referred to as the ordinary (O) mode of propagation because the RF electric and magnetic

fields for this mode are similar to the fields that an isotropic medium with a scalar permeability will support. If the saturated case of ferrite is considered, then this scalar permeability is given by μ_0 (free space permeability), while for the partially magnetized state the permeability μ_z value is given by Eq. 2.8 [10]. For the O-mode, any tuning or reconfigurability achieved here will be in the partially magnetized state because as soon as the saturation is achieved, the permeability value will reach the free space permeability value of 1, after which there will be negligible tuning regardless of what strength of field is applied. This is explained by Pozar in [10].

The second case is called the extraordinary mode (E-mode). The permeability experienced by a wave propagating in this mode is given by:

$$\mu_e = \frac{\mu^2 - \kappa^2}{\mu} \tag{2.10}$$

where μ and κ are the elements of the permeability tensor. Here, the propagating electric and magnetic fields are different to the RF fields which are observed in an isotropic medium hence this mode is regarded as extraordinary mode. For this mode of propagation tuning and reconfigurability will be achieved in the partially magnetized state as well as the saturated state. In the partially magnetized state, the tuning will be achieved by increasing the value of magnetization till saturation is achieved. Once M_s is achieved the tuning can still be observed by applying strong magnetic fields across the ferrite material. This type of tuning is achieved by moving the band of the gyromagnetic resonance with the applied magnetostatic field using Polder's equation which generally requires very high intensity of applied fields [10]. Therefore, it can be said that this mode of propagation is more flexible as compared to the O-mode as far as tunability is concerned.

2.2 Ferrite Based Designs in Literature

Ferrites have been effectively used by RF designers for tunable and reconfigurable microwave components. By controlling the magnetostatic properties of a ferrite with the help of a bias, one can control the behavior of the RF wave propagating through it. Using this property, different types of antenna, phase shifter and phased array designs have been reported in literature. In this thesis, the literature review on ferrite based designs is divided into following four parts:

i. Frequency Tunable Antennas

ii. Phase Shifters

iii. Polarization Reconfigurable Antennas

iv. Ferrite Low Temperature Co-fired Ceramic (LTCC) based designs using embedded bias windings

2.2.1 Frequency Tunable Antennas

An antenna implemented on a magnetic substrate can be tuned for its frequency of operation by applying magnetostatic fields across it. The frequency of operation of an antenna is dependent on the material properties such as permittivity and permeability. The bias magnetic fields vary the permeability experienced by the RF waves travelling through it, thus tuning the resonant frequency of the antenna. This technique has been employed by the designers to demonstrate efficient tuning of different types of antennas. One of the first demonstrations of a tunable antenna on a ferrite substrate was presented by Pozar [3]. The antenna was a rectangular patch

antenna designed to operate at 4.6 GHz. Different directions of magnetostatic bias were employed to understand the working of the antenna in the biased state. As such, a maximum tuning range of 39 % of the center frequency was obtained. However, the authors did not mention the bias strength that was required to achieve this result. In addition, no theoretical explanation was provided to support the measured tuning that was achieved from the design. This work was continued in [18], where a theoretical model was proposed to predict the performance of a circular patch antenna when it is designed on a normally biased ferrite substrate. The antenna demonstrated good tuning performance using external magnets that provide bias magnetic fields in the order of 2000 Oe. This was the first time that a theoretical model was presented to explain the tuning of a circular patch antenna on a saturated ferrite substrate. It is important to mention that although the two papers [3] and [18] are correlated; they presented antennas with different polarizations; one was linear while the later one was circular. Another problem with [18] was that the theory presented in that work was for a circular patch antenna while the measured results of a rectangular patch antenna were shown.

In 1992, following the work that Pozar presented, a yttrium-iron-garnet (YIG) based patch antenna was presented to operate at 5.84 GHz under unbiased conditions [19]. The substrate was biased using external magnets providing a maximum strength of 600 G. The tuning range thus obtained was 200 MHz which is 3.4 % of the center frequency. The important observation made in this work was that the reported antenna does not have a purely linear or circular polarization. The phase difference between the co-polarization and cross-polarization patterns was around 20° while their magnitudes were within a 3dB range of each other. The magnitudes of the two components do suggest that the antenna is circularly polarized rather than linear. However, the phase difference clearly shows that the antenna does not have pure circular polarization. The

authors did not explain this effect in detail, neither did they provide a theoretical or numerical analysis to explain these results. Nonetheless, frequency tuning was still reported in this work similar to the previous two papers.

G. M. Yang et. al., used a different substrate configuration to achieve tunability using ferrite materials. They used ferrite layers as superstrate on top of the patch antenna instead of using bulk ferrite as the substrate, as shown in Fig. 2.3 [20]. NiCo films were used as the ferrite layers on the antenna that was realized on an alumina substrate. When the antenna is loaded with different number of ferrite layers, change in the frequency of the antenna is observed. In addition to the tunability of the center frequency, an improvement in the gain of the antenna is also demonstrated. This is due to the superstrate effect which is achieved by loading the antenna with a high dielectric substrate. The authors claim the antenna to be frequency tunable with a range of 2% of the center frequency. However, the method used in this work is extremely inefficient. For a practical application, tuning the frequency of the antenna by varying the number of layers on top of the antenna is not feasible. The same group of authors published another work where tunability is achieved by biasing the ferrite layers instead of changing the number of layers [21]. They demonstrated a tuning range of 0.4 % by biasing the antenna with a magnetic field strength of 20 Oe. At a glance, the tunability results achieved from biasing the substrate look discouraging as compared to the ones achieved by changing the number of ferrite superstrate layers. However, a much better tunability range can be achieved, if stronger magnetic field strength is applied across the antenna. Field strength of 20 Oe is quite weak when external magnetic source is used. This is because of the strong demagnetization effect at the air to ferrite boundary as has been discussed in this chapter. Using a stronger magnetic field can result in much better tuning range, but the authors did not consider it in their experiments.

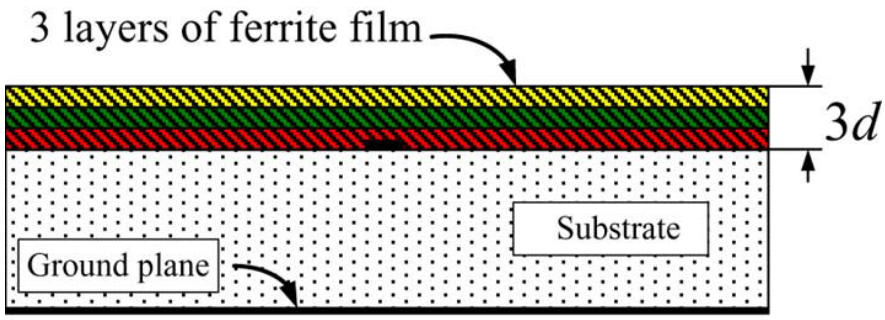

Fig. 2.3. Using ferrite layers on a patch antenna for frequency tunability [20]

Most of the work on ferrite based tunable antennas is on patch antennas. The reason is that the patch antenna design is simple, has a low profile and is easy to fabricate. Furthermore, it is heavily dependent on the substrate properties which makes it a viable option for the ferrite based tunable applications. The other antenna design which can be effectively used for such an implementation is Substrate Integrated Waveguide (SIW) based slot antenna. To prove this several different design configurations were published by L. R. Tan et. al. as shown in Fig. 2.4 [22-24] . The first two designs demonstrate a linearly polarized antenna which is tuned for its frequency response by the application of magnetic fields. The third design is a circularly polarized antenna which uses two slots that are perpendicular to each other and thus generate orthogonal electric field components. The circular polarization is maintained when the antenna is biased. This means that the axial ratio tunes with the center frequency of the antenna due to the change in the bias. The tuning range achieve through these three designs are 10.9%, 14.9% and 8 % around center frequency of 10 GHz, 9.2 GHz and 10 GHz respectively.

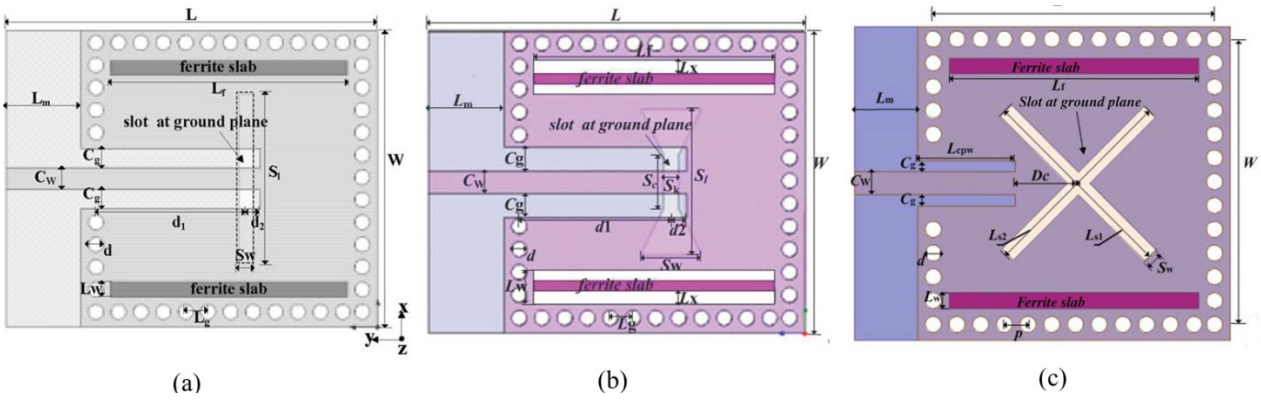

Fig. 2.4. Tunable ferrite SIW based slot antenna designs [22-24]

Two more antenna designs i.e. ferrite loaded cavity-backed slot antenna (CBS) and a half mode substrate integrated waveguide (HMSIW) antenna have also been reported in [25], [26] for the frequency tuning applications using ferrites as the substrate. The concept in both these designs is similar to the ones reported above. In a nut shell, it can be stated that ferrite is a viable medium for tunable antenna design applications. Applying the magnetostatic fields across the substrate changes its properties dynamically which allows the designers to control the center frequency of the antenna. A summary of ferrite based tunable antenna designs is given in table 2-1.

Table 2-1. Summary of ferrite based tunable antenna designs

Reference	Type of Antenna	Frequency [GHz]	Magnetic Field Strength	Tuning Range [%]
[3]	Patch	4.6	-	39
[18]		6	2000 Oe	40
[19]		6	600 Oe	3.4
[21]		2.1	20 Oe	0.4
[22]	SIW based Slot	10	0.335 mT	10.9
[23]		9.2	0.31 mT	14.9
[24]		9, 10	0.323 mT	8
[25]	CBS	1.4	855	10.7
[26]	HMSIW	5.5	0.32 mT	21

All the papers on the tunable antennas that have been discussed in this section have certain major issues associated with them. First of all, these designs rely on external magnets or electromagnets to provide the magnetic bias for the frequency tuning. Although the size of an electromagnet can vary depending on the strength of the magnetic field it can generate, but considering the values reported in table 2-1, it can be said that such designs will require electromagnets which are in the order of few m^3 in volume. The use of such large electromagnets will make the complete system bulky and non-integrable. Moreover, the fact that the magnetic source is external to the ferrite substrate means that there will be large demagnetization effect at the air-to-ferrite boundary resulting in inefficiency of the system. Finally, all these designs are operated in the saturated regime requiring strong magnetic fields. The focus of this thesis will be to resolve these issues by using multilayer magnetic substrates with integrated bias windings and operation in partially magnetized state as opposed to saturation.

2.2.2 Phase Shifters

In addition to antennas the other most popular component for ferrite designers has been phase shifter. There are different types of phase shifters that have been designed on ferrite substrates. Before starting the discussion on the designs themselves it is important that certain terminologies associated with the phase shifters and more specifically with the ferrite phase shifters are elaborated. These include:

i. Insertion Loss and Figure of Merit (FoM)

ii. Reciprocal and non-reciprocal phase shift

i. Insertion Loss and Figure of Merit (FoM):

When a signal is applied to any microwave device it goes through certain degree of attenuation. This attenuation is due to the losses present inside the device. These losses can be due to the material or the device itself. The attenuation level experienced by a signal through a microwave device is known as insertion loss (IL) usually measured in decibels (dB). For ferrites the loss is mainly due to the magnetic losses of the medium. For an ideal phase shifter the insertion loss is 0 dB but for the actual designs this value is almost impossible to achieve. As a result, the focus of a phase shifter design is to keep the losses as low as possible, while providing the required phase shift. Therefore, the performance of a phase shifter is characterized by two parameters i.e., insertion loss and phase shift. These two properties are assessed through figure of merit (FoM). FoM is defined as the phase shift achieved divided by the insertion loss.

$$\text{FoM} = (\text{Phase Shift})/(\text{Insertion Loss}) \tag{2.11}$$

The unit of FoM is °/dB. From the equation it is obvious that greater the value of FoM better the performance of the phase shifter.

ii. Reciprocal and Non-reciprocal Phase Shift:

Ferromagnetic/ferrite materials have anisotropic behavior when biased by a magnetostatic field. This means that the ferrite properties experienced by a wave in one direction must be different from that of the opposite direction. However, this depends on the direction of the bias magnetic field. If the direction of the bias in a ferrite material is altered it may result in a similar response in the two opposite directions of propagation. This can be explained by considering extraordinary (E) and ordinary mode (O) of propagation. For these two modes of wave propagation, the direction of bias is different. It is seen that for E mode the phase shift is non-

reciprocal while for O-mode it will be reciprocal. Due to this nature, ferrites can be used for reciprocal as well as non-reciprocal phase response. The reciprocal phase response is the case where the phase shift in the forward direction of propagation is equal to the phase shift in the reverse direction of propagation. To simplify this concept it can be said that the phase of S_{21} and the phase of the S_{12} will be the same for the reciprocal design (considering a two port phase shifter). For a non-reciprocal design the aforementioned values will be different giving rise to a differential phase shift. The differential phase shift can be defined as the difference of the phase between the two directions of propagation under biased condition i.e. $\angle S_{21} - \angle S_{12}$. These two terminologies are commonly used for ferrite based designs. For this thesis, the more important parameter is the difference between the phase of a wave in one particular direction in the biased and the unbiased conditions. This means at one time, the focus will be either on S_{21} or S_{12}. We define this phase shift as the uni-directional phase shift which is the difference between the phase before and after bias ($\angle S_{21(biased)} - \angle S_{21(unbiased)}$). The response of a phase shifter is always measured in degrees per unit length and will also be used for this work.

For magnetically biased phase shifting components different types of implementations have been studied. These variations are in the design as well as in the way they are biased by the magnetostatic sources. These design configurations can be divided in to the following four types:

a) Dual-mode ferrite phase shifters

b) Ferrite slab based phase shifters

c) Planar ferrite phase shifters

d) Ferrite SIW phase shifters

The most relevant among these types of phase shifter for this thesis is the SIW based designs and will be discussed in detail. The remaining three types are not directly related to the work that will be pursued in this thesis. However, a quick overview of these designs can be covered here.

The first among these designs is the dual-mode ferrite phase shifters [27]. These designs work on the principle of Faraday rotation where a magnetic field is applied parallel to the direction of propagation of the wave. As the field across the medium is varied it causes a change in the permeability of the medium hence providing variable phase shifts. As first of the phase shifter components using ferrite technology, dual-mode designs gained a lot of importance due to their superior performance in the era of 1970s. It has been observed that phase shifts of more than 400° can be achieved with an insertion loss of 2 dB resulting in FoM of >200°/dB [28]. A number of designs were reported using this design topology for ferrite phase shifters [29]-[34]. These designs demonstrated that phase shifts in the order of >100°/cm and FoMs of >200°/dB can be achieved from them. However due to their bulky nature, these designs were not sought after 1980s.

At the same time when dual-mode phase shifters were investigated, designs based on ferrite loading in the waveguides were also investigated for their response. These designs relied on the waveguides which were loaded with ferrite slabs along with a dielectric slab. Different design configurations were employed for realization of these phase shifters as shown in Fig. 2.5.

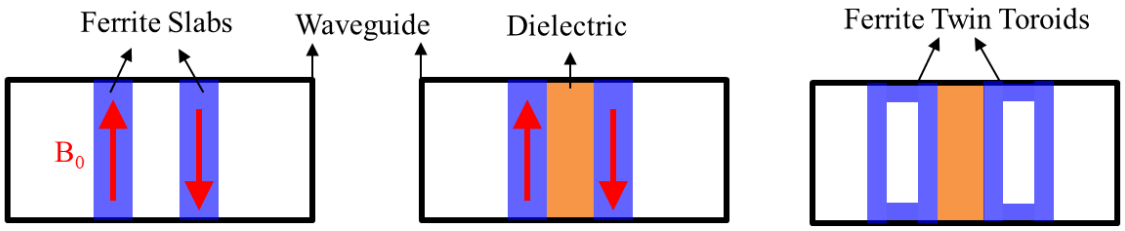

Fig. 2.5. Ferrite loaded waveguide phase shifters (a) rectangular ferrite slabs (b) ferrite slabs with dielectric loading (c) twin toroids with dielectric loading

The performance of these phase shifters were dependent on the thickness of the ferrite slab used inside the waveguide. The first implementation of this type of design was published in 1978 [35]. Using three different frequencies i.e. 35 GHz, 65 GHz and 94 GHz the authors reported phase shifts of 422°, 87° and 38° and FoMs of 603°/dB, 97°/dB and 25.33 °/dB respectively. There were some other designs using the same topology reported in the era of 1990s where decent phase shift and FoMs were achieved [36]-[38]. However not many designs have been reported using the ferrite loading technique after this. The reason is their fabrication is extremely challenging and costly. Especially at high frequencies their precise realization can be troublesome and therefore their implementation has died out in the research arena.

The third type of ferrite based phase shifters, found in the literature, are planar phase shifter designs. Due to the non-integrability of the first two topologies these types of phase shifters were pursued in the ferrite technology. Transmission lines such as slot line, coplanar waveguide (CPW), meander line and microstrip line were used for these planar design implementations [39]-[42]. Substrates such as yttrium-iron-granite (YIG) were used as the base ferrite materials. The resultant designs reported FoMs of >150°/dB but their main advantage was the use of relatively low magnetic field strength. These designs relied on bias fields in the order of few hundred of Oe which is still quite high but quite reasonable when compared with the other two

topologies discussed above. The main concern with these designs was their high insertion loss which was in the order of 3dBs. This was the reason that these designs fall out of research and not pursued any further.

2.2.2 (A) Ferrite SIW Phase Shifters

The advent of SIW technology encouraged the designers to pursue phase shifter designs using this technology. The performance of the waveguide ferrite phase shifters has shown results that are superior to the other technologies [27]. Thus, it was natural to investigate this design technique for ferrite mediums. The first implementation of a ferrite SIW based phase shifter was in 2010 [42], shown in Fig. 2.6. Duroid 6010 was used as the main substrate for the SIW design while two ferrite slabs were inserted inside the substrates to realize the dual-mode operation, as shown in Fig. 2.5. A coil system was attached on the top and bottom of the SIW structure and the structure is biased by using DC current. The coil generates magnetic flux inside the ferrite slabs in the opposite direction. When the current is passed through the coil it provides a differential phase shift of 300° at 24 GHz. The maximum magnetization generated inside the material is 3000 G which has been estimated by simulations. The authors did not report the magnetic field strength required to generate this magnetization inside the substrate but from the design aspects this value is deemed to be more than 1000 Oe.

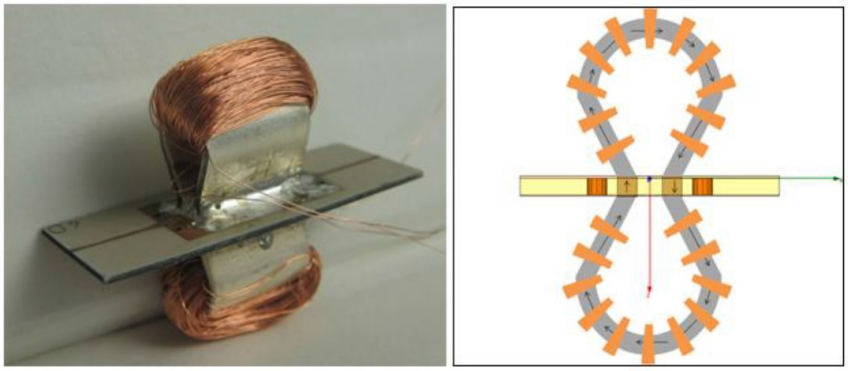

Fig. 2.6. Ferrite loaded SIW based phase shifter with external bias coil set up [43]

Using similar concept another design was done in 2013 where a single slab of ferrite was used in one of the halves of the waveguide, as shown in Fig. 2.7 [44]. It is not mentioned how the magnetic field is generated inside the substrate but from the design it appears that external magnets were used for this purpose. Field strength of 0.24 T was applied which resulted in a phase shift of around 400° with an insertion loss of around 2dB. The length of the phase shifter is around 2 cm. The results shown from these designs are quite encouraging for the use of ferrite based SIW technology, however they still do not solve the problems of previous demonstrations such as lack of integration, large sizes, use of external magnetic sources and required high magnetostatic field strengths.

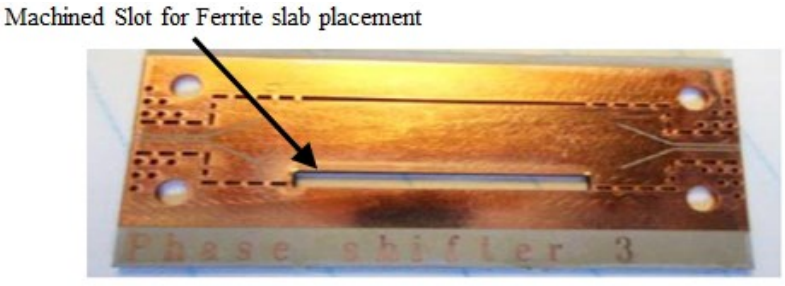

Fig. 2.7. Ferrite loaded SIW based phase shifter using external magnets [44]

2.2.2 (B) Summary of Ferrite Phase Shifters

Different types of phase shifter designs have been realized using ferrite or ferromagnetic materials. The results obtained from such designs are encouraging as far as their FoM and phase shift values are concerned. To summarize the work discussed in the last section, table 2-2 is compiled below.

Table 2-2. Summary of ferrite based phase shifter designs

Reference	Type of Design	Frequency [GHz]	Insertion Loss [dB]	Phase Shift [°/cm]	FoM [°/dB]
[28]	Dual Mode	35	2.2	118	205
[29]		70	1.4	150	257.1
[35]	Ferrite Slab Loaded SIW	35, 65, 94	0.7, 0.9, 1.5	123.03, 110.12, 59.4	603, 97, 25.33
[36]		35	0.6	-	750
[41]	Planar Transmission Line Based Designs	6.55	4.25	153.5	72
[42]		6.25	3.2	360	56.25
[43]	SIW	24	3.15	300	95
[44]		12.5-14	≤2	222.22	>200

It can be seen that ferrite based designs can generate phase shifts of more than 100° with reasonable values of insertion loss. The two characteristics missing in this table are the method by which magnetic field is applied to bias the substrate and the switching time of these designs. Like the antenna designs, phase shifters realized using ferrite materials also rely on external source of magnetic field. Therefore in general it can be said that they will require magnetic field strengths in the range of 1000s of Oe. This is one of the reasons why they are not seen as a very good option for present day applications. As far as switching time is concerned, ferrites have

switching speed in the range of $1\mu s$ to few μs [27]. Such switching speeds are generally acceptable for various applications however better speeds can be achieved with semiconductor based designs. However, we will focus ourselves on the ferrite based designs keeping in view the topic of this thesis.

2.2.3 Polarization Reconfigurable Antennas

In the last two sections, it was discussed how ferrite is used for the frequency tuning and phase shifting applications. This was accomplished by controlling the magnetostatic properties of the substrate using external biasing schemes such as magnets and electromagnets. Exploiting this characteristic, designers have also used magnetic mediums for radiation pattern reconfigurability. This includes steering the main beam of the antenna array and varying the polarization of single element antennas. For the beam steering realization, antenna designers use an array of patches on ferrite substrates as shown in Fig. 2.8 [45-47].

When the array substrate is biased, it changes the phase difference between the two elements due to the change in the permeability. This change in the phase between the antenna elements modifies the direction where the array has the maximum radiation, resulting in beam scanning. Though beam scanning has been shown through biasing of ferrite, the authors in [46, 47] observed that the application of magnetostatic bias also tunes the frequency of the array. This is expected as the resonant frequency is a function of the permeability of the substrate. This behavior is not useful for phased array applications as the antenna needs to be matched to the desired frequency only.

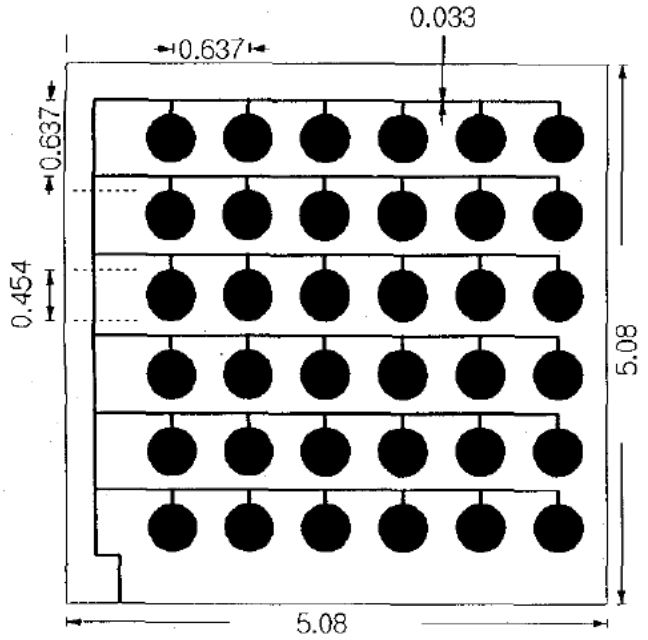

Fig. 2.8. Planar array of patch antennas on ferrite substrate [45]

Another interesting aspect has been observed related to the polarization of an antenna on biased ferrite substrates. This phenomenon was first discussed by D. M. Pozar and J. S. Roy in 1992 [18], [48], where a patch antenna performance on an axially biased ferrite was studied. Pozar presented a complete theoretical model of the circular patch antenna on a normally biased ferrite substrate. The theory revealed that in the biased condition a patch antenna demonstrates circular polarization of both sense i.e. left hand circular polarization (LHCP) and right hand circular polarization (RHCP) at different two frequencies. However, this theory was not verified by any experimental results.

Petosa et. al., presented two papers on dielectric resonator antennas, in which a ferrite cylinder was used as the dielectric medium [49], [50]. The author termed this antenna as ferrite resonator antenna (FRA). In the unbiased condition, the antenna works as a linear polarized antenna at its center frequency. When biased by a magnetic field which has both normal and

tangential components to the substrate, the antenna exhibited resonances at two different frequencies with two different sense of polarization. This effect is illustrated in Fig. 2.9 (referenced from [50]). It can be seen that in the conventional mode of operation the antenna works at a single frequency i.e. 7.35 GHz with linear polarization. However when biased, the reflection coefficient (return loss) of the antenna splits into two different matching points i.e. 6.8 GHz and 7.6 GHz. The authors mentioned these two frequency points as having circular polarization with opposite sense. It was claimed that the designed antenna operates at a frequency which is in between the resonance frequencies of the two nearly degenerate, mutually orthogonal modes and thus circular polarization is obtained. However, no evidence of this explanation was provided. Therefore, it can be said that the work which was presented up to this point was not able to explain the reasons as to why this frequency splitting is observed.

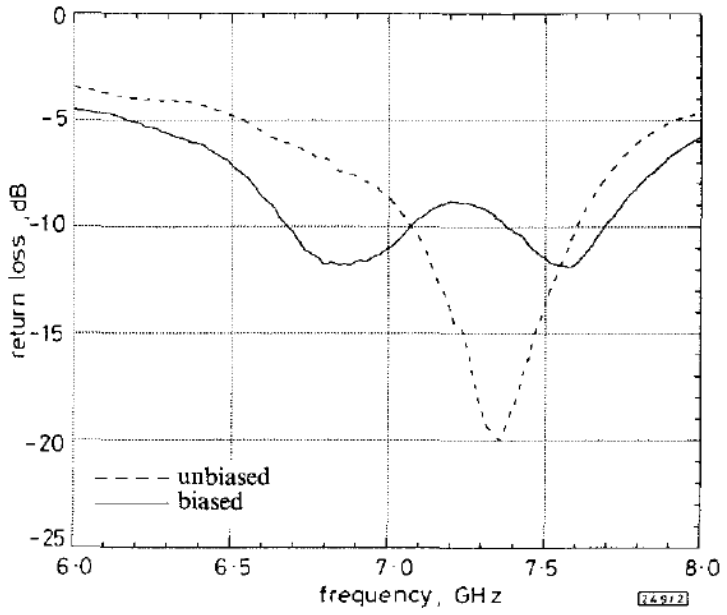

Fig. 2.9. Frequency splitting of an FRA antenna [50]

In 1997-98 R. J. Langley et. al. published three papers on annular ring patch antenna design realized on YIG substrate [51]-[53]. In the first two papers, measured results of the antenna were presented which showed the splitting of the resonant frequency when the substrate is biased. In the third paper, a complete theoretical model of the ring patch antenna on a saturated magnetic substrate was presented. This was the first time that a successful explanation of such polarization reconfigurability was proposed. Prototypes were fabricated to verify the cavity model that was proposed by the authors. A good match can be seen between the two results for different modes as shown in Fig. 2.10 below [53].

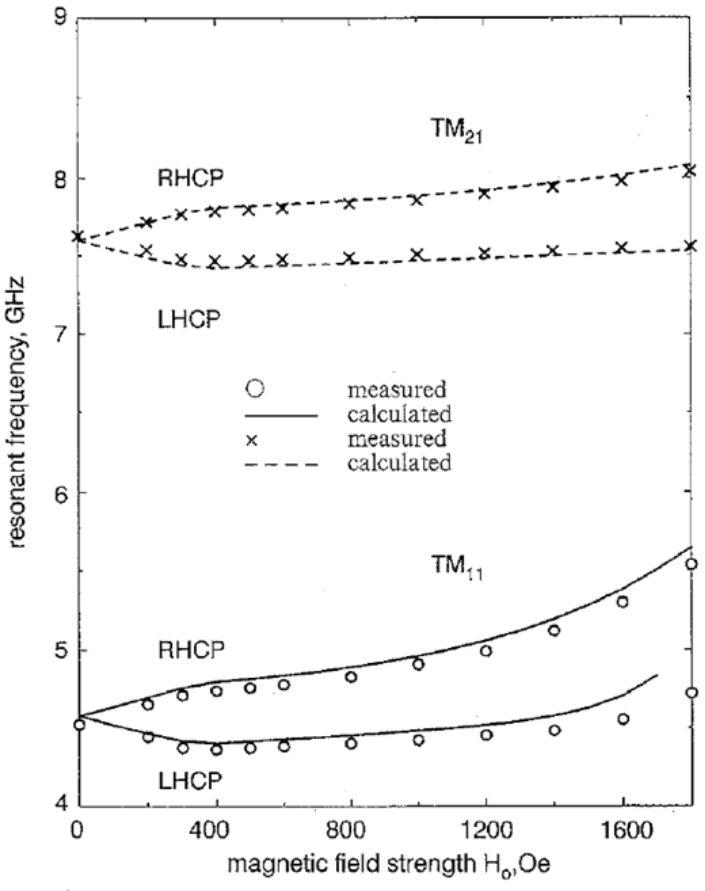

Fig. 2.10. Frequency response of annular ring antenna on ferrite substrate [53]

After Langley's work two more papers were published on the same polarization reconfigurable design [54], [55]. But the most comprehensive work in this regard is still the one reported by Langley [53]. The works reported in this section show the feasibility of polarization diversity that can be achieved using ferrite based antenna designs. Although the results reported in this section are encouraging, the designs still suffer from the same problems as reported before for the ferrite phase shifter designs and the tunable antenna designs. No work has been reported for the polarization reconfigurable patch antennas with their theory and operation in the partially magnetized state. This will be the focus of our work for polarization reconfigurable antennas i.e. operation in the partially magnetized state.

2.2.4 Summary of Literature on Bulk Ferrite Designs

It can be concluded from the discussion of this chapter that ferrite is a viable medium for frequency tunability and radiation pattern reconfigurability of microwave designs. However, there are many challenges/issues with the design approach that has been conventionally used with classical ferrites. These are:

i. Most of the ferrite based microwave passive designs are operated in saturated regime. This requires strong magnetic fields to bias the substrate which is usually accomplished by using external magnets or electromagnets. As a result all the designs reported in the literature are inefficient requiring high intensity of bias fields.

ii. The high intensity of the bias fields used in these designs is also because of the demagnetization effect. The tunable designs covered in this section either use external magnets or solenoid coils to provide the necessary magnetostatic bias. Since these magnetic sources are

external to the ferrite substrate they will suffer from demagnetization, which further reduces the efficiency of bulk ferrite based components.

iii. The use of the magnets/electromagnets makes the designs bulky and non-integrable. Compact size, light-weight and portability are some of the main needs of the modern communication systems. The large size of the electromagnets makes the ferrite designs unfit for these applications.

An elegant solution to the combined problem of bulky electromagnets and strong magnetostatic field requirements is to embed the bias windings in the ferrite substrate itself, below the microwave device. This can be done conveniently using an SoP (System on Package) based multilayer ferrite LTCC (Low Temperature Cofired Ceramic) substrate. Such a design will not only reduce the overall size of the system but will also reduce the required field strengths by avoiding the demagnetization effect and also by operating in the partially magnetized state rather than saturation hence improving the efficiency of the system.

2.2.5 Ferrite Low Temperature Cofired Ceramic (LTCC) Based Designs Using Embedded Bias Windings

System on package (SoP) concept provides a unique way of integrating the system components vertically instead of horizontally. This enables the designers to reduce the overall size of the system immensely. SoP integrates multiple functions into a single, compact, low cost and high performance packaged module [56], [57]. It reduces the system size and cost considerably by transforming millimeter-scale discrete components into micrometer or

nanometer-scaled embedded thin-film components [58], [59]. The vertical integration of actives and passives using SoP is shown in Fig. 2.11.

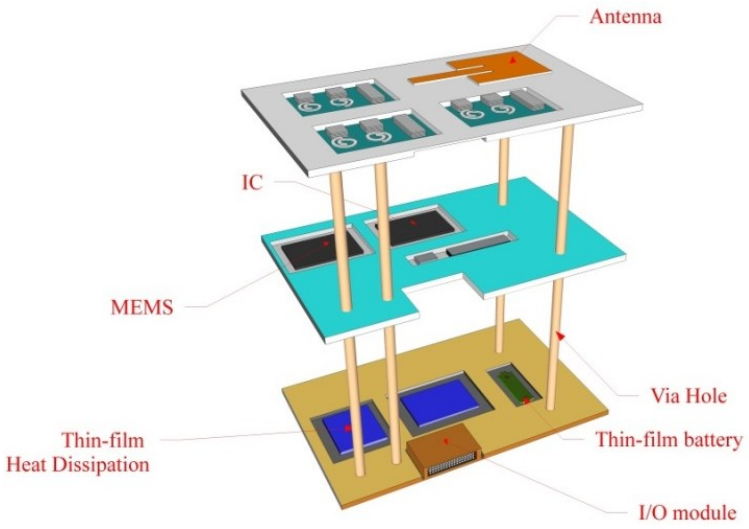

Fig. 2.11. System on Package (SoP) Concept

The most commonly used technology for SoP is Low Temperature Co-fired Ceramic (LTCC). LTCC is a mature technology that is being commercially used. Being ceramic based, it is hermetic and, therefore, is a very good packaging material; it is also very suitable for RF applications and supports multi-layer integration up to over 50 layers. Moreover the low loss nature of LTCC at microwave and millimeter-wave frequencies makes it extremely suitable for efficient antenna design.

In the last decade two ferrite LTCC tape systems have been introduced by Ferro Corporation (Ferro A6-S) and ESL Electro Science (ESL40012) [60], [61]. These mediums allow the realization of multilayer ferrite based microwave designs which can reduce the size of the module by 3D integration and cut down the cost by fabrication in large scale. The vertical integration method of the LTCC technology enables the use of embedded bias windings inside

the magnetic medium as opposed to the use of external magnets. As a result the problems of the traditional ferrites which include bulkiness, large size, inefficiency, non-integrability and non-portability cab be resolved by the new ferrite LTCC medium. Using the concept shown in Fig. 2.11, tunable, miniaturized and efficient antennas can be implemented.

As with any new material in the microwave engineering, these two tape systems also needed to be characterized for their high frequency properties. The fact that these materials are magnetic in nature means that they should also be studied for their magnetic behavior which includes properties such as saturation magnetization, remanence, and coercivety. For this purpose, the magnetostatic and microwave characterization of these substrates are reported in [60], [62]. Table 2-3 summarizes the magnetostatic properties of the two ferrite LTCC material systems.

Table 2-3. Characteristics of Ferro A6-S and ESL 40012 [60], [62]

Material	Saturation Magnetization $4\pi M_s$ G	Remanence G	Coercivety Oe	Squareness
Ferro A6-S	2300	1380	28	0.6
ESL40012	4000	2500	5.4	0.625

The authors of both the manuscripts also studied the high frequency characteristics of the materials. For this purpose ring and cavity resonators were used in [60] and [62] respectively. The dielectric constant of Ferro A6-S and ESL40012 was found to be 11.0 ± 0.5 (@ 20 to 40 GHz) and 13.9 ± 0.5 (@ 9.6 GHz) respectively. This high value of dielectric constant is expected from a ferrite material. The loss tangent values were quite close for the two material systems i.e.

0.004. This value of loss tangent is quite acceptable for ferromagnetic materials which are generally deemed lossy.

2.2.5 (A) Full Mode Asymmetrically Biased LTCC Based SIW Phase Shifter

Using the characterization of Ferro A6-S, a full mode SIW ferrite phase shifter employing the new LTCC technology was demonstrated in [9]. This was the first and only realization of a ferrite SIW phase shifter using this medium. For the first time, the electromagnets were replaced by embedded bias windings. The design concept and implementation of embedded windings inside the phase shifter are shown in Fig. 2.12 [9]. The authors studied the theoretical model of this design and presented a closed form transcendental equation that can predict the differential phase shift of any ferrite phase shifter design. The proposed theoretical model showed that a full mode asymmetrically biased phase shifter can generate differential phase shifts in the order of 500°/cm with FoM of 600 °/cm.

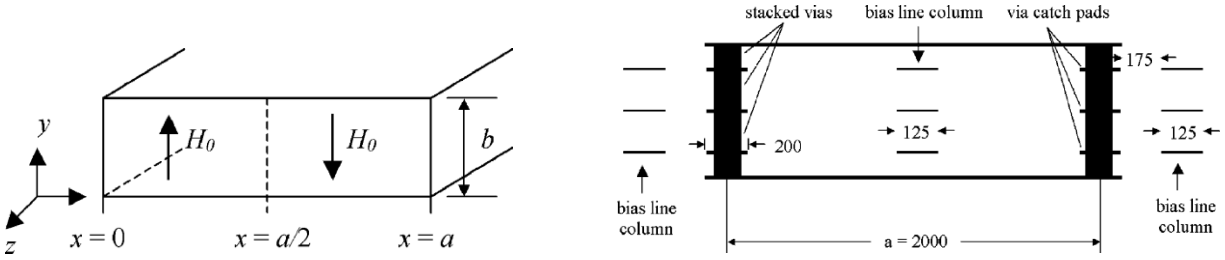

Fig. 2.12. (a) Ferrite filled asymmetrically biased SIW phase shifter concept (b) Implementation of bias windings inside the phase shifter design [9]

The bias fields applied to achieve such values were in the range of few thousands A/m or tens of Oe. This shows a reduction of almost 90 % in the bias field strengths as compared to the

design reported in Table 2-2 of this thesis. Although the proposed design showed promising results in theory there were a number of problems associated with the actual fabricated design. The fabricated phase shifter could only show a maximum phase shift of 52.8° (14.67 °/cm) as opposed to the proposed theory which means that there is a huge discrepancy between the predicted and measured results. The insertion loss of the phase shifter was around 3.6 dB which is extremely high as compared to some of the bulk ferrite phase shifters. Finally, the bias windings used in that work was neither optimized to reduce the current requirements nor was it placed in the best possible way. Even with all these issues, the design reported in [9] is quite intriguing as it was the first ever demonstration of a microwave component in ferrite LTCC technology. This work opened a new door of research in the domain of ferrite based tunable and reconfigurable microwave components.

2.2.5 (B) Ferrite LTCC Based Tunable Patch Antenna

Similar to [9], the authors in [63] used the new ferrite LTCC tape system (ESL40012) for implementation of a tunable microwave component on it. Here, the authors designed a simple linearly polarized patch antenna with embedded bias windings using the 3D integration concept in SoP approach. The fabricated image of the embedded bias windings is shown in Fig. 2.13. Both the solenoid and toroid windings were used for the substrate characterization while the solenoid windings were also used for tuning the frequency of the antenna. The antenna was designed to operate at 12 GHz so as to avoid low field losses of the medium since the f_m of ESL40012 is 11.2 GHz. The design showed a tuning range of 4 % using the bias fields of similar strength as [63] which again proves the viability of this new integration approach. However similar to the phase shifter design, the tunable antenna realization also had several issues

associated with it. There were no theoretical or simulation models presented in this work, as a result it can be stated that the authors did not investigate the reasons for achieving the frequency tunability. In addition to this, the embedded bias windings used in this paper were integrated in between the antenna and its ground plane which means that the RF fields of the antenna were adversely affected by the presence of metallic lines in their path. Therefore, poor gain values were obtained from the designed antenna. A downside which is common between this work and [9] is that the authors in both the manuscripts never considered the operation of the microwave components (i.e. phase shifter and antenna) in the partially magnetized state. The use of the embedded windings remarkably reduces the required field strength to bias the ferrite medium but at the same it means that the substrate is being operated in the partially magnetized state rather than saturation. The authors did not consider the magnetization state of the medium properly which resulted in discrepancy between theory and measurements for the phase shifter design [9] while no theory or simulations were presented for the tuning of the patch antenna [68]. The above-mentioned short comings and issues will be dealt with in this thesis.

(a) (b)

Fig. 2.13. Embedded bias windings (a) solenoid (b) toroid [62], [63]

2.3 Conclusion

Ferrites are magnetic dielectrics which have been used for design of tunable and reconfigurable RF and microwave elements. The tunability/reconfigurability was achieved by using external magnets or electromagnets to bias the substrate on which the component was realized. This approach provided interesting results for military and space applications. However, the bulky nature of the designs (due to the use of large electromagnets) rendered them unfit for the modern applications where system size is one of the main challenges. The external source to bias the material also resulted in demagnetization affects which in turn increased the required magnetic field strength outrageously. Therefore these designs were not only large they were also highly inefficient and non-integrable.

The advent of the ferrite LTCC technology showed that ferrite can still be a good solution to the tunable and reconfigurable requirements of the modern communication systems. The prototypes fabricated using the multilayer fabrication technique allows the use of embedded bias windings instead of external electromagnets. This new approach of vertical integration using multilayer fabrication processes can significantly resolve the drawbacks due to which ferrites have not been pursued as a research area in the recent years. The concerns of size, high magnetic field strength, portability and integrability can all be addressed using the new approach and will be the topic of research for this thesis.

Chapter 3

Ferrite LTCC Based Tunable Antennas

In this chapter, tunable antenna designs realized with ferrite LTCC technology using embedded windings are discussed. The designs include a linear polarized rectangular patch antenna and a helical antenna. A theoretical model is presented for the patch antenna on a biased ferrite substrate which is backed up by simulations and measurements. The helical antenna is an extension of the work shown in the patch antenna design. These two designs show how multilayer LTCC technology can provide miniaturized, efficient, and portable ferrite components.

3.1 Linear Polarized Patch Antenna

The design concept for the patch antenna implementation using ferrite LTCC is shown in Fig. 3.1. The antenna is designed using the top layers of the substrate while the bias windings are realized in the bottom layers. A ground plane is used in between the antenna and the bias windings. This ground plane will shield the antenna from the bias windings and will improve the radiation performance of the antenna, as opposed to [63], where the solenoid windings were embedded between the antenna and the ground plane. In this section, the theory, simulation, and design of the antenna with the embedded bias windings are discussed.

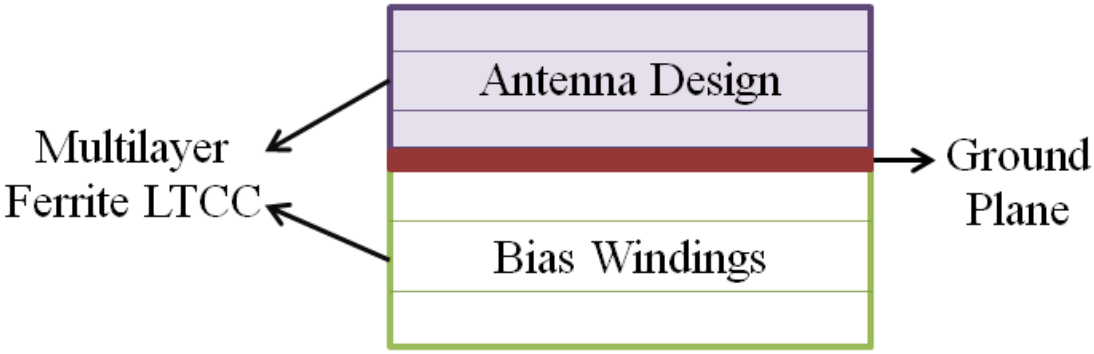

Fig. 3.1. Design concept for ferrite LTCC based patch antenna

3.1.1 Mathematical Model

As discussed in the last chapter, a ferrite medium is modeled by the Polder's equations when saturated [10]. However, these equations are not applicable to a partially magnetized ferrite substrate. When using the saturated case for a microwave design, the initial relative permeability of the material is typically assumed to be 1 (free space permeability); however, this is not true for frequencies close to f_m. This assumption can create a considerable mismatch between the actual performance of a prototype realized on such a substrate compared to the expected response. To overcome this discrepancy, a closed-form equation was proposed by Schlomann to predict the permeability of the material in its completely demagnetized state [15]. In addition to the demagnetized state, the elements of the permeability tensor μ and κ do not agree with the Polder's equations in the partially magnetized state. To address this, a new set of equations have been presented in [11] and [16], which have been experimentally verified in [17]. This work employs the theoretical analysis presented in [17] to derive equations that predict the frequency tuning of a patch antenna on a partially magnetized ferrite substrate.

3.1.1(A) Partially Magnetized Ferrite

The equations that explain the behavior of a magnetic material in its partially magnetized state Eq. 2.6 to Eq. 2.8 [17]:

$$\mu'_o = \frac{2}{3}\left[1 - \left(\frac{\gamma 4\pi M_s}{f_{res.}}\right)^2\right]^{\frac{1}{2}} + \frac{1}{3}$$

$$\mu = \mu'_o + (1 - \mu'_o)\left(\frac{M}{M_s}\right)^{\frac{3}{2}}$$

$$\kappa = n\frac{\gamma 4\pi M}{f_{res.}}$$

All of the parameters in the above equations have been discussed except for n. The coefficient n shows the deviation of κ from Rado's model in the partially magnetized state. In general, Rado's model is accurate when $f_{res.} \geq 2f_m$; thus, n can be neglected for this frequency band. However, when $f_{res.} < 2f_m$, considerable deviation is observed between Rado's model and the actual medium response [17]. This deviation is quantified in terms of the coefficient n. The coefficient n is dependent both on the frequency and strength of magnetization. Since n is only weakly dependent on the magnetization, it is neglected in this work for simplicity. The dependence of n on frequency, however, must be considered.

Another important factor is the gyromagnetic resonance, which occurs near the Larmor frequency where the ferrite medium is lossy. To avoid these losses and the low-field losses, it is necessary to operate at a frequency that is higher than the Larmor frequency (f_0) and the magnetization frequency (f_m). Ten layers of ferrite LTCC (ESL40012) are used in this work that has a saturation magnetization (M_s) of 4000 G, resulting in a magnetization frequency of 11.2 GHz [63]. To avoid low-field losses, a value of 13 GHz has been selected as the resonant

frequency of the antennas. The strength of the magnetic fields used in this work is low. Therefore, the Larmor frequency will be easily avoided at 13 GHz. It was observed in [22] that at 13 GHz *n* can vary between 0.6 and 0.7, but the authors in that work did not verify this deviation experimentally. Their work was based on numerical computation. Therefore, in this work, this value was varied from 0.5 to 0.7 to obtain the best match between the theory and the measurements. It was observed that $n = 0.5$ provides a good agreement between the theory, simulations, and measurements, as discussed in Section 3.3. As a result, this value is kept constant in this thesis for all of the designs.

After understanding the basic magnetostatic properties of the ferrite, now it is easy to evaluate the microwave electric and magnetic fields of the antenna under biased conditions. For the patch antenna TM^z mode of operation is solved [64]. The application of Ampere's Law for this mode of operation yields

$$-\frac{\partial h_y}{\partial z} = j\omega\varepsilon e_x \tag{3.1}$$

$$\frac{\partial h_x}{\partial z} = j\omega\varepsilon e_y$$

$$\frac{\partial h_y}{\partial x} - \frac{\partial h_x}{\partial y} = j\omega\varepsilon e_z$$

Eq. 3.1 is independent of the permeability of the material and is unaffected by the bias. In order to apply Faraday's Law, the permeability tensor for each bias direction must be defined. Two different direction of bias will be studied for the patch antenna.

3.1.1 (B) Extraordinary Mode using Z-Bias

The permeability tensor takes the following form when the direction of the bias is in the Z

direction:

$$\boldsymbol{\mu} = \mu_0 \begin{bmatrix} \mu & -j\kappa & 0 \\ j\kappa & \mu & 0 \\ 0 & 0 & \mu_z \end{bmatrix} \tag{3.2}$$

where μ_0 is the free space permeability. For a saturated ferrite μ_z is equal to 1; however, for the partially magnetized state it can be computed from Eq. 3.3 [17]:

$$\mu_z = \mu'_o \left(1-\left(\frac{M}{M_s}\right)^{\frac{5}{2}}\right) \tag{3.3}$$

Faraday's Law then yields,

$$\frac{\partial e_z}{\partial y} - \frac{\partial e_y}{\partial z} = -j\omega\mu h_x - \omega\kappa h_y \tag{3.4}$$

$$\frac{\partial e_x}{\partial z} - \frac{\partial e_z}{\partial x} = \omega\kappa h_x - j\omega\mu h_y$$

$$\frac{\partial e_y}{\partial x} - \frac{\partial e_x}{\partial y} = 0$$

In this work, the length L of the patch is the largest dimension, which means that TM^{100} is the resonant dominant as illustrated in Fig. 3.2. Using this mode will imply that $\frac{\partial}{\partial y} = \frac{\partial}{\partial z} = 0$ and $e_x = e_y = 0$. Taking this into account, Eq. 3.1 and Eq. 3.4 can be reduced to the following three equations:

$$\frac{\partial h_y}{\partial x} = j\omega\varepsilon e_z \tag{3.5a}$$

$$j\omega\mu h_x = -\omega\kappa h_y \tag{3.5b}$$

$$\frac{\partial e_z}{\partial x} = -\omega\kappa h_x + j\omega\mu h_y \tag{3.5c}$$

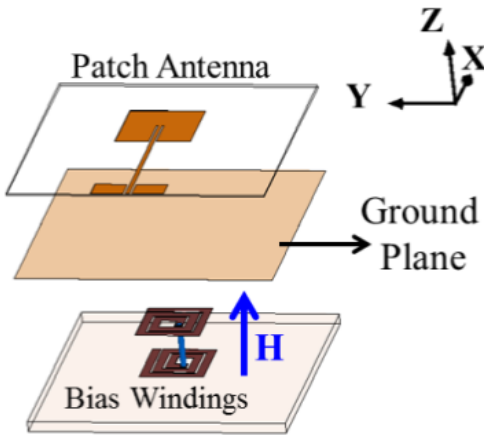

Fig. 3.2. Solenoid winding for the E-mode (Z bias, reduced number of layers and turns are shown for clarity)

From the above equations, the following wave equation is obtained:

$$\frac{\partial^2 h_y}{\partial_x{}^2} + k_x{}^2 h_y = 0 \tag{3.6}$$

where,

$$k_x = \omega\sqrt{\mu_e\,\varepsilon} \tag{3.7}$$

$$\mu_e = \frac{\mu^2 - \kappa^2}{\mu} \tag{3.8}$$

Solving Eq. 3.6 and applying the boundary condition $h_y = 0\ at\ x = 0$ results in the following solution:

$$h_y = A\,sin(k_x x) \tag{3.9a}$$

Now h_y can be used to determine the other components, i.e. e_z and h_x.

$$h_x = j\frac{A\kappa}{\mu} sin\,k_x x \tag{3.9b}$$

$$e_z = -j\frac{Ak_x}{\omega\varepsilon} cos\, k_x x \tag{3.9c}$$

Applying the boundary condition $h_y = 0\ at\ x = L$ to compute the wave number k_x and comparing it to Eq. 3.7 for the dominant modeTM^{100} results in the following expression for the E-mode resonant frequency:

$$f_E = \frac{1}{2L\sqrt{\mu_e\,\varepsilon}} \tag{3.10}$$

where f_E is the resonant frequency of the patch antenna for the E-mode. If Eq. 3.10 is compared to the resonant frequency f_{res} of a demagnetized patch antenna, the following ratio is obtained:

$$\frac{f_E}{f_{res}} = \frac{\sqrt{\mu'_o}}{\sqrt{\mu_e}} \tag{3.11}$$

Eq. 3.11 shows the dependence of the resonant frequency of the patch antenna on the permeability of the substrate in the extraordinary mode. If μ_e (effective extraordinary permeability or E-mode permeability) is greater than μ'_o then the frequency of the antenna will decrease and vice versa.

3.1.1 (C) Ordinary Mode using Y-Bias

A similar analysis to the E-mode is done on the patch antenna for the O-mode. For this mode, the design concept with the bias windings is shown in Fig. 3.3:

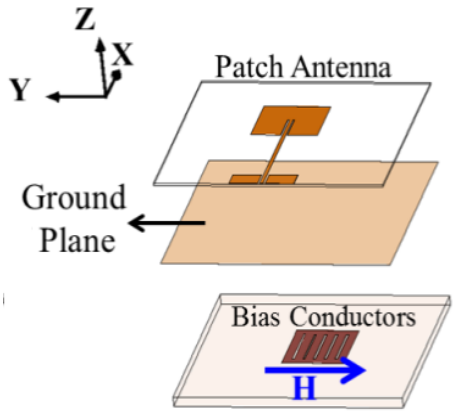

Fig. 3.3. Bias windings for the O-mode

The permeability tensor takes the following form for a magnetic field in the Y direction or along the width of the patch which corresponds to the O-mode:

$$\boldsymbol{\mu} = \mu_0 \begin{bmatrix} \mu & 0 & -j\kappa \\ 0 & \mu_y & 0 \\ j\kappa & 0 & \mu \end{bmatrix} \tag{3.12}$$

Applying Faraday's Law for this case results in,

$$\frac{\partial e_z}{\partial y} - \frac{\partial e_y}{\partial z} = -j\omega\mu h_x \tag{3.13}$$

$$\frac{\partial e_x}{\partial z} - \frac{\partial e_z}{\partial x} = -j\omega\mu_y h_y$$

$$\frac{\partial e_y}{\partial x} - \frac{\partial e_x}{\partial y} = \omega\kappa h_x$$

Again, considering the TM^{100} mode and simplifying Eq. 3.1 and Eq. 3.13 yields,

$$\frac{\partial h_y}{\partial x} = j\omega\varepsilon e_z \tag{3.14a}$$

$$\omega\kappa h_x = j\omega\mu h_x = 0 \tag{3.14b}$$

$$\frac{\partial e_z}{\partial x} = j\omega\mu_y h_y \tag{3.14c}$$

For this mode the same wave equation is obtained as in Eq. 3.6 but with a different wave number:

$$k_x = \omega\sqrt{\mu_y\,\varepsilon} \tag{3.15}$$

where μ_y is given by Eq. 2.8 but with magnetization in the Y-direction instead of Z. A very interesting point to note here is that for this mode only h_y and e_z are the non-zero field components, which is similar to a patch antenna on an isotropic medium. Therefore, the mode is known as ordinary but with a variable permeability that is controlled by magnetic bias. Applying the same boundary conditions yields the O-mode resonant frequency, f_o which, when compared to the resonant frequency of the demagnetized patch, yields:

$$\frac{f_o}{f_{res}} = \frac{\sqrt{\mu'_o}}{\sqrt{\mu_y}} \tag{3.16}$$

Similar to the E-mode, the resonant frequency of the O-mode decreases with an increase in μ_y and vice versa.

Using this theory, tuning is primarily achieved via the large change in the magnetization (M) that occurs in the partially magnetized state and not by the bias field H_0. Once saturation is

reached ($M=M_s$), Eq. 2.6 to Eq. 2.8 assume their usual Polder forms and further tuning can only be accomplished by large changes in the bias field H_0, which was the traditional way of tuning the ferrite antennas. Using the partially magnetized tuning mechanism, high magnetization field strengths are avoided, making this a much more efficient means of tuning the antenna.

3.1.2 Magnetostatic Simulations

CST EM Studio was used to design and optimize the bias windings whereas CST Microwave Studio was used to design the antenna for this work. These two solvers can be used in conjunction to simulate the antenna in the presence of the magnetostatic fields. Unfortunately, this joint simulation environment option is only valid for the saturated ferrite case. Therefore, a different simulation strategy is adopted here to simulate the antenna in the partially magnetized state. Initially, the bias windings are simulated in the magnetostatic solver to observe the magnetization generated by them. The magnetization value obtained is used to determine the elements of the permeability tensor through Eq. 2.6 to Eq. 2.8, and the permeability tensor obtained from the above equations is used in the high frequency simulator for antenna simulations in the partially magnetized state. Using a single value of magnetization for the complete antenna substrate assumes uniform bias fields under the antenna, which is not true for the actual measurements and can result in a deviation between the theory and the measurements. Therefore, a strategy was devised to model the non-uniform fields in the simulator, though the theoretical model will still depend on the uniform case.

The magnetostatic characterization of ESL40012 is presented in [62], [63]. The initial *B(H)* curve obtained from those measurements are shown in Fig. 3.4 (a) and has been used in this work to optimize the bias windings for both the E and O modes. For the E-mode patch, a

solenoid winding is designed using the bottom five layers of the substrate to produce a Z-directed magnetostatic bias field. For the O-mode, six parallel conductors of equal width are realized on the top of the fifth layer to produce Y-directed fields. The placement of these windings under the patch is shown in Fig. 3.2 and Fig. 3.3. The ground plane is realized in the sixth layer whereas the patch antenna is implemented on the top layer (i.e. the tenth layer), which means that the patch antenna uses four layers of the substrate. The ground plane is used in between the antenna and the windings such that the RF fields of the patch remain unaffected by the presence of DC bias conductors.

Magnetostatic simulations are performed on the bias windings to determine the strength of the magnetic fields for different current excitations. The bias windings generally produce non-uniform magnetostatic fields. Therefore, to model these fields under the patch antenna, magnetic fields in each layer produced by different current excitations are recorded. For this purpose, three lines, one along each axis (i.e. X, Y, and Z) are modeled in each layer under the patch antenna. The values of the magnetic fields obtained from these three lines, for a given current excitation, are averaged to obtain a single value for each layer. In this way, each layer can be modeled with a different magnetization. However, these simulations reveal that the fields are maximum and are close to each other in strength in the two layers above the ground plane. Therefore, these two layers are modeled with a single magnetization value. The third and the fourth layers above the ground plane have values that are 50 % and 20 % of the maximum value and are modeled accordingly. The horizontal and vertical lines in each layer, where the fields are recorded, are shown in Fig. 3.4 (b).

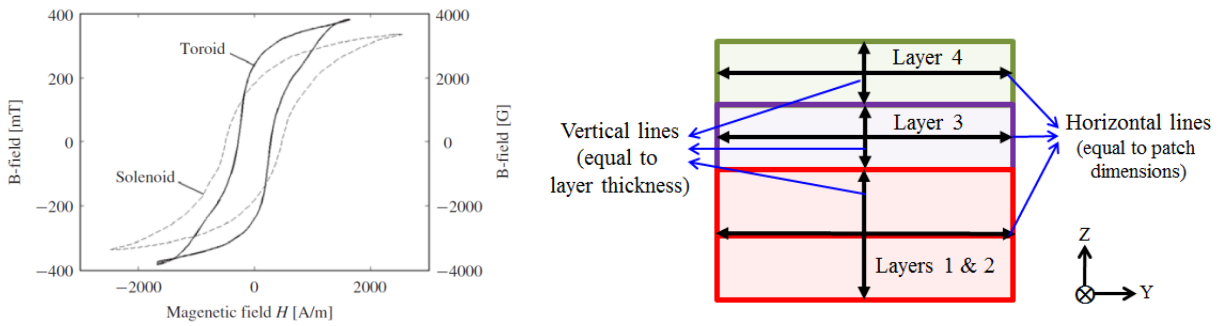

Fig. 3.4. (a) Measured $B(H)$ curve of ESL40012 [62], [63] (b) Four layers of the substrate shown with the horizontal and vertical lines along three axes (X, Y and Z, the line along X axis is going into the page and has same length as the Y line) where the magnetostatic fields are observed and averaged to model the non-uniform fields under the patch antenna

The horizontal lines used for these simulations are equal to the bias windings dimensions while the vertical lines are equal to the layer thickness. These simulations also reveal that for the E-mode, the top layer of the patch antenna substrate has a stronger tangential field component than the normal field component with respect to the antenna and the substrate. Therefore, in the microwave simulations for the E-mode, two different cases have been modeled for the non-uniform bias. One with all the layers biased in the Z direction and the other with the bottom three layers biased in the Z direction and the fourth layer biased in the Y direction. For the O-mode bias windings, the magnetostatic fields above the ground plane are strongest in Y-direction (desired direction) in all layers of the substrate. Therefore, for this mode, all of the layers are modeled with the Y-directed fields but with different bias strengths.

The solenoid windings used for the E-mode, are composed of nine turns per layer, resulting in a total of 54 turns. The conductor width used for this design is 100 µm with a pitch of 50 µm. The total size of the solenoid is 3 mm x 3 mm, as shown in Fig. 3.5 (a). The magnetic field strength (H) measured in Oersteds (Oe) and the magnetization ($4\pi M$) in Gauss (G) that are

simulated for the bottom two layers of each current excitation are shown in Fig. 3.5 (b). The values of *H* for the third and the fourth layer are 50 % and 20 % of this maximum value. Overall, these simulations demonstrate that a current of 180 mA is sufficient to saturate the ferrite substrate through this optimized solenoid winding, compared to the 500mA used previously [67]. For the O-mode patch, six parallel conductors (450 µm wide with 100 µm spacing) are used on the fifth layer to produce a Y-directed field. These conductors produce a maximum H value of 14 Oe for a current excitation of 1600 mA. Similar to the E-mode, the magnetostatic solver is used to determine the field strength produced by a particular bias current value in each layer.

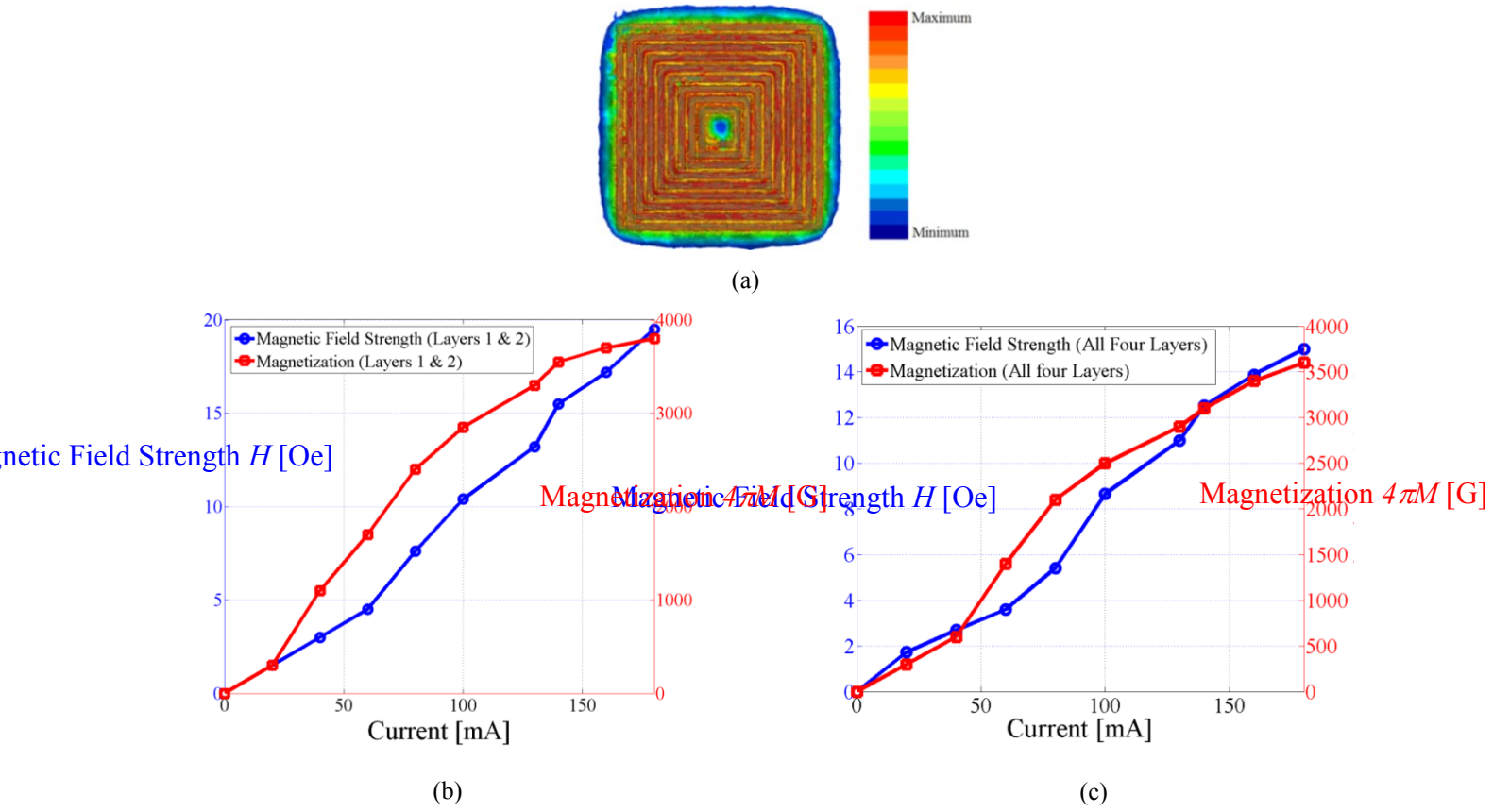

Fig. 3.5. (a) Magnetostatic simulation of bias windings for the E-mode, Magnetic field strength and magnetization produced by the bias windings (b) in the bottom two layers (c) at the center of the substrate

Although the modeling of the non-uniform fields under the patch antenna is closer to the actual scenario, it cannot be used for the theoretical model. The theoretical model requires a single value of the magnetic field or magnetization for a single current excitation in the complete antenna substrate. This means that for the theory, each layer cannot be treated individually. Therefore, to predict the tuning of the antenna, using the theory, the magnetostatic fields are observed at the center of the patch antenna substrate, which is shown in Fig. 3.5 (c). The magnetization value obtained at the center of the substrate for a current excitation is then used in Eq. 2.6 to Eq. 2.9 to evaluate the resonant frequency of the patch antenna using Eq. 3.11 and Eq. 3.16.

3.1.3 Microwave Characterization

The microwave properties of ESL40012, such as dielectric constant (ε_r) and loss tangent ($\tan\delta$), have been presented in [62]; where the demagnetized permeability of the substrate was assumed to be 1. Because of this assumption, there could be an error in the dielectric constant reported there. Section 3.2.1 explained that the demagnetized permeability of a magnetic material is less than 1, especially for frequencies close to f_m. If the frequency of operation is greater than $2f_m$ then the demagnetized permeability can be taken as 1. However, in this case, the frequency of interest is 13 GHz which is close to f_m. Therefore, it is necessary to characterize the substrate again at 13 GHz. For this purpose, a ring resonator and a T resonator have been designed on ESL40012. The ring resonator is an edge-coupled design with a diameter of 2.35 mm while the length of the T resonator is 1.87 mm. The fabricated photographs of the two resonator designs are shown in Fig. 3.6 (a) and (b) respectively with their measured response shown in Fig. 3.7.

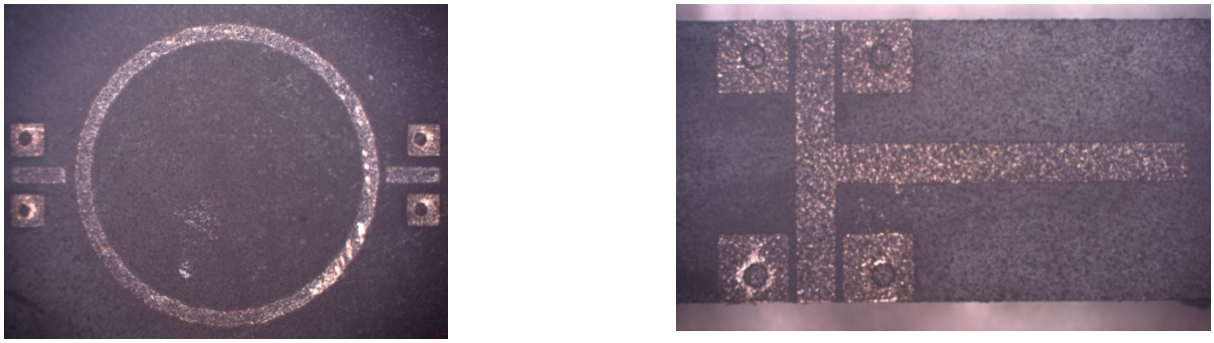

(a) (b)

Fig. 3.6. Fabricated (a) ring resonator (b) T resonator

The fundamental frequency of the ring is approximately 12.7 GHz while that of the T resonator is 12.9 GHz. To extract the dielectric constant, it is important to evaluate the demagnetized permeabilities at these frequencies using Eq. 2.9 such that this value can be utilized in Eq. 3.17. The demagnetized permeability of ESL40012 at 12.9 GHz is 0.664. At 12.7 GHz, which is the resonant frequency of the ring, the value of demagnetized permeability will be close to 0.664. Therefore, this value is kept constant for both of these frequencies. The equation for the resonance of the ring resonator and the T resonator are given by following equations [65], [66]:

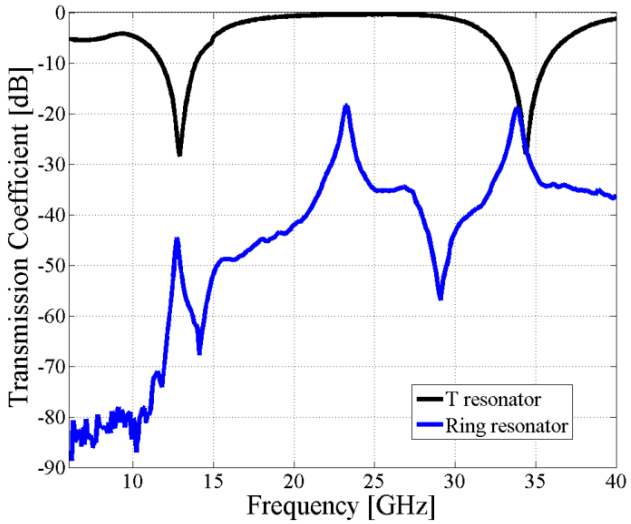

Fig. 3.7. Measured transmission coefficient of the resonators

$$f = \frac{mc}{2\pi r\sqrt{\mu'_o \varepsilon_{eff}}} \tag{3.17a}$$

$$f = \frac{mc}{4L\sqrt{\mu'_o \varepsilon_{eff}}} \tag{3.17b}$$

where m is the resonance mode which will be 1, 2, 3….for the ring resonator and 1, 3, 5… for the T resonator; c is the speed of light; r is the radius of the ring; ε_{eff} is the effective permittivity; L is the length of the T resonator; and μ'_0 is the demagnetized permeability. The measured dielectric constants of ESL40012 at different frequencies obtained from Eq. 3.17(a) are summarized in Table 3-1. These values demonstrate a tolerance of approximately 8 %.

In addition to dielectric constant, it is important to characterize the substrate for its loss tangent. To do this, the quality factor is extracted from the measured results of the T resonator, which is necessary to compute the value of the loss tangent. Both the loaded and unloaded quality factors are required. The loaded quality factor is the Q without removing the load, which

is due to the connected measurement equipment, while the unloaded quality factor is dependent on the loaded Q and the insertion loss of the resonator [67]. The two quality factors are given by the following equations:

$$Q_L = \frac{f}{BW_{3dB}} \tag{3.18a}$$

$$Q_u = \frac{Q_L}{\sqrt{1-2\times 10^{\frac{IL}{10}}}} \tag{3.18b}$$

where Q_L and Q_U are the loaded and unloaded quality factors, IL is the insertion loss, and BW_{3dB} is the 3dB bandwidth of the resonator. Once the unloaded quality factor is known, it can be converted into loss (α_{tot}) using Eq. 3.19 [68]. The total loss (α_{tot}) is composed of the loss due to the dielectric (α_d), radiation (α_r), and conductor (α_c) losses. The conductor loss is calculated using Agilent's ADS line calculator while the radiation loss, being small, has been neglected. The remaining dielectric loss can be used to evaluate the loss tangent given by Eq. 3.20 [68]. The loss tangent obtained from these calculations is summarized in Table 3-1 with the dielectric constant at different frequencies.

$$\alpha_{tot} = \alpha_d + \alpha_r + \alpha_c = \frac{8.686\pi f\sqrt{\varepsilon_{eff}\mu'_0}}{cQ_u} \tag{3.19}$$

$$tan\delta = \frac{\alpha_d\lambda_0\sqrt{\mu'_0\varepsilon_{eff}}(\varepsilon_r-1)}{8.686\pi\varepsilon_r\mu'_0(\varepsilon_{eff}-1)} \tag{3.20}$$

Table 3-1: Microwave characteristics of ESL40012

Frequency (GHz)	Dielectric Constant (ε_{eff})	Demagnetized Permeability μ'_o	Loss Tangent $\tan\delta(1 \times 10^{-3})$
12.9	14.5	0.664	4
23.2	13.7	0.9	8.5
33.8	13.2	0.96	4

From table 3-1 it can be observed that the demagnetized permeability is considerably less than 1 for the frequencies close to f_m while it is almost equal to 1 for frequencies greater than $2f_m$. The microwave characteristics summarized in the above table can now be used for the antenna design in the demagnetized state.

3.1.4 Antenna Design

The microwave simulation strategy is shown in Fig. 3.2 and Fig. 3.3. Initially, a relative demagnetized permeability of 0.68 obtained from Eq. 2.9 at 13 GHz is used to simulate the antenna without any bias. The total thickness of the module is 580 μm (58 μm for each layer). A 13 GHz inset fed microstrip patch antenna with dimensions of 3.6 mm × 3.4 mm is realized on the top (10^{th}) layer. An impedance bandwidth of 1.5 % with a gain of 3.6 dBi is obtained in simulations. The simulated impedance performance and 3D radiation pattern of the antenna are shown in Fig. 3.8 (a) and 3.8 (b) respectively. This gain and the stable radiation pattern highlight the importance of placing the ground plane in between the antenna and the bias windings. The high dielectric constant (ε_r=14.5) and the relatively small thickness (232 μm) of the substrate are

the suspected causes of the slightly lower gain of the patch antenna compared to the conventional values.

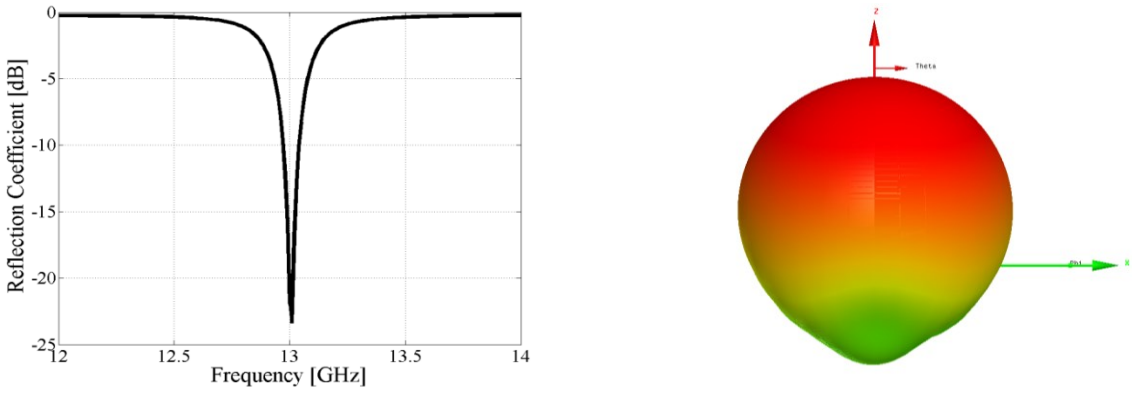

(a) (b)

Fig. 3.8. Simulated results of patch antenna (a) Reflection Coefficient (b) 3D radiation pattern

The antenna frequency tuning simulations in the biased case are done using the non-uniform fields shown in Fig. 3.5 (b). The magnetization values obtained from the magnetostatic simulations are used to evaluate the elements of the permeability tensor. The tensor thus obtained is used in the full-wave microwave simulator to perform the antenna simulations in the biased condition. These simulations reveal that for the bias strength of 19 Oe (180 mA) the antenna demonstrates a tuning range of 1240 MHz for the E-mode. Moreover the bias windings employed in this work are able to reduce the field strength by more than 90 % compared to what is typically needed when an external electromagnet is used [62]. Simulations are also carried out with three layers under the patch antenna assigned a Z directed bias with the fourth layer assigned a Y directed bias for the E-mode. However, the results obtained from these simulations are quite similar to the initial simulations where Z-directed bias fields are used in all four layers. Similar to the E-mode, the O-mode simulations have been done using non-uniform fields under

the patch antenna. These simulations exhibit a tuning range of 680 MHz. The detailed comparison between these simulated results with the theory and measured results will be presented in the next section.

3.1.5 Fabrication and Measurements

The ferrite LTCC patch antenna modules are fabricated at VTT Electronics in Finland. An X-ray image of the fabricated embedded solenoid winding and a picture of the fabricated antenna are shown in Fig. 3.9 (a) and (b) respectively. A microstrip line is used for the RF excitation and the magnetic bias is provided through DC pads on the top layer.

(a) (b)

Fig. 3.9. (a) X-ray image of fabricated bias windings for Z bias (b) Fabricated antenna

3.1.5 (A) Frequency Tuning for E-Mode Prototype Antenna

The measured tuning response of the patch antenna with an applied Z bias is shown in Fig. 3.10. The fundamental mode of the unbiased patch is at 13.1 GHz, which compares well with the theory and simulations. Furthermore, as the current in the windings is increased, the frequency of the patch decreases, which is in agreement with Eq. 3.11. A maximum bias current of 180 mA is

used for this mode which tunes the antenna down to 11.85 GHz as shown in Fig. 3.10. Increasing the current beyond 180 mA can damage the narrow bias conductors (100 µm wide). The measured tuning range of 1.25 GHz is more than twice what was achieved in [62], with a 64 % reduction in the bias current.

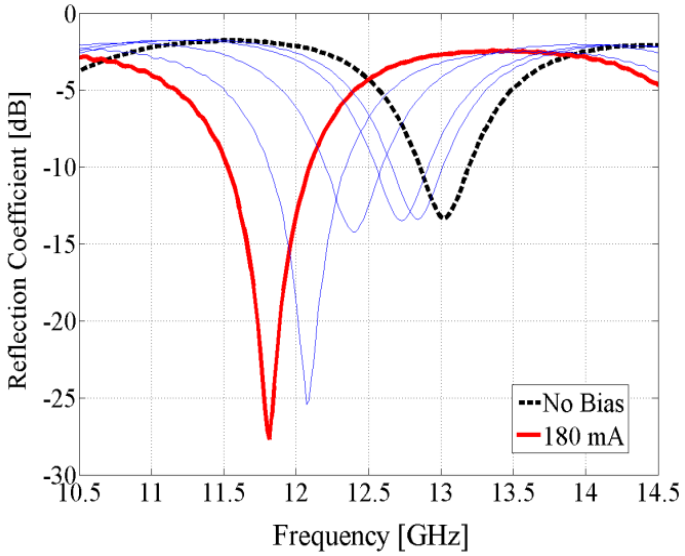

Fig. 3.10. Measured frequency response for the E-mode (the curves from right to left are for 0 mA, 45 mA, 75 mA, 120 mA, 165 mA, and 180 mA)

A comparison between the theoretical, simulated, and measured results is shown in Fig. 3.11. A strong agreement can be observed among these results. The measured results exhibit a tuning range of 1250 MHz, compared to the values of 1240 MHz and 1050 MHz that were predicted by the simulations and the theory, respectively. A slight deviation between the theory and the measurements is observed, which can be attributed to the inability to use the non-uniform fields in the theoretical model and the heating of the substrate due to the bias current. Moreover, the ideal TM mode assumed in the theory is not completely accurate for the actual measurements. Nonetheless, the general agreement between the two results indicates that the proposed theory is

a good starting point for predicting the tuning range of an antenna in a few minutes in the partially magnetized state which would otherwise require rigorous simulations and may also require many hours.

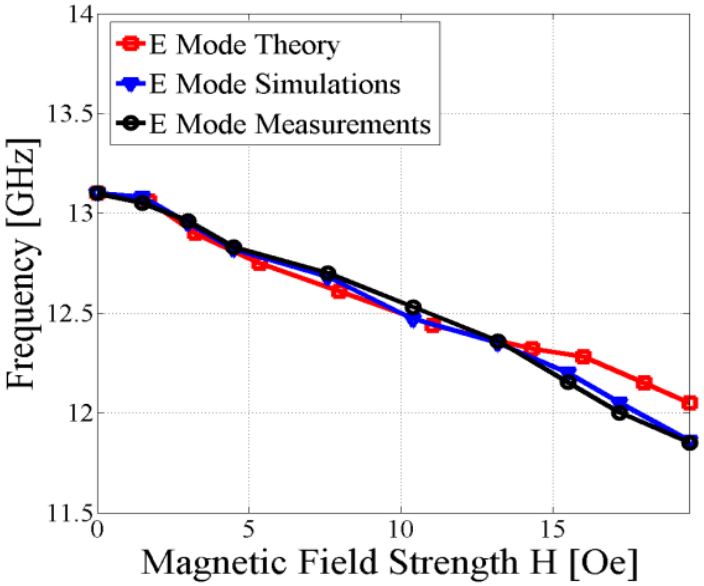

Fig. 3.11. Theory vs. simulations and measurements for the E-mode

3.1.5 (B) Frequency Tuning for O-Mode Prototype Antenna

The O-mode prototype with a bias in the Y direction is measured in the same fashion. The measured results exhibit a tuning range of 650 MHz which is in agreement with the simulations (680 MHz) and theory (770 MHz) as shown in Fig. 3.12. The lower tuning range for this mode compared to the E-mode is due to the weaker magnetic fields produced by the wide bias conductors (400 μm wide) for a large value of current (1600 mA). Increasing the current beyond this value can provide a better tuning range, but it may damage the bias conductors.

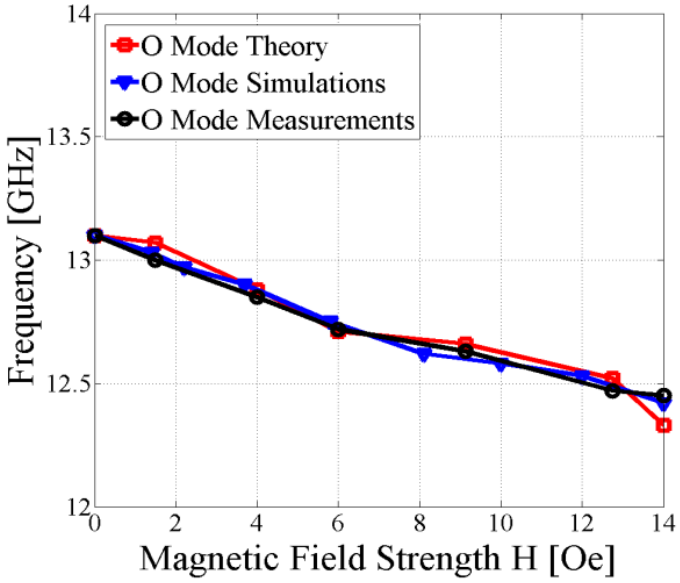

Fig. 3.12. Theory vs. simulations and measurements for the O-mode

3.1.6 Gain and Radiation Pattern Measurements

For the radiation pattern measurements in the biased state, DC connections to the substrate are made via wires that are soldered to bias pads on the top layer. In the absence of these wires, DC probes must be used to provide the required bias. A photograph of the biased substrate connected to an SMA cable for radiation pattern measurements is shown in Fig. 3.13. Co-polarized radiation pattern measurements were performed over a range of −180° to +180° along the E and H planes of the antenna for different bias conditions. The simulated and measured radiation patterns with no bias and with bias for the E-mode are shown in Fig. 3.14 and Fig. 3.15. For clarity, the normalized pattern for the two extreme states are shown (i.e. unbiased, 0 mA, and maximum bias,180 mA). A maximum gain of 3.0 and 3.2 dBi was measured for the unbiased and biased states, respectively. A tilt can be observed in the E plane which is due to the presence of the SMA connector. Since the size of the antenna is small, its radiation pattern is affected by the

presence of a metallic connector in its E plane. This tilt in the measurements has been verified by modeling the SMA connector in the simulations. The maximum cross polarization level is lower than 15 dB without any bias, which decreases to 20 dB in the presence of the bias. This value is typical for ferrite-based substrates [10], [63].

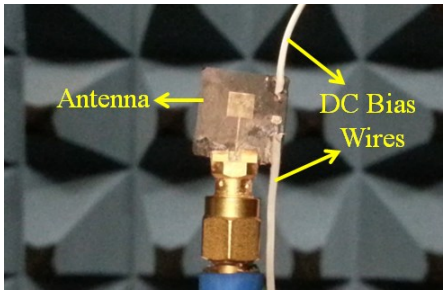

Fig. 3.13. Radiation pattern measurement under biased condition

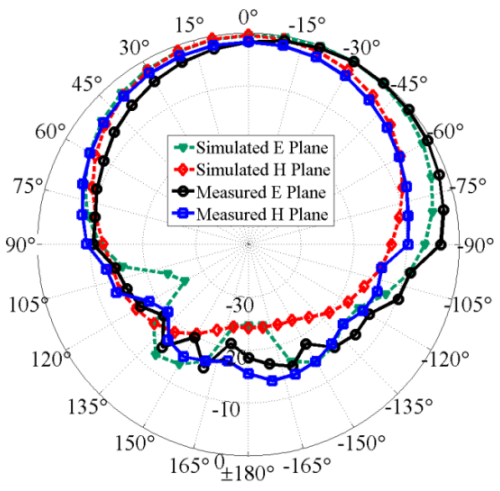

Fig. 3.14. Simulated and measured radiation pattern with no bias

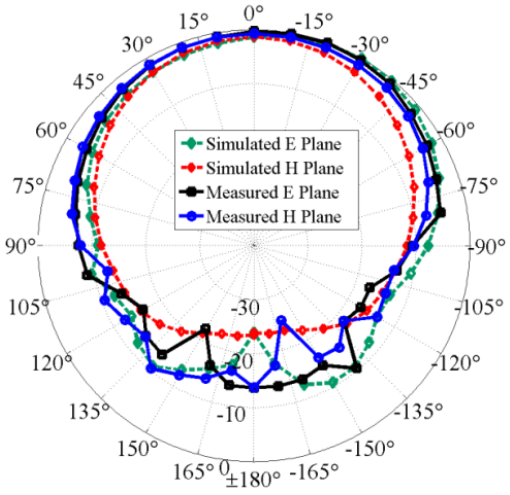

Fig. 3.15. Simulated and measured radiation pattern in biased state (180mA)

The radiation pattern and gain measurements of the O-mode are performed in a manner similar to the E-mode. These results confirm that the antenna radiation characteristics of the patch are almost identical with and without the bias. The tuning range achieved from the patch antenna in this work is superior to the only other ferrite LTCC based tunable antenna design [68]. In addition, the bias current used in this work is lower than the one that was used previously. To highlight the advantages of the patch antenna design presented here, a comparison between this work and the literature is summarized in Table 3-2.

Table 3-2: Comparison between results shown in [63] and this work

Literature	[63]	This work
Center Frequency (GHz)	12	13
Tuning Range	4 %	10 %
Current (mA)	500	180
Mode	Only O-mode	Both E and O mode
Theory	Not discussed	A model has been proposed

3.2 Helical Antenna

The tunable patch antenna design of the last section provides a perfect platform to investigate other types of microwave antennas and passive components in the new multilayer ferrite technology. The use of the embedded windings reduces the size considerably compared to when external electromagnets were used for the tuning. However, the windings occupy a major chunk of the layers that were used in the patch antenna implementation. Out of ten layers, six layers in the patch antenna design were occupied by the windings, which is 60 % of the total space. In addition to occupying space, the conductors of the bias windings should be carefully embedded

in the antenna package such that they do not affect the radiation or impedance performance of the antenna. The ground plane of the patch antenna was used as an isolator between the antenna and the bias windings. Both the problems of size and placement can be resolved if the antenna structure itself can work as a bias winding. A dual-purpose design is needed for such an implantation.

For such a realization, a magnetically tunable helical antenna which does not require separate bias windings is proposed. A helical antenna design is an ideal candidate that can work as a bias winding while radiating RF waves. But to achieve this, the antenna must be optimized to work as a solenoid winding. A challenge that will be encountered in such an approach is that the same helical structure will be excited by both RF and DC signals, which means that a mechanism is required to isolate the two frequencies. Usually, RF and DC signals are isolated using RF chokes and DC blocks with high frequency components. The same technique is used with the ferrite LTCC based helical antenna by monolithically integrating open circuit stubs (RF chokes) and a blocking capacitor (DC block) in the same package. This is one of the key merits of the LTCC technology that will be exploited for this particular design.

3.2.1 Design Concept and Optimization

A helical antenna is a travelling wave antenna that radiates in bore-sight in the axial mode. The size of a helical antenna dictates its center frequency. Generally, the circumference of the antenna should be equal to one-wavelength of the center frequency. Here, the antenna was designed for the center frequency of 13 GHz as was the case for the patch antenna. As a proof-of-concept, ten layers of the substrate are used. Among these ten layers, six layers are used for the antenna design, the bottom three layers are used for the feed network, and the top layer is

utilized for DC bias pads. The antenna design with the integrated RF choke and DC block capacitor is shown in Fig 3.16.

The circumference of the helical antenna for a center frequency of 13 GHz on ESL 40012 substrate is approximately 7 mm; this circumference value results in a radius of 1.15 mm ($r = C/2\pi$). Using this radius, the conductor width of the antenna is optimized at 0.75 mm for the best impedance match through microwave simulations. A width of 0.75 mm results in an inner radius of 0.75 mm and an outer radius of 1.5 mm. These dimensions are used for all six turns of the antenna. The interlayer conductors are connected using vias with a diameter of 200 μm.

Initially, the antenna is simulated without any magnetic bias. The simulated impedance performance of the antenna is shown in Fig. 3.17 (a). The reflection coefficient results show that the antenna has two poles at 12.95 GHz and 13.3 GHz, respectively. The pole at 13.3 GHz represents the original dimensional resonance of the antenna ($C \sim \lambda_g$), whereas the pole at 12.95 GHz is due to the mutual reactance between the turns of the antenna, as observed in simulations. The simulated radiation pattern shown in Fig. 3.17 (b) demonstrates a bore-sight maximum radiation pattern, as expected from an axial mode helical antenna. A simulated gain of 2.1 dBi is achieved at 13.1 GHz, which is low due to the high dielectric constant of the ferrite material.

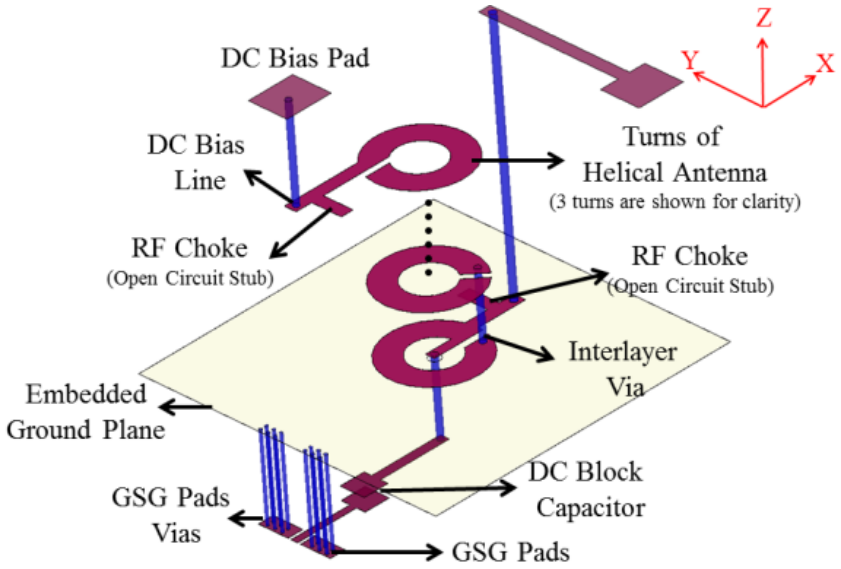

Fig. 3.16 Helical Antenna Design Concept

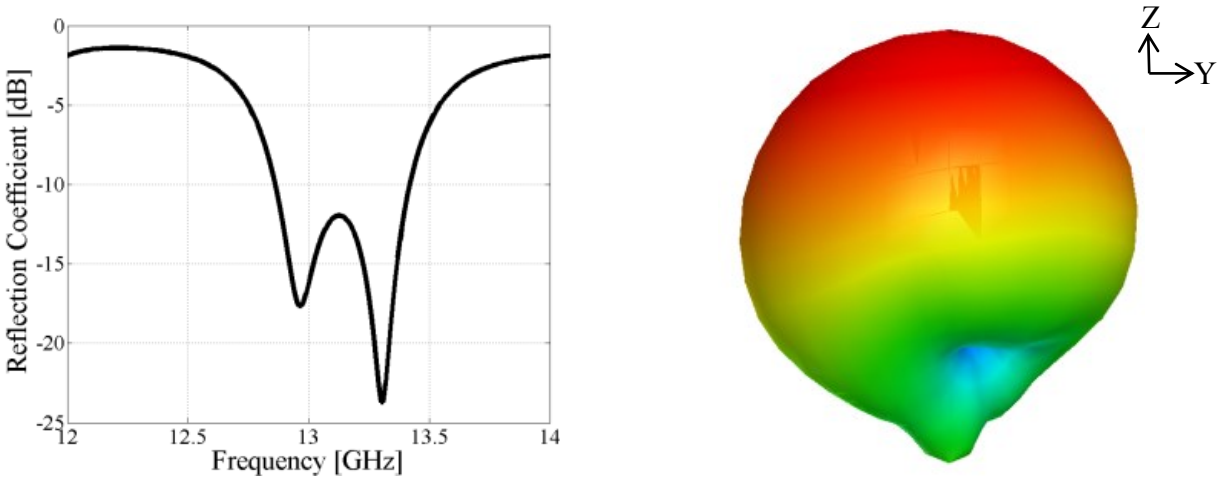

(a) (b)

Fig. 3.17 (a) Simulated reflection coefficient (b) Simulated 3D radiation pattern of the helical antenna

3.2.2 Magnetostatic Simulations

As discussed previously, the helical antenna needs to act as the bias winding as well. For this purpose, the optimized antenna structure is simulated in CST EM Studio to assess its

magnetostatic behavior. A helical antenna is a solenoid structure for a magnetostatic bias. Conventionally, a ferrite-core solenoid has the strongest magnetic field at its center along the axis of the solenoid, due to the presence of a magnetic core. However, in this work, the solenoid winding is completely surrounded by the ferrite material. Thus, the magnetostatic fields will not be concentrated at the center of the solenoid. Rather, the strongest fields are observed around the conductors themselves. This effect is illustrated in Fig. 3.18 (a), where the red region shows the area of the strongest magnetostatic fields and the yellow area in the middle of the solenoid has a field strength that is 10% of the red region. CST EM simulations demonstrate that the area with 10% of the maximum fields (i.e. the yellow region) starts at a distance of 100 μm from the inner conductor edge and at 250 μm from the outer edge of the solenoid. This information is utilized in the microwave simulator by defining the red region with a magnetic field value of H and the yellow region by a magnetic field value of $0.15H$.

The consequent values of magnetization M in the two regions can be evaluated using the B(H) curve of ESL40012. A graph showing the relationship between the DC current excitation, the magnetic field strength (H), and the magnetization ($4\pi M$ in G) generated in the red region is plotted in Fig. 2(b). As expected, the strength of the magnetic field (H) increases with the applied bias current in the windings. The maximum current in this plot has been restricted to 1100 mA, which is expected to be the largest current that can be safely applied to these windings without damaging them (as was observed in the measurements). This current value provided a maximum magnetization of 3300 G, which is sufficient for operation in the partially magnetized state but not to saturate the ferrite material.

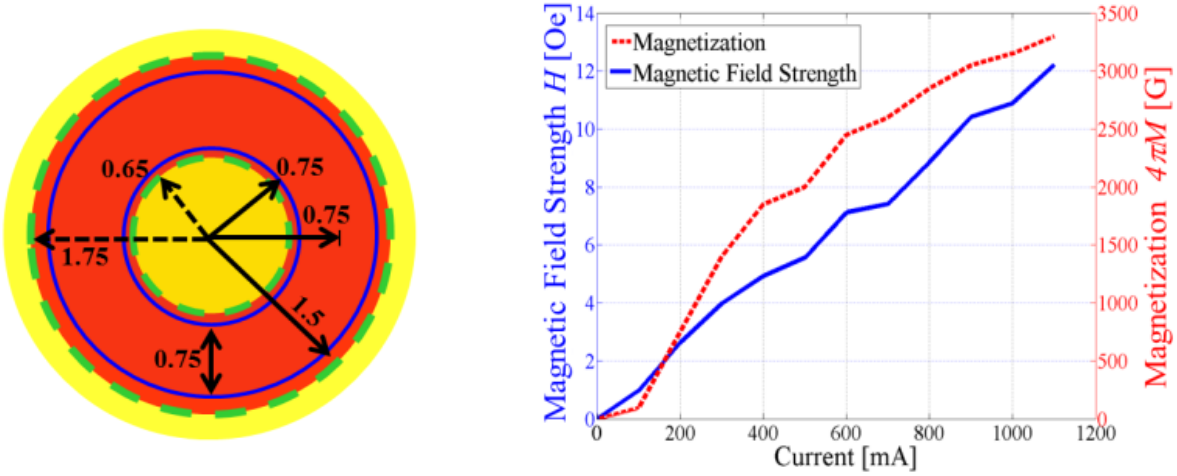

(a) (b)

Fig. 3.18 (a) Magnetostatic field strength regions in helical antenna (shown from the top view), dashed lines outline the boundary of field regions and solid blue lines outline the boundary of conductors, units are in mm) (b) Current versus magnetic field strength and magnetization (for red region of Fig. 3.18 (a))

3.2.3 Feeding Arrangement

Before simulating the antenna in the biased state, a mechanism is needed to isolate the DC bias and the high frequency excitations at their respective inputs. This is a challenge and the novelty of this design. To accomplish this, the DC blocking capacitor and RF choke are used with the helical antenna structure in the same manner as are used for a microwave amplifier (Fig. 3.16). Since the design is in a multilayer substrate, the best approach is to monolithically integrate them with the antenna. This will allow the design to operate without any external surface-mount components thus maintaining its compactness. The DC block capacitor consists of two parallel metallic plates with an area of 0.81 mm x 0.81 mm, which results in a capacitance of 0.77 pF. To take advantage of the DC block capacitor, it is also used for impedance matching by canceling the small input inductance of the antenna. The two plates of the capacitor are

implemented on the bottom two layers of the antenna substrate whereas the antenna's ground plane has been realized on the third layer. One of the plates of the capacitor is connected to the microstrip feed line while the other plate is attached to the first turn of the antenna using an inter-layer via. In this way, no part of the DC current of the antenna can flow to the RF feed line. For the RF chokes, two quarter-wave open circuited stubs are connected to the first and last turns of the antenna, as shown in Fig. 3.16. The DC bias is applied to a bias line which connects the stubs to the antenna terminals. At first, the antenna is simulated with the DC block and RF choke to verify its performance at its center frequency without any bias. Once the antenna has been integrated with the DC block and RF chokes it can be simulated in the partially magnetized state.

3.2.4 Frequency Tuning Simulations

For the antenna simulations in the partially magnetized state, the information obtained from the magnetostatic simulation is used. 'Full Permeability Tensor' option of CST Microwave Studio is used for these simulations as was the case for the patch antenna. The elements of the tensor are defined using Eq. 2.6 to Eq. 2.8. Two regions of the substrate, as shown in Fig. 3.18 (a), are simulated with different magnetization strengths. The value of the corresponding magnetization for different current excitations is obtained from Fig. 3.18 (b). Both the regions are strongly biased in the Z direction, therefore the permeability tensor is defined accordingly. As the magnetization of the substrate is increased, it is observed that the center frequency of the antenna decreases which in agreement with the patch antenna design. This tuning response is due to the increase in the effective permeability of the material with the increase in the bias strength. For a maximum magnetic field strength (H) of around 12 Oe (3300 G), the center frequency of the antenna reduces to 12.05 GHz. This results in a tuning range of almost 1 GHz. The gain and the

radiation performance of the antenna do not vary much with the applied bias which is desired for a tunable antenna. The frequency tuning simulations of the antenna will be further discussed along with the measurements in the next section.

3.2.5 Impedance and Radiation Pattern Measurements

A photograph of the fabricated antenna is shown in Fig. 3.19 (a). The antenna is completely embedded inside the substrate but its top turn can still be seen. Two DC wires are soldered on the contact pads to provide the magnetostatic biasing. The RF ground plane is embedded inside the substrate and is not externally visible. To make it accessible for the RF excitation, two ground pads are provided near the microstrip feed line and are connected to the ground plane using vias (illustrated in Fig. 3.16). In this way the antenna can be tested using an SMA connector or a ground signal ground (GSG) probe.

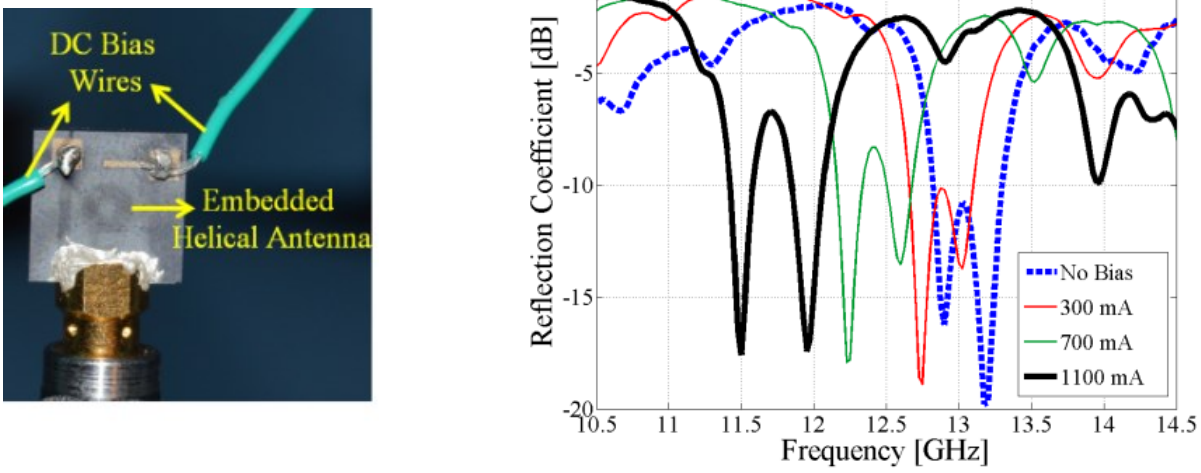

(a) (b)

Fig. 3.19. (a) Fabricated antenna with DC wires (b) Measured reflection coefficient (S_{11}) of the antenna

The impedance measurement of the helical antenna is performed using an SMA connector. In the absence of the DC current, the antenna operates at 13.1 GHz which is similar to the simulated center frequency. As the DC current is passed through the antenna, its resonant frequency decreases, which is expected given the frequency tuning simulations. The measured impedance performance of the antenna is shown in Fig. 3.19 (b). A maximum DC current value of 1100 mA is passed through the antenna which tunes it down to 11.8 GHz. A measured tuning range of 1300 MHz was obtained from the fabricated antenna design which is slightly more than the simulated value of 1050 MHz. Further tuning can be obtained if more current can be passed (until the saturation magnetization is achieved). However, for this design, the current is limited to 1100 mA (as stated in Section 3.2.2).

The pole that is closer to f_m = 11.2 GHz experiences more variation in the effective permeability than the pole that is away from f_m. This is true for any microwave component on a biased ferrite. The frequency that is closer to f_m is affected more by the applied bias than the one away from it, as demonstrated by the combination of Eq. 3.8 and Eq. 3.11. Due to the different tuning percentage of the two poles, a slight decrement in the bandwidth of the antenna is observed. The bandwidth, for now, is not a serious concern; therefore, it is not optimized any further. However, future designs can be optimized so that the bandwidth of the antenna remains unchanged. A good match was observed between the simulated and measured tuning range as shown in Fig. 3.20. The small difference between the simulated and measured frequency range may be due to the heating of the substrate, which may change its magnetization. Other than this small deviation, there is a strong correlation between the tuning ranges of the two results.

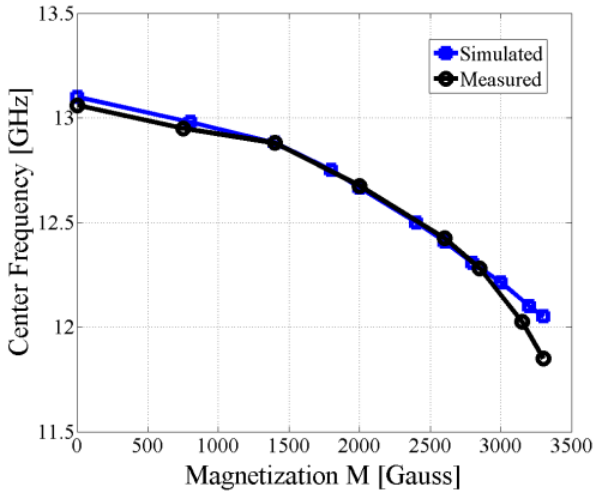

Fig. 3.20. Comparison between the simulated and measured tuning range

For the radiation pattern and gain characterization, the antenna is initially measured without applying any DC bias. A measured gain of -0.3 dBi is obtained at the center frequency of the antenna. This value is 2.4 dB lower than the simulated gain of 2.1 dBi. The investigation of this discrepancy revealed that the additional loss in the measurements is due to the surface roughness of the conductor. The two tunable antennas, the patch and the helical, were fabricated in two separate runs. As a result, the surface roughness issue was not observed in the patch antenna, but its value in the second run has severely altered the measured gain from the simulated value. The measured surface roughness of the conductor in the helical design is 1.5 μm for a total conductor thickness of 3.5 μm. To study its effect on the antenna performance, microwave simulation of the helical design is repeated with the measured conductor surface roughness. The new simulations reveal that the measured surface roughness reduces the antenna gain to -0.7 dBi as opposed to 2.1 dBi. This translates to a change of 26 % in the efficiency of the antenna (from 47% to 21 %). Therefore, improving the surface roughness of the conductor will improve the gain performance of the antenna.

As mentioned previously, ferrite ESL 40012 is a relatively new tape system and its fabrication process is not completely mature. Thus, a number of issues, such as weak adhesion between the conductor and the substrate, warpage, and cambering of the substrate have been experienced during the fabrication of the prototype. However, it is expected that with the maturity of the fabrication processes, these issues can be resolved and the performance that is achieved in the simulations can be reproduced in the measurements. The simulated and measured normalized radiation pattern of the antenna in two principle planes for the no bias case is shown in Fig. 3.21. Some ripples can be seen in the measured pattern for Phi = 0 plane at Theta =-90°. These ripples are due to the connector which is mounted at this position and has a considerable size compared to the antenna. The axial ratio was measured at approximately 20 dB which indicates the linear polarization of the antenna. A graph showing the gain versus frequency response for the unbiased case is plotted in Fig. 3.22. The three cases, simulated with and without conductors, surface roughness, and measured results, generally follow the same trend.

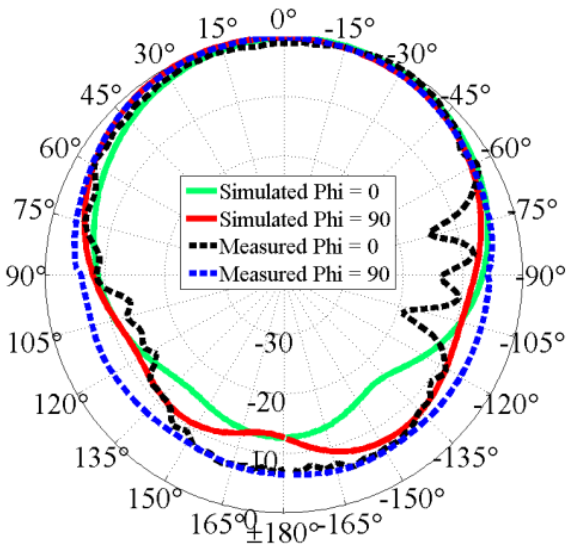

Fig. 3.21. Simulated and measured radiation pattern for no bias

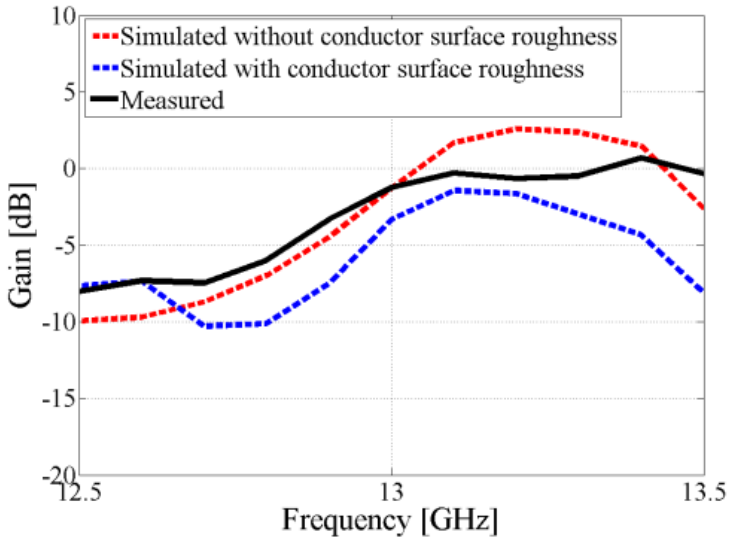

Fig. 3.22. Gain vs. frequency of the antenna for the unbiased state

Once the antenna had been measured for the unbiased condition, it was measured for its radiation performance in the biased state. The radiation pattern of the antenna does not change substantially from the unbiased state. The maximum gain value is tilted at 30°, in the Phi = 0 plane due to the connector. For the biased state of 1100 mA, the maximum gain of the antenna at 11.8 GHz changes by 0.4 dB of its gain value in the unbiased state. The simulated and measured radiation patterns of the antenna in the biased state of 1100 mA are shown in Fig. 3.23, which shows a good match between the two results. Ripples are also seen in the radiation pattern of the antenna in the biased state due to heat generation which have been smoothen out.

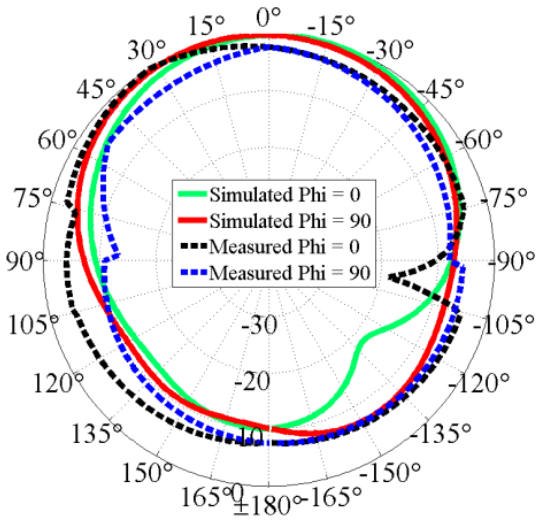

Fig. 3.23. Simulated and measured radiation pattern for 1100mA

3.3 Conclusion

This chapter covers the design and implementation of two different tunable antennas using multilayer ferrite LTCC substrate. As opposed to the conventional use of electromagnets with ferrites, embedded bias windings are used to magnetize the substrate. This concept enables the operation of the antenna in the partially magnetized state. Such a design realization reduces the required magnetostatic field strength by more than 90%. The absence of the electromagnets means that the major drawback of classical ferrite designs (i.e. bulkiness) has been overcome. These new designs are efficient, portable, light-weight and integrable in modern communication systems. Using the proposed concept, a frequency tuning of 10 % was achieved from the antenna designs with acceptable gain and radiation performance.

Chapter 4

Ferrite LTCC Based Half Mode SIW Phase Shifter for Phased Array Applications

After studying the theory and design of the tunable antennas in the multilayer ferrite LTCC technology, a half mode SIW phase shifter operated in the partially magnetized state is investigated in this chapter. As discussed in Chapter 2, SIW technology has recently been examined for the design of ferrite phase shifters. Due to their superior integrability compared to some traditional ferrite designs, SIW technology is selected for this work. The chapter also addresses the integration of the phase shifter design in a patch antenna array for beam steering applications.

4.1 Half Mode SIW Phase Shifter

Phase shifters are integral microwave components that are typically used in phased antenna arrays for beam scanning purposes. The purpose of a phase shifter is to provide the required phase change between the antenna elements of a phased array. This phase difference between the antenna elements results in the steering of the main beam of the array design. One way to control the phase of the microwave signal is by subjecting it to a magnetic bias on a ferrite substrate. Using this methodology various types of phase shifter designs have been implemented with the magnetic mediums [27]-[42]. These designs had the problems of large size and integrability and as a result, they did not gain popularity. To bring the ferrite phase shifters back to the main stream communication systems, ferrite LTCC technology is a viable solution. To prove this, an

attempt was made in [9] to demonstrate an antisymmetrically biased, waveguide-based phase shifter. Although the design had several drawbacks, such as the use of the saturated region to predict the phase shifter performance, unoptimized bias windings, poor placement of bias windings inside the waveguide, and the use of full mode operation which required two different bias windings, it did provide a new direction of research in the area of ferrite-based phase shifter designs. The problems observed in that work are addressed in the design presented here to show the advantages of the multilayer ferrite technology.

4.1.1 Mathematical Model and Design

The design concepts of full mode and half mode SIW phase shifters are shown in Fig. 4.1. Although only the half mode design is studied in this thesis, the full mode concept is also shown to provide a clear distinction between the two designs. The use of a perfect magnetic boundary at 'x = a' in the half mode waveguide renders it similar to a full mode waveguide in terms of the RF performance, which can be understood from the image theory [14]. This approach is expected to reduce the power consumption, as it requires a single bias winding for DC excitation as opposed to the full mode design that requires two different sets of bias windings for each half of the waveguide.

First, the theory of the phase shifter must be studied in order to understand its operation in the partially magnetized state. The material definition is similar to the definition that is used in for the theory of the patch antenna. The difference is the mode of operation and the wave propagation. The waveguide mode used for the phase shifter is transverse electric (TE) as opposed to the transverse magnetic (TM) mode used for the patch antenna. Using the dominant TE mode with propagation in the Y-direction and applying Ampere's law yields:

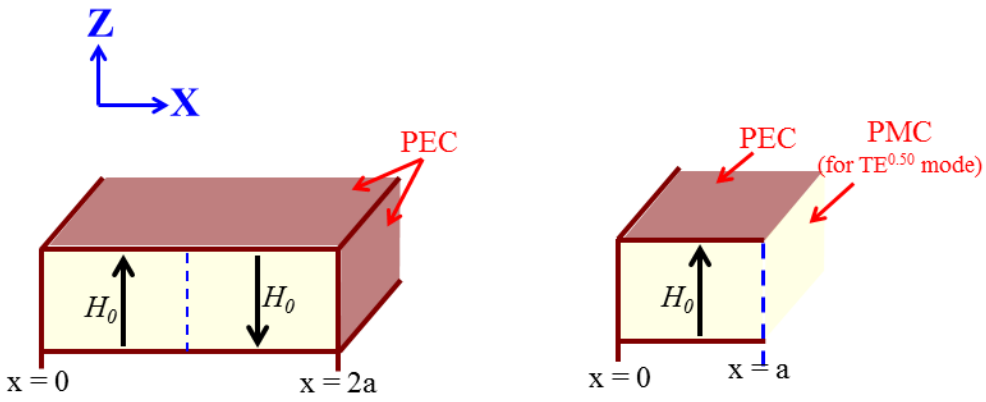

(a) (b)

Fig. 4.1 (a) Full mode asymmetrically biased SIW phase shifter (b) Half mode SIW phase shifter

$$-j\beta h_z + \frac{\partial h_y}{\partial z} = j\omega\varepsilon e_x \tag{4.1}$$

$$\frac{\partial h_z}{\partial x} - \frac{\partial h_x}{\partial z} = 0$$

$$\frac{\partial h_y}{\partial x} + j\beta h_x = j\omega\varepsilon e_z$$

which are independent of the permeability of the material and are unaffected by the bias direction. The magnetostatic bias for the phase shifter is applied in the Z direction, which results in the permeability tensor of Eq. 3.2. The Z direction of bias was considered as it gives the best phase shifter performance for the waveguide phase shifters [9], [36], [43]. Using the permeability tensor of Eq. 3.2 and applying Faraday's law results in:

$$-j\beta e_z = -j\omega\mu h_x - \omega\kappa h_y \tag{4.2}$$

$$\frac{\partial e_x}{\partial z} - \frac{\partial e_z}{\partial x} = \omega\kappa h_x - j\omega\mu h_y$$

$$j\beta e_x = -j\omega\mu_z h_z$$

The width of the phase shifter is the dominant dimension, which means that $TE_{0.50}$ is the dominant mode of propagation, i.e., $\frac{\partial}{\partial z} = 0$ and $e_x = h_z = 0$. It is important to clarify that $TE_{0.50}$ is used as the dominant mode instead of TE_{10} due to the half mode design. Taking this into account, Eq. 4.1 and Eq. 4.2 can be reduced to the following three equations:

$$\frac{\partial h_y}{\partial x} + j\beta h_x = j\omega\varepsilon e_z \tag{4.3a}$$

$$-j\beta e_z = -j\omega\mu h_x - \omega\kappa h_y \tag{4.3b}$$

$$\frac{\partial e_z}{\partial x} = -\omega\kappa h_x + j\omega\mu h_y \tag{4.3c}$$

From the above equations, the following wave equation is obtained:

$$\frac{\partial^2 e_z}{\partial x^2} + k_x{}^2 e_z = 0 \tag{4.4}$$

where k_x is the wave number and μ_e is the extraordinary permeability as expressed through the following equations:

$$k_x = \sqrt{\omega^2 \mu_e \varepsilon - \beta^2} \tag{4.5}$$

$$\mu_e = \frac{\mu^2 - \kappa^2}{\mu} \tag{4.6}$$

Applying the boundary condition $e_z = 0 \; at \; x = 0$, will result in the following solution to Eq. (4.4):

$$e_z = A \sin k_x x \; e^{-j\beta y} \tag{4.7}$$

Eq. 4.7 shows that the electric field inside the waveguide is sinusoidal as long as $\omega^2\mu_e\varepsilon > \beta^2$; otherwise the field propagating inside the waveguide will be hyperbolic. Now e_z can be used to determine the other field components, i.e. h_x and h_y:

$$h_x = -\frac{Ak_x}{\omega\mu_e\varepsilon}\left[\beta sink_x x + \frac{\kappa k_x}{\mu} cosk_x x\right] \tag{4.8}$$

$$h_y = \frac{Ak_x}{\omega\mu_e\varepsilon}\left[jk_x cosk_x x + j\frac{\kappa\beta}{\mu} sink_x x\right] \tag{4.9}$$

Applying the boundary condition $h_y = 0\ at\ x = a$ results in:

$$\kappa\beta + \mu\sqrt{\omega^2\mu_e\varepsilon - \beta^2}\ cot(a.\sqrt{\omega^2\mu_e\varepsilon - \beta^2}) = 0 \tag{4.10}$$

Eq. 4.10 shows that if the bias inside the waveguide is changed, it will change μ and κ, eventually changing μ_e. This will cause a change in β, which will be reflected in the overall phase at the output. The closed form equation obtained from the above derivation is a transcendental equation and therefore needs to be solved graphically to obtain a solution. For this purpose, zeros of LHS of the equation are plotted for different bias strengths versus β. This generates the roots of the equation for different states of magnetization. These roots of β are subtracted from the phase constant in the unbiased state, which is obtained by traditional waveguide theory of the TE mode of propagation. A plot showing the difference between the phase shifts in the unbiased ($\beta_{unbiased}$) and biased (β_{biased}) states is plotted against the applied magnetic field, shown in Fig. 4.2. This plot is generated considering the forward propagation only. From this plot, the phase shift at any given magnetization, $4\pi M$, can be predicted. Thus, the

proposed theory can be used to predict the achievable phase shift due to an applied bias with simple equations. To validate this theory, the design and measurements of the phase shifter are discussed in the following sections.

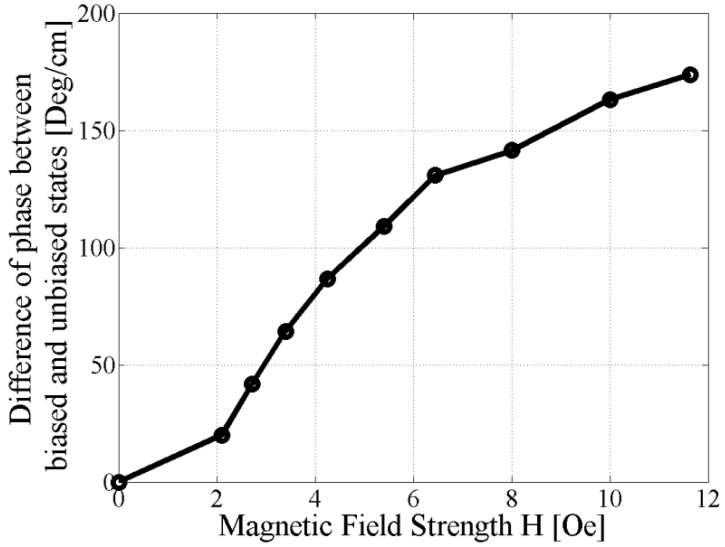

Fig. 4.2. Phase shift versus magnetic field *H* strength at 13 GHz

4.1.2 Phase Shifter and Bias Windings Simulations

The magnetostatic fields inside the waveguide are generated by the embedded bias windings. To design and optimize the bias windings CST EM Studio was used while the phase shifter was simulated in CST Microwave Studio. First, the bias windings will be simulated to record their performance which in turn will be used for the high frequency simulations of the phase shifter. In total, ten layers of ESL40012 are used for the realization of the phase shifter, as shown in Fig. 4.3. The top four layers were used for the phase shifter design, while the ground plane was implemented on the sixth layer. The remaining bottom five layers were used for the bias winding design. The phase shifter is fed using a microstrip to the rectangular waveguide flare (RWG), as

shown in Fig. 4.3. The width of the half mode SIW is 2.39 mm, which enables its operation at 13 GHz. The frequency of operation is kept the same as the patch antenna given the properties of the substrate. The length of the feed line with the RWG flare is 5 mm, which results in a total phase shifter length of 15 mm.

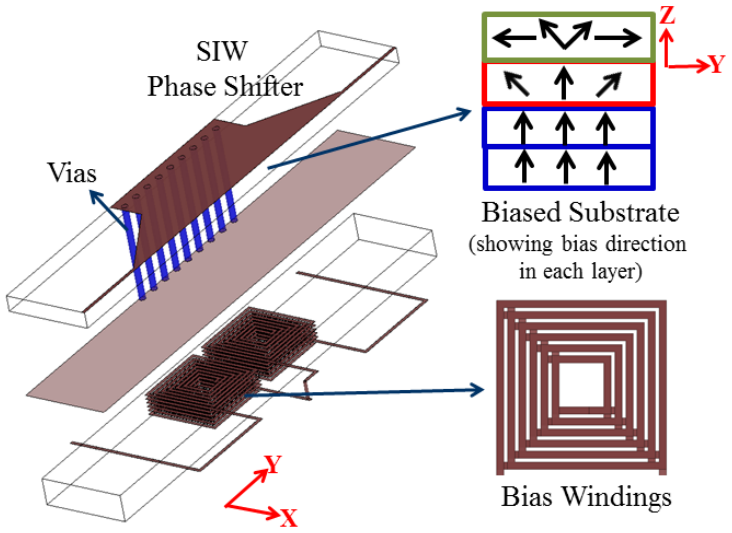

Fig. 4.3. The phase shifter design showing the magnetostatic fields in the biased substrate and the bias windings

4.1.2 (A) Magnetostatic Simulations

The magnetostatic bias required by the phase shifter is provided by two solenoid bias windings, realized in the bottom five layers of the substrate. The windings are used in series under the phase shifter to bias a region of 5 mm. Each solenoid winding is composed of six turns per layer resulting in a total of 36 turns. As with the two antenna designs, the bias windings for the phase shifter will also generate non-uniform *H* fields and need to be modeled accordingly using the magnetostatic simulator. The exercise conducted for these simulations is similar to the one that was used for the patch antenna design and therefore, it will not be repeated here.

In summary, each phase shifter layer is recorded for the magnetic field strength generated by the DC current in the windings. The bottom two layers of the waveguide are modeled as one while the top two layers are simulated individually. The magnetostatic fields produced in the bottom two layers of the phase shifter for different current excitations are shown in Fig. 4.4. The third and fourth layers above the ground plane have *H* values that are 50 % and 20 % of the value of the bottom two layers. In addition, the fields in the fourth layer are directed along the Y axis as shown in Fig. 4.3. As a result, in the microwave simulator, two sets of simulations are performed for the case of non-uniform simulations: first with all the layers biased in the Z direction and second where three layers are biased in the Z direction and the fourth layer is biased in the Y direction.

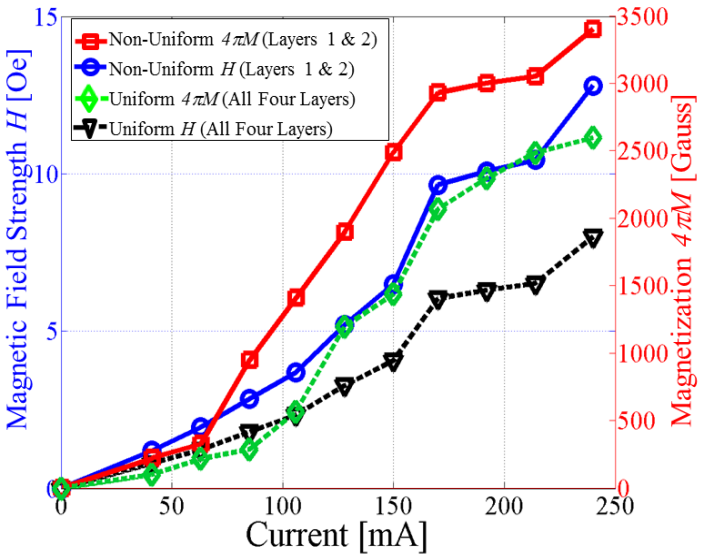

Fig. 4.4. Magnetic field strength, *H,* and magnetization, *4πM,* produced by the bias windings for DC current excitation showing both uniform (for theory) and non-uniform case (for simulations)

Although the modeling of the non-uniform fields above the ground plane is closer to the actual scenario, it cannot be used for the theoretical model. The theoretical model requires a

single value of H ($4\pi M$) for a single current excitation in the complete substrate. Therefore, to predict the phase shift using the theory, the magnetostatic fields are observed at the center of the phase shifter substrate and are shown versus current in Fig. 4.4 (labelled as Uniform H and $4\pi M$). The field values obtained from these simulations were also used to model uniform fields in the high frequency simulator and to compare the results with the theory.

4.1.2 (B) Microwave Simulations

The magnetostatic simulations discussed in the last section can be used to simulate the phase shifter in the high frequency simulator. Using the 'full permeability tensor' option of CST Microwave Studio, a ferrite substrate can be modeled in the partially magnetized state. Here, Eq. 2.6 to Eq. 2.8 are used to define the permeability tensor of the substrate which ensures the operation of the phase shifter in the partially magnetized state. The design is thus simulated in the biased state for both non-uniform and uniform bias shown in Fig. 4.4. These simulations show that for a bias current of 240 mA, phase shifts of 149 deg/cm and 155 deg/cm are achieved for the uniform and non-uniform bias respectively. Comparing these results with the theory (Fig. 4.2), a closer match is observed between the theoretical model and the uniform simulation case, which was expected. The theoretical model predicts a phase shift of 141.4 deg/cm. However there is not a significant difference between the non-uniform case and theory but to obtain a closer match between the theory and simulations two different cases were studied in the magnetostatic solver. The non-uniform modeling is more accurate and closer to the actual scenario, as explained in the next section where the measured results are discussed.

4.1.3 Measurements of the Half Mode SIW Phase Shifter

The fabricated phase shifter and an X-ray image of the fabricated embedded solenoid winding are shown in Fig. 4.5 (a) and 4.5 (b), respectively. The total volume of the phase shifter is 4 mm x 15 mm x 0.58 mm. The measured results of the fabricated phase shifter exhibit an impedance bandwidth of 600 MHz with an insertion loss of 1.5 dB, as shown in Fig. 4.6. The fundamental mode of the unbiased design is at 13.1 GHz, which compares well with the theory and simulations. The measurements show that the phase shift experienced by the forward propagating wave (S_{21}) decreases with the increasing current in the bias windings. A maximum bias current of 240 mA results in a phase shift of 83.2°. This value corresponds to a total measured phase shift of 166.4°/cm. A plot between the measured phase shift and the DC current excitation is shown in Fig. 4.7. The phase shift shown in Fig. 4.7 is the difference between the phase of the biased and unbiased transmission coefficients ($\angle S_{12\text{-}unbiased} - \angle S_{12\text{-}biased}$). Increasing the current beyond 240 mA can provide better phase shifts but at the same time can damage the bias windings. Excluding the transition loss of 1 dB from the insertion loss, the fabricated phase shifter demonstrates an FoM of almost 83.2°/dB.

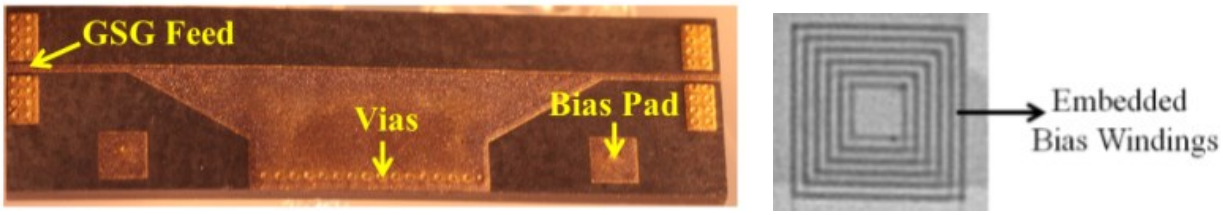

(a) (b)

Fig. 4.5. (a) The fabricated phase shifter; (b) an X ray image of embedded bias windings

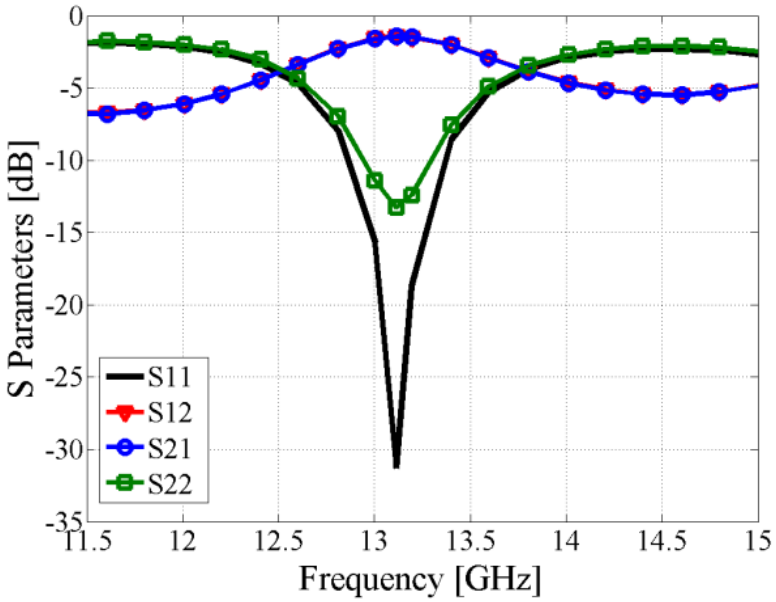

Fig. 4.6. Measured S parameters of the phase shifter

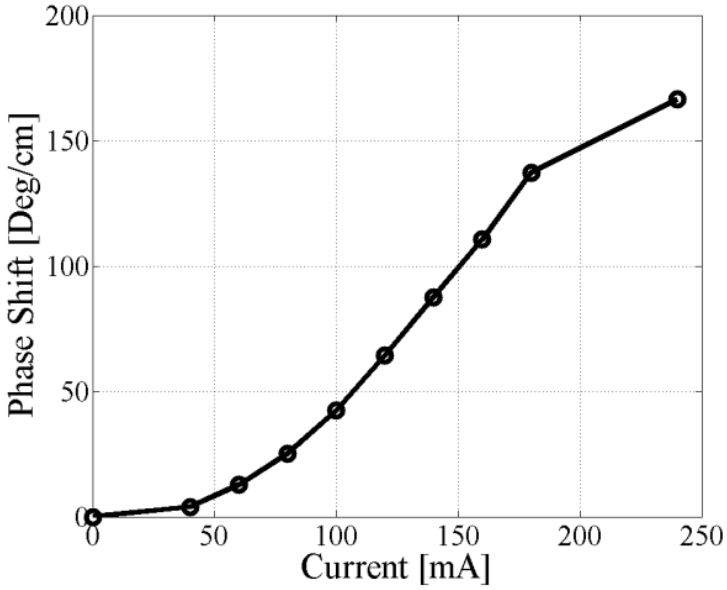

Fig. 4.7. Measured phase shift versus current

A strong agreement can be observed between the analytical model and the simulations with the uniform bias, as shown in Fig. 4.8 (a). The strategy devised for the microwave simulations

with the non-uniform bias results in a good match with the measured results, as demonstrated in Fig. 4.8 (b). The theory, simulations, and measured results generally follow the same trend over the frequency band of 13 GHz to 14 GHz. An average error of 10 % is observed between the theory and measurements. These results indicate that the error between theory and measurements is quite acceptable which provides a validation for the proposed theoretical model. The importance of the theoretical model can be understood from the fact that it can predict the phase shift of a ferrite-based design in a matter of minutes, which otherwise requires rigorous simulations (magnetostatic and microwave) for several hours on a high-end machine. Thus, the proposed theoretical model is useful for the quick evaluation of such a phase shifter design.

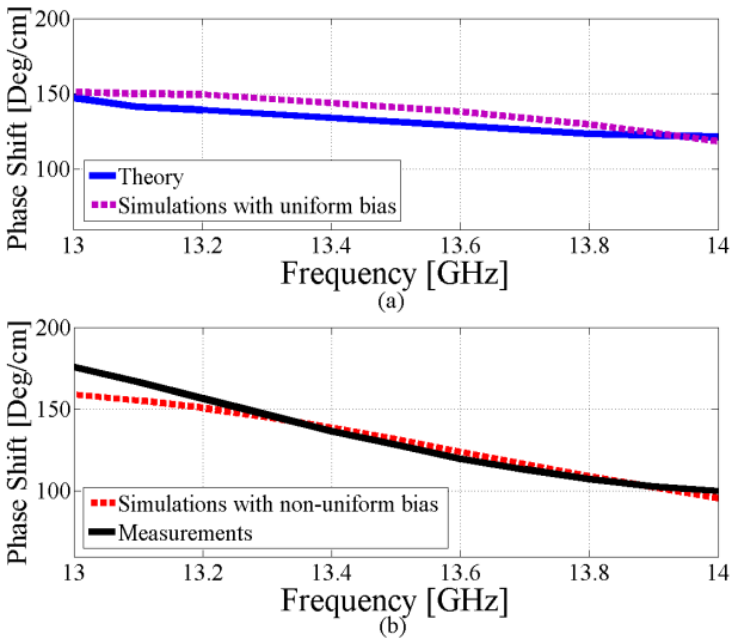

Fig. 4.8. (a) Theory versus simulations with uniform bias for $4\pi M$ = 2600 G (b) Simulations with non-uniform bias versus measurements for maximum bias of $4\pi M$ = 3450 G

A comparison between this work and the only previously reported ferrite LTCC phase shifter is presented in Table 4-1. Although [9] reports the differential phase shift as opposed to the uni-

directional phase shift reported in this work, the comparison provides an idea of the performance of the two designs.

Table 4-1: Comparison of the proposed design with the only other ferrite LTCC based design

Reference	Current [mA]	Phase Shift [deg]	FoM [deg/dB]	Size mm^3
[9]	500	52.8	14.66	29.4
This work	240	83.2	83.2	8.3

4.2 Phased Array Antenna

The half mode SIW phase shifter implemented in the ferrite LTCC technology is used in a patch antenna array to demonstrate beam steering. For this purpose, a two-element array with a phase shifter integrated between them is designed as shown in Fig. 4.9. The size of the phased array is 12 mm x 24 mm x 0.58 mm. Two 3.5 mm long patch antennas separated by a distance of 10 mm ($0.44\lambda_0$) are simulated on four layers of ESL 40012 substrate. The feed line of 50 Ω has a width of 150 µm, which is divided into two segments that each have a width of 80 µm. The ground plane of the phase shifter, used to isolate it from the windings, also acts as the ground plane of the antenna array. Initially, the antenna array is simulated in the unbiased state to optimize its response at 13 GHz, which is the operating frequency of the phase shifter. A gain of 4.5 dBi with an impedance bandwidth of 1.5% is achieved from the optimized design.

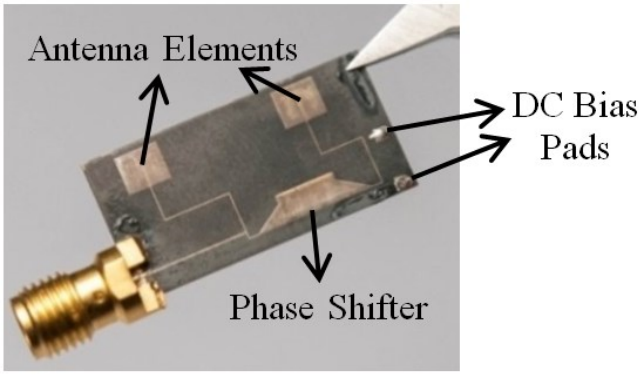

Fig. 4.9. Fabricated phased array antenna

4.2.1 Beam Steering Simulations

For the biased simulations, the phase shifter is magnetized using the magnetostatic simulations explained in Section 4.1.2 (A). Since the non-uniform bias in the phase shifter is close to the actual scenario, the phased array antenna is simulated with the non-uniformly biased phase shifter. These simulations show that for a maximum bias of 3450 G (240 mA), the phased array antenna demonstrates a beam steering of 40° at its center frequency. The maximum gain of the antenna is reduced by 0.8 dB, which is expected from a phased array design. The phase shifter is integrated into the H plane of the antenna array; hence, the steering is also observed in the H plane (XZ plane). The impedance performance of the antenna is not affected by the biasing of the phase shifter as illustrated in Fig. 4.10 where the reflection coefficient of the array in the unbiased and biased states is shown. The radiation pattern of the antenna in the H plane for the bias states of 0 mA, 120 mA (1700 G), and 240 mA (3450 G) are shown in Fig. 4.11. For the two biased states, beam steering values of 24° and 40 ° has been achieved respectively.

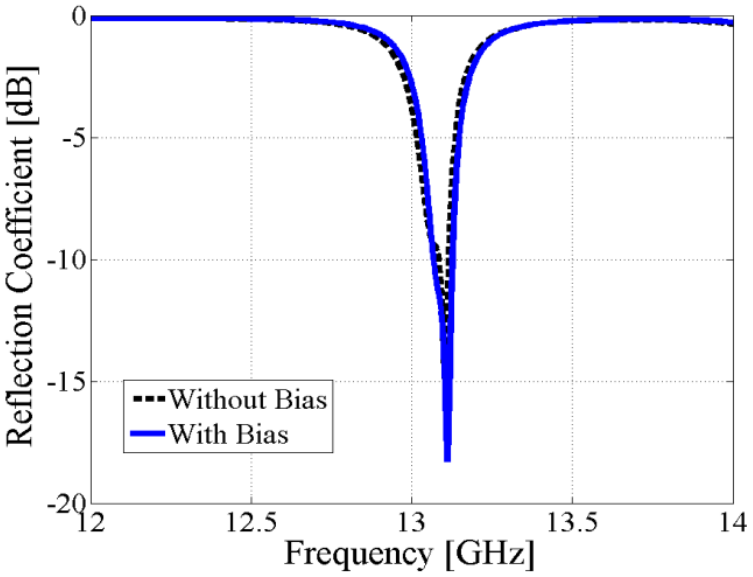

Fig. 4.10. Simulated reflection coefficient of the antenna array in the biased and unbiased states

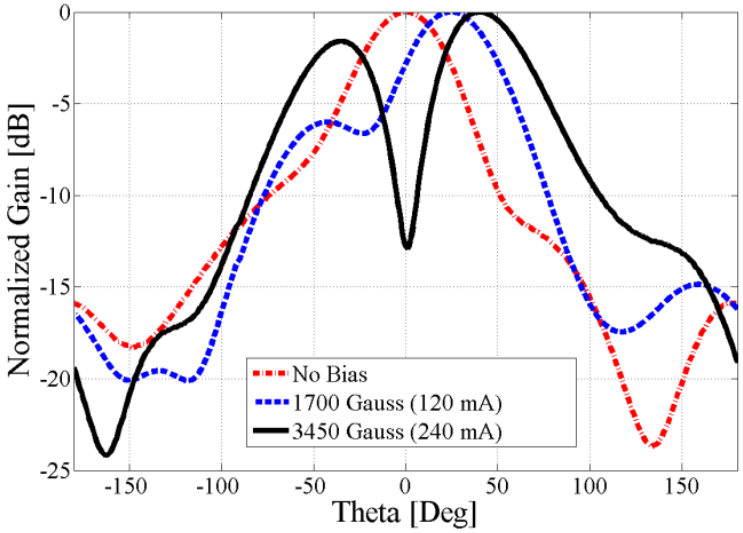

Fig. 4.11. Simulated radiation pattern of the array in H plane for bias states of 0 G, 1700 G and 3450 G

4.2.2 Measured Results

An SMA connector is mounted on the fabricated antenna array for impedance and radiation pattern measurements as shown in Fig. 4.9. Measurements performed in the unbiased state show

that the array is operating at a center frequency of 13.4 GHz instead of the designed frequency. The investigation revealed that the fabricated patch antennas have a length of 3.2 mm instead of 3.5 mm. This new length of the antenna along with the tolerance (~10%) of the dielectric constant is used in the microwave simulator to match the measured impedance performance. Fig. 4.12 shows that a good match has been achieved between the measured and post-measurement simulation results for the impedance of the antenna.

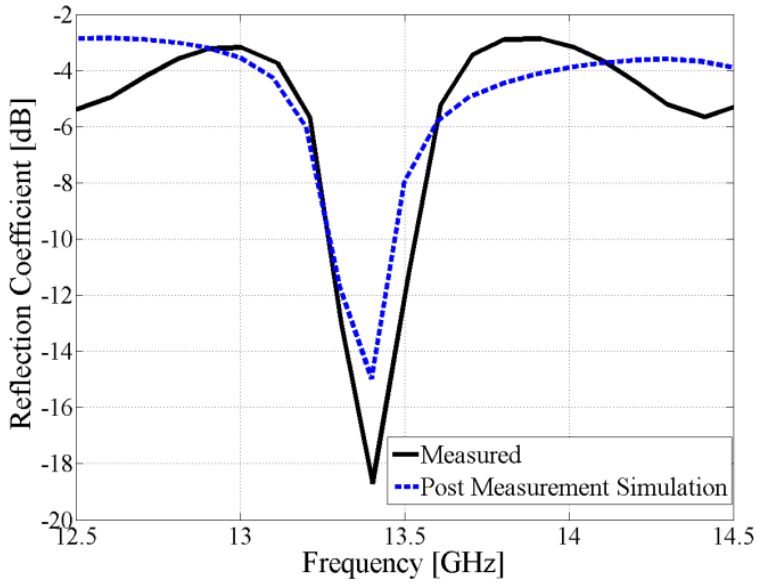

Fig. 4.12. Measured and post measurement simulated S11 of the phased array

The measured maximum gain of the antenna is 1 dBi instead of the simulated value of 4.5 dBi. This change in the measured gain is due to the surface roughness of the conductor that was used for the antenna fabrication. This problem of surface roughness is similar to the one observed in the case of the helical antenna. As explained in Chapter 3, ESL 40012 is a new experimental tape system that has a number of issues with its fabrication process. These issues can cause a deviation between the measured results of an actual prototype and the simulated results.

However, it is expected that with precaution in future fabrication runs, these issues can be resolved and the same performance as indicated by the simulations can be achieved. To verify this, the antenna array was simulated with the measured conductor roughness to determine its effect on the gain and radiation performance. These simulations showed that simulating the array with a surface roughness of 1.5 μm in a conductor thickness of 3.5 μm can reduce the gain to 0.94 dBi. The post measurement simulation value is close to the measurements and proves that the degradation in the gain is due to the surface roughness.

The array was then measured for its radiation performance in the biased state. The measured beam of the antenna array in the H plane for three different conditions (one unbiased and two biased states) is shown in Fig. 4.13. Beam steering of 16° and 30° was obtained for the current values of 120 mA and 200 mA, respectively. During the antenna array measurements in the biased states, heating of the windings is observed. Therefore, a maximum current of 200 mA was used, which reduces the beam scanning from 40° to 30°. Some ripples are observed in the radiation pattern of the antenna which have been smoothen out for clarity. In order to verify these results, post-measurement simulations were also conducted on the modified patch antenna array. The new simulations show that for the bias strengths of 120 mA (1700 G) and 200 mA (3100 G), the maximum gain of the antenna steers to 18° and 28°, respectively. The simulated and measured results of the antenna array are summarized in Table 4-2. A good match can be observed between the simulated and measured angles at which the antenna gain is maximal in the H plane.

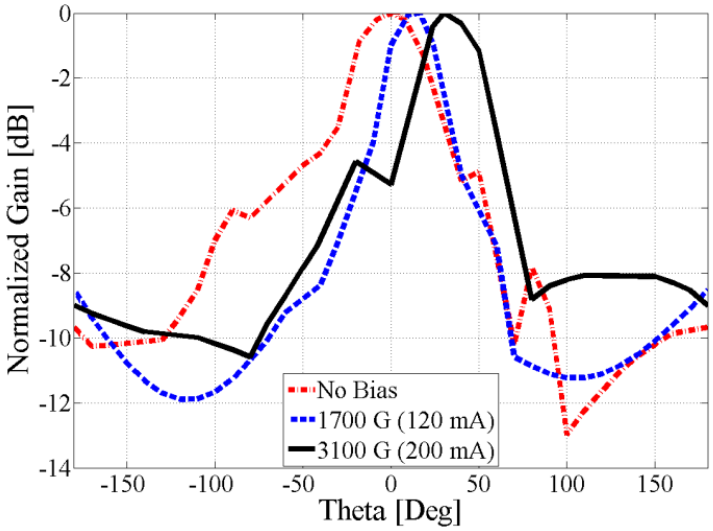

Fig. 4.13. Measured radiation pattern of the phased array for different bias conditions (0 mA, 120 mA and 200 mA)

Table 4-2: Post-measurement simulation and measured beam steering of the phased array at 13.4 GHz

Current [mA]	Magnetization $4\pi M$ [G]	Post Measurement Simulation Beam Steering	Measured Beam Steering
No bias	0	0°	0°
120 mA	1700	18°	16°
200 mA	3100	28°	30°

The use of a single phase shifter in a two element antenna array means that it can only scan the beam in one direction of the antenna plane. Using two phase shifters (i.e., one for each antenna element) can result in a beam steering of almost ±30°, providing twice the coverage angle.

4.3 Conclusion

A half-mode SIW ferrite LTCC based phase shifter, suitable for monolithic integration with the beam scanning antenna array elements, is presented in this chapter. The use of multilayer substrate allows the placement of embedded bias windings, which negate the use of external magnets, reducing the demagnetization effect. A simple theoretical model is presented in this work, which can predict the performance of the phase shifter. A good match has been obtained between the theoretical model, simulations, and measurements for the phase shifter design. As a proof of concept, the phase shifter design is integrated into an antenna array to demonstrate beam steering. A measured beam steering of 30° has been achieved in the H plane of the fabricated antenna array. The design has a small form factor of 12 mm x 24 mm x 0.58 mm, and a weight of 1g, making this concept highly suitable for applications requiring miniaturized, light-weight, reconfigurable components.

Chapter 5

Polarization Reconfigurable Patch Antenna Realized Through Low Cost Additive Manufacturing

In the last two chapters, we have covered the design of tunable and reconfigurable antennas and phase shifter using ferrite LTCC technology. This chapter covers the theory and design of a polarization reconfigurable circular patch antenna. Although the ferrite LTCC based modules worked well, the cost of fabrication is quite high and increases exponentially as the number of layers increase. In addition to the primary goal of investigating the polarization re-configurability of ferrite based antennas, we intend to explore low cost fabrication methods, such as additive manufacturing (printing) in this chapter. For this, a custom in-house printing process has been developed which involves a novel magnetic ink that has been used to print the magnetic substrate. The conductor layers have been realized using inkjet printing. Similar to the previous chapters, this chapter also presents a theoretical model which is compared with simulations and measurements.

5.1 Mathematical Model

For the mathematical model, a circular patch antenna with its geometry shown in Fig. 5.1 has been studied on a partially magnetized substrate. The radius of the antenna is labelled as ‘a’. Due to the structure of the antenna, cylindrical coordinate system has been used contrary to the

previous two chapters where rectangular coordinate system was used. The theoretical analysis is based on the cavity model of the patch antenna.

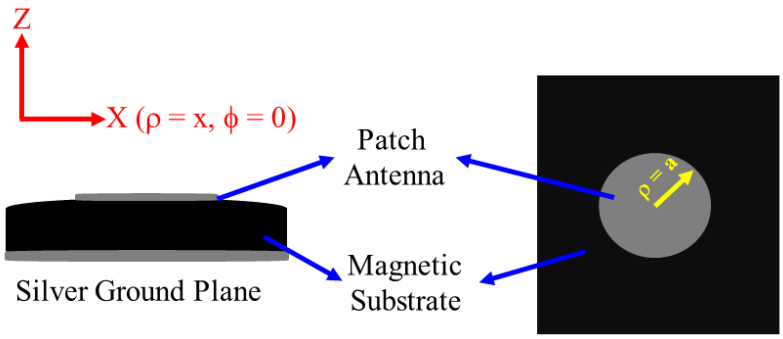

Fig. 5.1. Stack up and the geometry of a circular patch antenna on a magnetic substrate

The substrate is considered to be biased in the Z direction which results in the permeability tensor of Eq. 3.2 (previously described in chapter 3), where the elements of the tensor are defined by Eq. 2.6 to Eq. 2.8 (previously described in chapter 2). Using the permeability tensor of Eq. 3.2, Ampere's and Faraday's laws are applied on the partially magnetized patch antenna for TM^z mode.

Application of Ampere's Law for dominant TM_{11} results in:

$$\frac{1}{\rho}\frac{\partial(\rho h_\phi)}{\partial z} - \frac{1}{\rho}\frac{\partial(h_\rho)}{\partial z} = j\omega\varepsilon e_z \tag{5.1}$$

where $\frac{\partial}{\partial z} = 0$ which causes the two electric field components i.e. e_ρ and e_ϕ to be 0. Applying Faraday's Law using the permeability tensor for the Z direction of bias provides the following:

$$\frac{1}{\rho}\frac{\partial(e_z)}{\partial\phi} = j\omega\mu h_\rho - \omega\kappa h_\phi \tag{5.2}$$

$$\frac{1}{\rho}\frac{\partial(e_z)}{\partial\rho} = j\omega\mu h_\phi + \omega\kappa h_\rho$$

Simplifying Eq. 5.1 and Eq. 5.2 together gives rise to the following wave equation:

$$\nabla^2 e_z + k^2 e_z = 0 \tag{5.3}$$

where,

$$k = \omega\sqrt{\mu_e\,\varepsilon} \tag{5.4}$$

$$\mu_e = \frac{\mu^2 - \kappa^2}{\mu} \tag{5.5}$$

In all of the above equations μ and κ are elements of the permeability tensor in the partially magnetized state while k is the wave number and μ_e is the permeability for the extraordinary (E) mode. The solution of the above wave equation is given below.

$$e_z = \{AJ_1(k\rho) + B\,Y_1(k\rho)\}(Ce^{j\phi} + De^{-j\phi}) \tag{5.6}$$

where J_1 and Y_1 are Bessel and Hankel functions of the first kind and the first order. A, B, C and D are the coefficients for the functions used in the above solution. Since Y_1 (Hankel function) is infinity for $\rho = 0$ i.e. the origin (antenna is centered at origin), therefore Eq. 5.6 is reduced further by using $B = 0$. Now the electric field component e_z can be used to compute the magnetic field component. Here it is important to concentrate on h_ϕ, since the boundary condition at $\rho = a$,

enforces h_ϕ to go to zero. This is because the walls of the patch antenna substrate are assumed to be perfect magnetic conductors, similar to the patch antenna in chapter 3. Therefore h_ϕ will be,

$$h_\phi = \frac{j\kappa}{\omega\mu\mu_e}\{\frac{1}{\rho}jAJ_1(k\rho)(Ce^{j\phi} - De^{-j\phi}) - \left(-j\frac{\mu}{\kappa}\right)AJ_1{}'(k\rho)(Ce^{j\phi} + De^{-j\phi})\} \tag{5.7}$$

Enforcing the boundary condition on $h_\phi = 0$ at $\rho = a$, results in the following solution:

$$J_1{}'(ka) \pm \frac{\kappa}{a\mu}J_1(ka) = 0 \tag{5.8}$$

Eq. 5.8 is the closed form solution to find out the resonant frequency of the antenna using its roots and is consistent with the findings of Pozar in [18]. However, the contribution of this work is to incorporate the partial magnetization regime into the theoretical analysis. In order to compute the resonant frequency, the LHS of Eq. 5.8 is plotted for different magnetization strengths. The zeros of the plot are used to evaluate the resonant frequency of the antenna. However, it is exceedingly important to clarify that Eq 5.8 is a combination of two equations with different roots. The roots of these equations correspond to circular polarization. The root of one equation corresponds to one sense of polarization, while the other equation gives the frequency for the opposite sense of polarization. This means that when a ferrite or a magnetic medium is biased normally, it causes a circular patch antenna to resonate at two different resonant frequencies with two different senses of circular polarization. If the direction of bias is reversed, the two resonant frequencies exchange the sense of polarizations. This phenomenon happens because the coefficient m in TM_{mn} mode of propagation is an integer that can have both positive and negative values [18]. For this work, TM_{11} mode is considered which implies that the

values of m are ±1. The two opposite signed values correspond to two different sense of rotation or polarization i.e. left hand and right hand. In the unbiased state these two polarizations have the same frequency of operation and thus the antenna works as a linearly polarized antenna. However, a biased ferrite causes these modes to split and resonate at different frequencies due to different permeabilities experienced by the two modes (refer to Eq. 5.8). As a result, a linear polarized antenna starts behaving as a circular polarized antenna working at differently tuned frequencies.

5.2 Printed Magnetic Substrate Characterization

As mentioned at the beginning of this chapter, low cost additive manufacturing is explored for the realization of the polarization reconfigurable antenna. The additive manufacturing technique is gaining a large amount of interest due to its low cost, as well as its easy and fast prototyping capabilities [69]. The ability to deposit material only where it is required in a digital fashion, as compared to the subtractive technologies which depend on etching or removing the undesired material, results in no, or low, material waste. Moreover, it is a completely digital process, which means that no expensive masks are required for printing.

A custom magnetic ink based on Fe_2O_3 nanoparticles has been developed for this work. The magnetic substrate used for the antenna design is realized by printing with this magnetic ink (see the details in the fabrication section, i.e. section 5.4). It is important for the antenna design that the newly printed magnetic substrate be characterized for its material properties, both i.e. magnetostatic and microwave properties.

5.2.1 Magnetostatic Characterization

Vibrating Sample Magnetometer (VSM) is used for the hysteresis loop, B(H) curve, measurement of the magnetic ink. The substrate without any metallic layers on it is placed within the VSM. The VSM generates an alternating magnetic field for the measurement of the B(H) curve. For the printed substrate the measured results are displayed in Fig. 5.2. The ink reveals a saturation magnetization ($4\pi M_s$), coercive field (H_c) and remanent magnetization (B_m) of 1,560 G, 46 Oe and 350 G respectively. Among these, the key property is the saturation magnetization, which dictates the magnetization frequency of the material ($f_m = \gamma 4\pi M_s = 4.37$ GHz). For microwave designs, it is recommended that the center frequency should be higher than the magnetization frequency of the medium to avoid any low field losses [63]. The curve shown below will also be used to simulate the bias windings of the magnetostatic simulator. Another important characterization is related to the high frequency properties of the material. Therefore, once the material has been characterized for its magnetostatic properties, and its low loss region is known, a suitable resonant frequency can be selected for the resonator for the purpose of microwave characterization. The magnetic nature of the ink, as is shown in these measurements, appears suitable for tunable microwave components.

5.2.2 Microwave Characterization

A coplanar waveguide (CPW) based ring resonator is designed and fabricated on the top of the printed magnetic substrate, as shown in Fig. 5.3 (a). The resonator has been inkjet printed on the magnetic substrate using a custom silver ink. The details of the fabrication can be found in Section 5.4. The ring is designed with a radius of 6.75 mm, having a conductor width and gap of

2.5 mm and 200 µm respectively. Keeping in mind the typical dielectric constant of the ferrite materials ($\varepsilon_{eff.} \sim 14$), the dimensions of the ring are appropriate for a resonant frequency of 2 GHz.

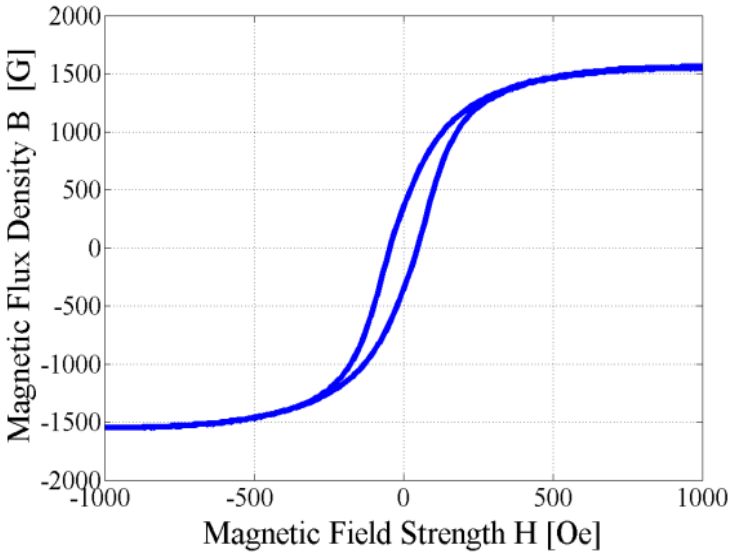

Fig. 5.2 Measured $B(H)$ curve of printed Fe_2O_3 (magnetic) ink

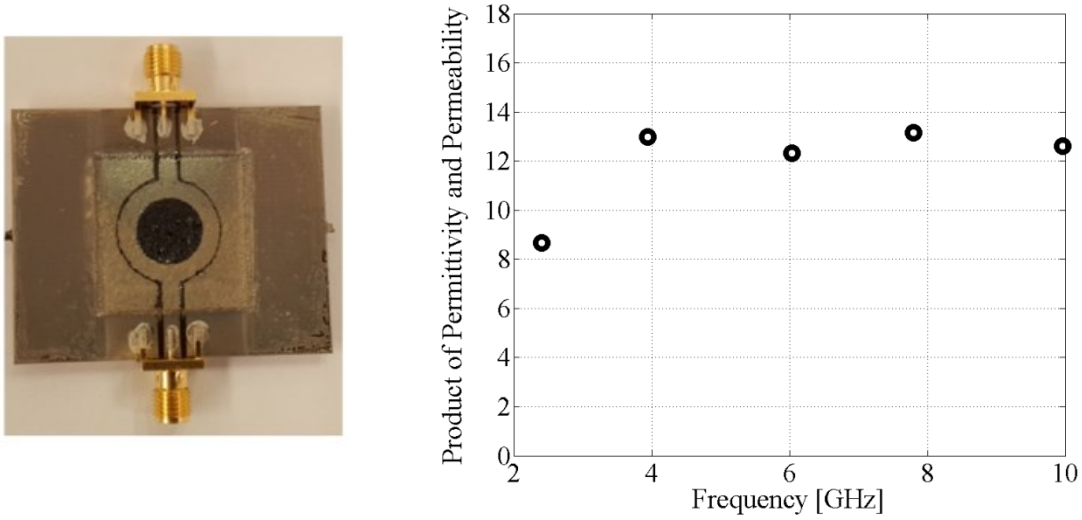

(a) (b)

Fig. 5.3 (a) Fabricated ring resonator (b) Product of permittivity and permeability of the magnetic ink

The resonator has been characterized for its S parameters from 1 GHz to 10 GHz. The fundamental resonance of the design is measured at 2.4 GHz. These results are used to extract the dielectric constant of the material. Since this is a magnetic material, the result obtained from the equation will give a product of the initial permeability and permittivity. This product is displayed in Fig. 5.3 (b). As can be seen, the value of this product varies with respect to the frequency, which is expected due to the varying initial permeability of the ferrite material [60]. The demagnetized permeability of a magnetic material is given by Eq. 2.8 [15] and can be used here to isolate the two quantities. Using this equation, the permittivity and permeability of the medium at different frequencies are listed in Table 5-1. Frequencies above f_m are considered in the table since these are the frequencies that can be used for the antenna design. For the initial design of any microwave device this product can directly be used in the equation of the resonant frequency. In addition to the dielectric constant, the loss tangent ($\tan\delta$) of the material is also calculated from the measured results. The conductor losses are calculated using the transmission line calculator of Agilent ADS. The measured conductivity of the metal is 5×10^6 S/m, which is used to evaluate the conductor loss for different frequencies. Once the conductor loss is known, the dielectric loss of the material can be evaluated. The loss tangent of the substrate at frequencies below f_m is relatively higher. For example, at 2.4 GHz and 4 GHz, the loss tangent values are 0.13 and 0.015 respectively. This is due to the low field losses of the magnetic material in the absence of the magnetic bias [63]. However, the loss tangent value at frequencies above f_m is in the acceptable range. For example at 6 GHz, its value is 0.007. Therefore, 6 GHz is used as the design frequency for the patch antenna design.

Table 5-1: Permittivity and permeability of the magnetic ink at different frequencies

Frequency [GHz]	Demagnetized Permeability (μ'_o)	Permittivity (ε_{eff})
6.04	0.796	15.5
7.9	0.86	15.29
9.9	0.9	14.2

5.3 Design and Simulations

The substrate properties obtained in the characterization section above can now be used for the design and simulations of the antenna as well as the bias windings. Similar to previous chapters, the simulations will be comprised of two parts, magnetostatic and microwave simulations. The magnetostatic simulations are carried out in CST EM Studio, while the CST Microwave studio is used for the high frequency simulations. The magnetostatic simulations for the circular patch antenna design are carried out in two steps. In the first step, the substrate is modeled using the embedded bias winding (consistent with the methods in chapter 3 and 4), while in the next step, an external electromagnet is used to bias the substrate. Since the magnetostatic simulations with the embedded windings have the exact same steps as in the previous chapters and have been discussed in detail before, it is unnecessary to repeat them here. The external electromagnet is used due to a number of complications with the inkjet printed windings (the details of which will be discussed in the fabrication section, i.e. section 5.4). Simulations using an external magnet will be covered in the following sub-section.

5.3.1 Magnetostatic Simulations Using Electromagnet

The strategy implemented for the simulation of an electromagnet in the magnetostatic simulator is displayed in Fig. 5.4. The set up shows that an electromagnet with a variable applied magnetic flux density (B) is defined inside the simulator. For any actual electromagnet, the applied B is known and defined by the user. Therefore, in the simulator, the B from the electromagnet can be defined and consequently, the magnetization ($4\pi M$) generated inside the substrate can be recorded. To accomplish this, the strength of the field is observed at the center of the substrate. Three lines, one along each axis (i.e. X, Y and Z), are used on which the fields are observed. The dimensions of the three lines are equal to the size of the substrate, which is 24 mm x 24 mm x 1.5 mm respectively. The field strengths obtained from the three lines are averaged in order to generate a single value for the internal magnetization ($4\pi M$) inside the substrate versus the applied magnetic flux density (B). The results obtained from this simulation are shown in Fig. 5.5. As the applied magnetic field is increased, the magnetization inside the substrate increases as expected. For a magnetic flux density of 2,800 G, the internal magnetization is recorded at roughly 1,400 G, which means that the material is almost saturated. To maintain the operation in the partially magnetized state, this is the highest value of the applied field used in the simulations.

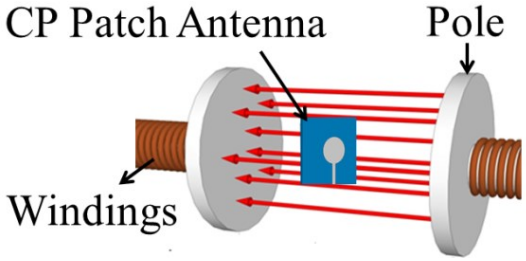

Fig. 5.4. Biasing the antenna substrate using electromagnet in CST EM Studio

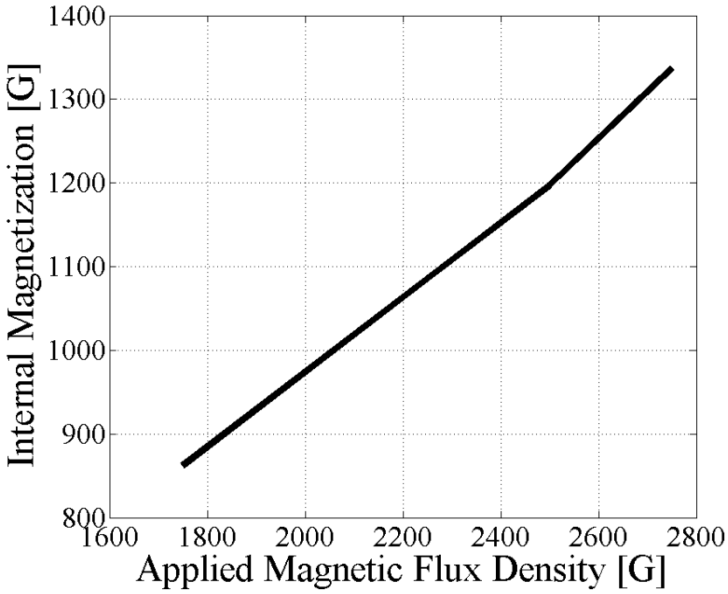

Fig. 5.5. Magnetization inside the substrate vs applied magnetized field from the electromagnet

The magnetostatic modeling of the electromagnet and the windings can now be used to perform the microwave simulations of the antenna in the biased conditions.

5.3.2 Microwave Simulations

Initially, the circular patch antenna is designed on the magnetic substrate without any bias. The antenna is optimized to operate at 6 GHz using the dielectric and magnetic properties of the material. These properties include the dielectric constant, the demagnetized permeability and the loss tangent obtained from section 5.2. The optimized antenna has a radius of 4.1 mm on a substrate thickness of 1.5 mm. The antenna is fed at the edge with a microstrip feed therefore it needs to be matched using an open circuit stub. The open circuit stub has a length of 3.5 mm and is 1.6 mm away from the edge of the antenna. The inset feeding technique cannot be used here because the circular polarization of the antenna will be disturbed due to the discontinuity in the

patch structure. Therefore, instead of using inset feed, a conventional microstrip stub matching is employed in this design. The simulated impedance and radiation performance of the antenna are presented in Fig. 5.6. A maximum gain of 3.34 dBi is obtained from the antenna at 6 GHz. Once the antenna has been optimized for its performance in the unbiased state, it can be simulated for the partially magnetized state.

Initially the antenna is simulated with a uniform bias changing the magnetization of the antenna from 0 to its saturation magnetization of 1,540 G. The simulation results reveal the frequency splitting of the antenna. As expected in the biased state, the antenna resonates at two different frequencies with opposite senses of polarization. This means that a linearly polarized antenna will start behaving as a circularly polarized antenna. These results are consistent with the proposed theory. In simulations, one polarization tunes from 6 GHz to 6.4 GHz, while the other polarization tunes from 6 GHz to 5 GHz. If the direction of the applied bias is reversed, then the senses of polarization change for the two tuning frequencies, which means that if the 6 GHz to 6.4 GHz band was showing LHCP for one direction of bias, then it will show RHCP for the opposite bias direction and vice versa. This is also consistent with the proposed theoretical model. Similar trends of frequency tuning and polarization reconfigurability are observed when the antenna is simulated using the magnetostatic simulations of the bias windings, which models the non-uniform bias inside the magnetic medium. The actual comparison between the theory and the simulation will be discussed in detail with the measurements to avoid any repetition of the current discussion.

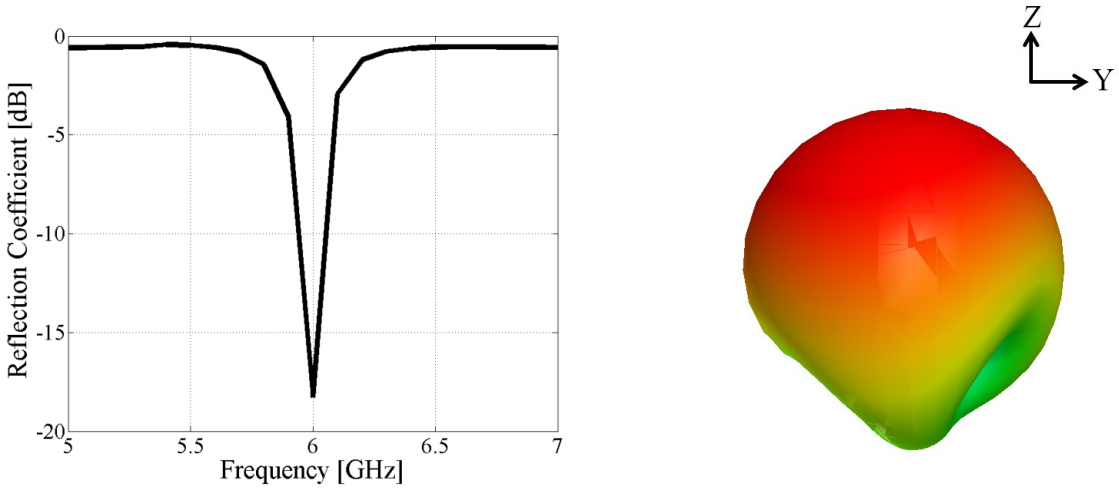

(a) (b)

Fig. 5.6 Simulated results of circular patch antenna (a) Reflection coefficient (b) 3D radiation pattern

5.4 Antenna Fabrication and Measurements

In this work, a fully printed process, utilizing a custom ferrite (Fe_2O_3) based magnetic ink for functional substrate printing and a custom silver-organo-complex (SOC) ink for metal traces printing, is presented which was reported in [70]. The magnetic ink is prepared by mixing iron oxide (Fe_2O_3) nanoparticles in SU-8 epoxy resin. Fe_2O_3 nanoparticles with an average particle size of 20 nm were synthesized using a simple solution process. The as-synthesized iron oxide nanoparticles are chemically functionalized with oleic acid so as to be compatible with UV-curable epoxy resist. The next step is to mix the functionalized iron oxide nanoparticles with the SU8 2000 (Microchem) epoxy resist in 50:50 weight % ratio for formulating ink paste. Once the ink paste is ready, it can be printed using a manual screen printing technique, such as squeegee. The steps for the fabrication process are displayed in Fig. 5.7. Initially, a slot is created in the base material using LPKF Protomat S103 (Fig. 5.7 (a)) to facilitate the printing of the magnetic ink for a precise substrate thickness of 1.5 mm. FR-4 is used as a frame with a sacrificial paper in

the back to provide support for the magnetic ink. This is done because initially the ink is in liquid form and needs a support substrate until it is sintered. Once the ink solidifies, due to the sintering process, it can be separated from the holder, which in this case is an FR-4. Any other substrate material may also be used as the support substrate for this fabrication process. Once the ink is printed, it is pre-baked and cured using an ultraviolet (UV) source for 30 min, as shown in Fig. 5.7 (b). Once cured, the magnetic substrate is cut through and separated from FR4 as shown in Fig. 5.7 (c). The paper in the back of the magnetic substrate is removed by immersing it in warm water for 10 min. A 10 μm smoothening layer of '3D vero black plus' material is then inkjet printed and photo-cured on top of the magnetic substrate. In the next step, the SOC ink is deposited on top and bottom of the substrate using inkjet printing. A total of 8 layers of SOC ink are printed and cured using infrared (IR) heating for 5 min. Both sides of the magnetic substrate are printed with the smoothening layer and the SOC ink as shown in Fig. 5.7 (d). After the printing of the conductor layer for ground plane, an isolation layer is realized through printing of Vero ink on this ground plane, shown in Fig. 5.7 (e) (in the figure it is shown upside down). The purpose of this layer is to provide insulation between the ground plane and the bias windings. The final step of fabrication is the printing of the windings as illustrated in Fig. 5.7 (f).

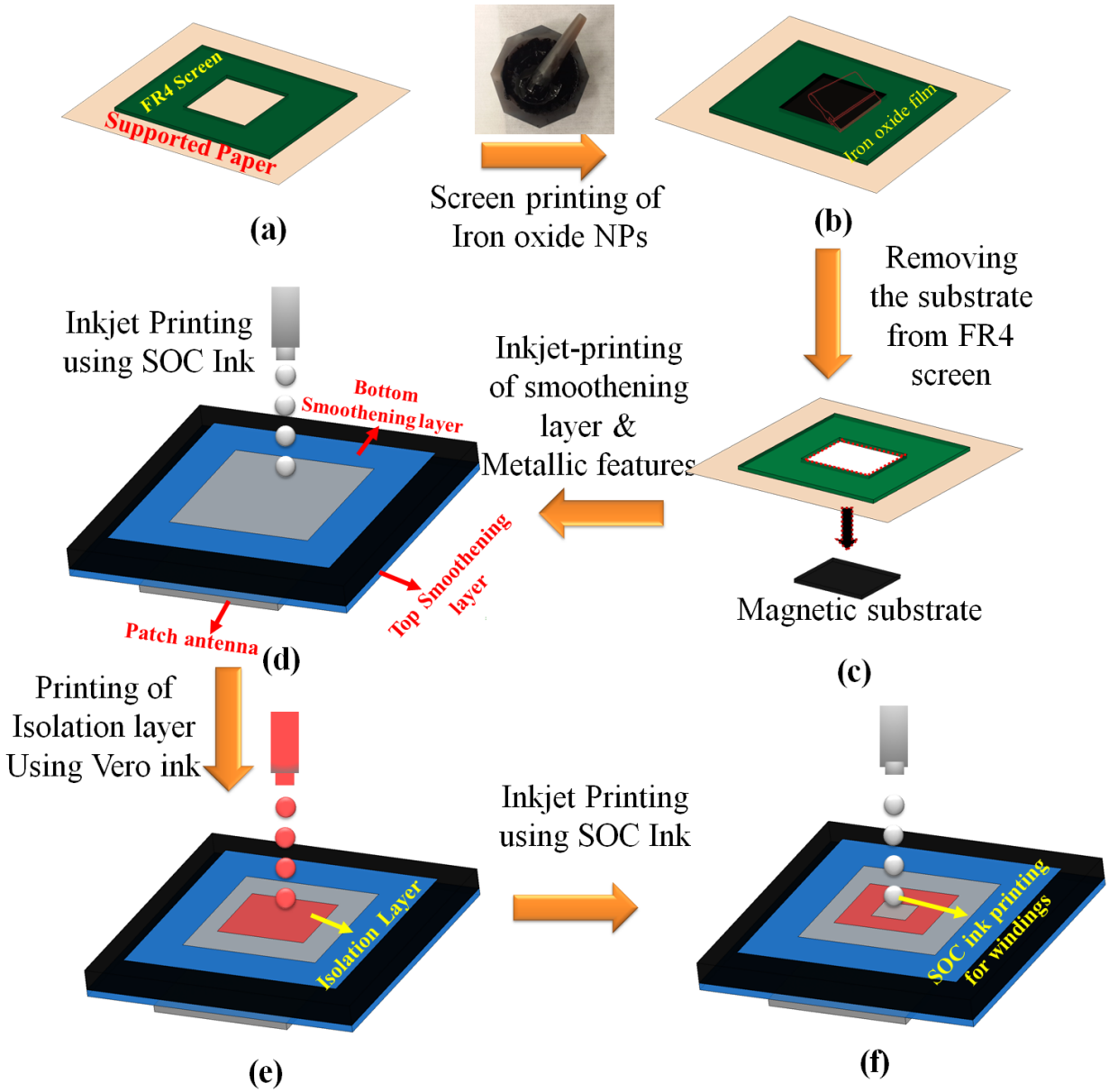

Fig. 5.7. Fabrication process for the magnetic ink substrate (a) FR4 screen with supported paper at the back (b) Screen printing (squeegee) of iron oxide ink (c) After curing cutting the solid magnetic substrate from the FR4 screen (d) Printing of smoothening layer and SOC (metallic) layer on both sides of the substrate (e) Printing of Vero ink which serves as isolation layer (f) Printing of SOC ink on the isolation layer for bias windings implementation

The printing of the antenna and the ground plane did not pose any significant challenges, however major issues were observed in the printing of the isolation layer and the bias windings. After printing of the isolation layer and curing it, big trenches and holes were observed on the surface of the isolation layer, as shown in Fig. 5.8 (a). Initial investigation suggests that these trenches and holes were formed due to the evaporation of the trapped solvent from the Vero ink during the curing process. Due to these holes the conductor layer (for bias windings shown in Fig. 5.8 b) printed on top of the isolation layer, got short circuited with the ground plane which is right underneath the rough isolation layer. A possibility to resolve this issue is to try different inks for the isolation layer instead of the Vero ink, such as polymer based ink SU-8. Another serious issue which came across during the printing process was large surface roughness of the magnetic substrate. The Profilometer measurement showed that the magnetic substrate has an RMS surface roughness of 4.5 μm. This high value of roughness not only complicated the remaining steps of fabrication but also affected the antenna performance. Nonetheless, this is a completely new process with a new magnetic ink and this is the first demonstration of a fully printed magnetically controlled antenna and it is bound to have some imperfections. With repeated experiments, it is expected that the process will improve and at maturity will be as good a platform for tunable and reconfigurable microwave components as some of the other processes, such as Ferrite LTCC. Since optimization of the printing process is not the major focus of this work, no more time was invested on this aspect of the work. With the initial experiments, we prepared a working prototype which could be tested but without the embedded bias windings. And since the major goal of demonstrating polarization diversity with magnetic control can be shown with this prototype, we moved on to characterization of this prototype with external electromagnets. Having said that, the final goal of this work will still be to integrate the

embedded windings within this fully printed process, however in respect of timeline of this thesis, it will be considered as future work to be taken in the group.

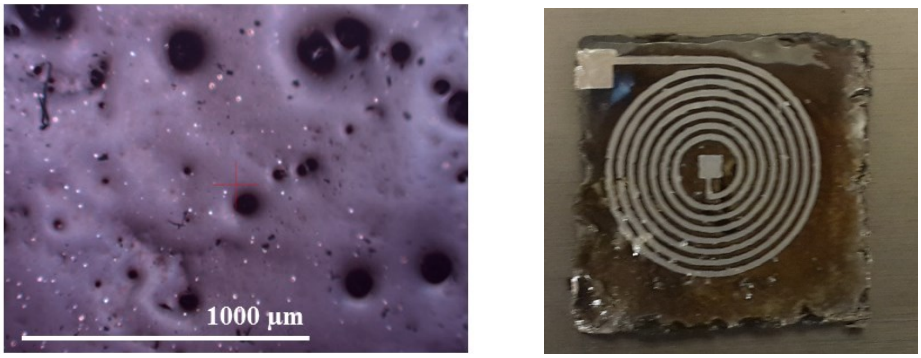

(a) (b)

Fig. 5.8. (a) Holes on the surface of the isolation layer (b) Printed windings

5.4.1 Impedance Measurements

The photograph of the fabricated antenna is included in the inset of Fig. 5.9. An SMA connector is mounted on the antenna through a conductive silver epoxy (CW-2460 of Chemtronics) for its impedance and radiation pattern characterization. As expected, the antenna works at 6 GHz in the unbiased state, as shown in Fig. 5.9. Some loss can be seen in the impedance plot of the antenna as the curve does not go close to 0 dB of return loss. It is also expected because of the large surface roughness of the magnetic substrate. The conductor layer printed on the fabricated substrate is only 2 µm which means that the conductor layer will also be rough due to the surface roughness of the underneath substrate.

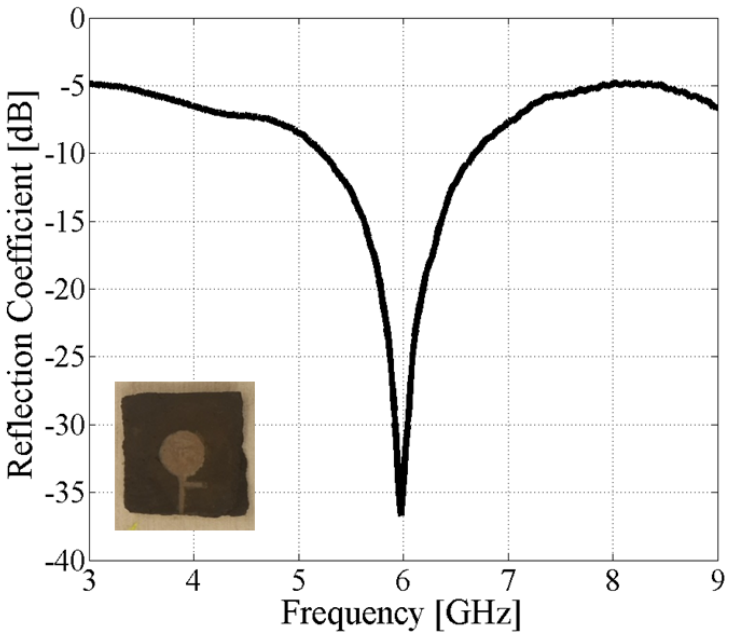

Fig. 5.9. Measured reflection coefficient of the antenna with an image of fabricated module

For characterization under biased condition, the antenna is placed between the poles of the electromagnet whose magnetic field is varied to test the antenna under varying bias conditions. The antenna is placed in a way that the applied direction of bias is normal to the surface of the antenna. As has been seen in theory and simulations, biasing the antenna causes a split in the resonance frequency of the antenna. As the strength of the magnetic bias is increased the two frequencies tune away from each other. A plot showing the comparison between the three results i.e. theory, simulations and measurements is shown in Fig. 5.10. A good agreement can be observed between these results which validates the theoretical analysis. From the simulations, it is known that the two frequencies will have circular polarization with opposite sense of rotation. One of the polarizations is referred to as P1 while the other one is named as P2. Each polarization (P1 or P2) can either be LHCP or RHCP depending on the direction of the bias. For

+Z direction of bias P1 is observed to be LHCP while P2 is found to be RHCP. If the direction of bias is reversed to –Z direction then the two polarizations will interchange.

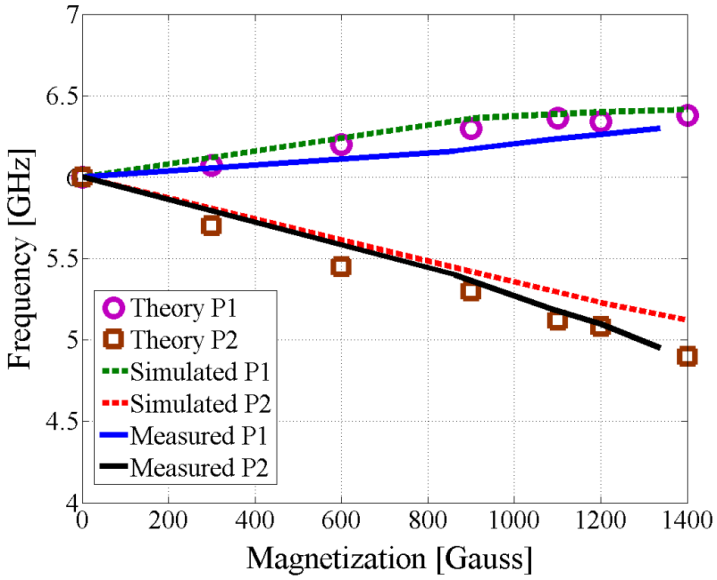

Fig. 5.10. Frequency splitting of the circular patch antenna due to the applied magnetostatic bias

Although the phenomenon of frequency splitting has been observed in the impedance measurements, the polarization is yet to be determined for the fabricated antenna. This means that the antenna needs to be characterized for its gain and radiation performance in the biased conditions. Unless the axial ratio of the antenna has been measured, it cannot be said with surety whether the antenna is actually circularly polarized.

5.4.2 Radiation Pattern Measurements

The radiation pattern of the antenna is initially measured in the unbiased state at 6 GHz. A good agreement can be seen between the simulated and measured radiation performance from

Fig. 5.11. A slight tilt is observed in the measured radiation pattern of the antenna in Phi = 0° plane. This is the plane where the connector of the antenna is mounted due to which the maximum gain of the antenna is at θ = 15°, instead of θ = 0°. This is consistent with the measurements of the patch antenna and the helical antenna reported in chapter 3. Also, some ripples can be seen in the Phi = 0° plane, which can be a combine affect due to the large surface roughness (4.5 μm for a conductor thickness of 2 μm) and the presence of the connector in this plane. Having said that, most of the large ripples are concentrated in the region beyond ±70° where the radiation of patch is almost 10 dB less as compared to the maximum gain.

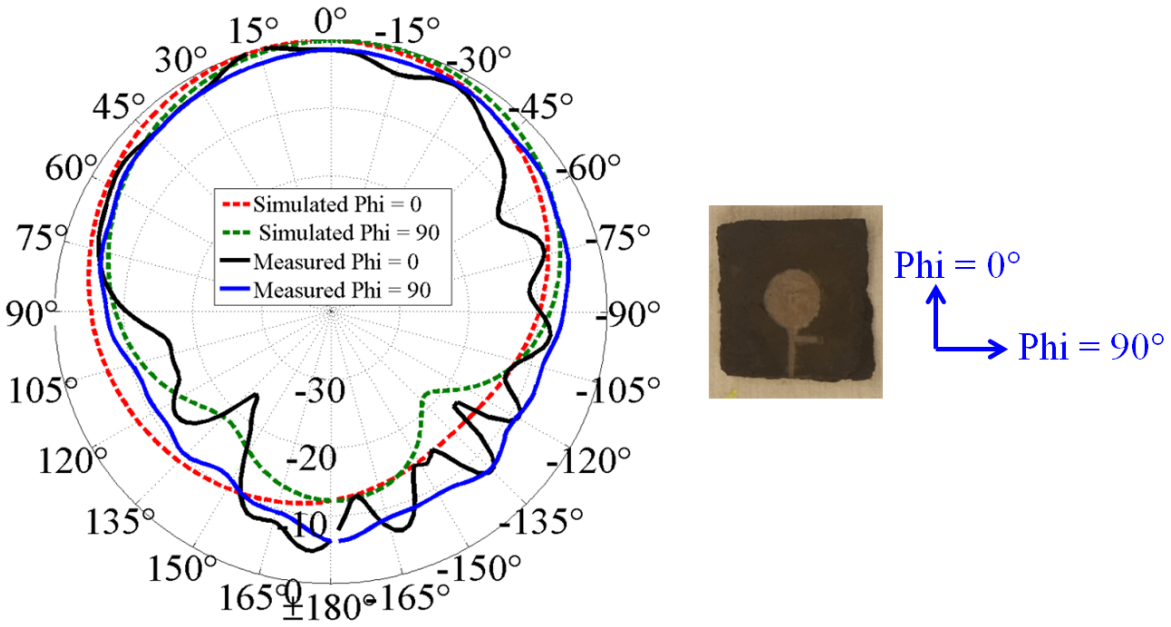

Figure 5.11. Simulated and measured radiation patterns in the unbiased state with the antenna coordinate system

Ideally the radiation characteristics of the antenna should be measured in an anechoic chamber with the required magnetic source. However, it is not possible to accomplish this task

due to the use of electromagnet as the source for generating the required magnetic field strength. Therefore, people have been using electromagnets to bias the substrate and observe the consequent radiation characteristics of the antenna. Using electromagnet inside a chamber is not practically feasible. The size of an electromagnet which can provide the required field strength is usually in the order of 60 cm x 50 cm x 40 cm as shown in Fig. 5.12 (a). This kind of structure cannot be used in an anechoic chamber. Instead of an electromagnet, a permanent bar magnet can be used in the chamber, as shown in Fig. 5.12 (b). The size of this magnet (50 mm x 1 mm x 1 mm) is suitable for radiation pattern measurements inside the chamber but such a magnet cannot generate stronger magnetic fields to overcome the demagnetization effect. Therefore, to further verify the proposed theory and simulations a measurement set up was devised. A non-magnetic receiving antenna was used on one port of the vector network analyzer (VNA) while the transmitting port was connected to the magnetic antenna under test. The transmission coefficient S_{21} was then measured for horizontal and vertical polarizations of the receive antenna by rotating it 90° for each measurement, as shown in Fig. 5.13. This was done for different values of the applied magnetic field. The ratio of the two perpendicular amplitude components gives the axial ratio at a particular frequency. Using the frequencies from Fig. 5.10, the axial ratio was measured and is shown in Fig. 5.14. The general trend of this graph is that the axial ratio becomes lower with the applied magnetic field. This trend is also consistent with the simulations. The reason for the trend is the magnetization state of the medium. As the ferrite medium approaches saturation, more dipole moments align with the applied bias fields. At saturation, all the dipoles are aligned with the magnetic field providing a fixed axis for the RF magnetic field to rotate hence providing better circular polarization. Mathematically this happens because near saturation the two orthogonal components of the fields have almost equal

magnitude due to which better circular polarization is obtained near saturation as is explained in [18], [53]. Furthermore, slight variation in the AR value can be due to the environment in which the antenna is measured. Since the antenna is placed in between the poles of the electromagnets it is bound to have some reflections. Nonetheless, the measured results still validate the circular polarization of the antenna in the biased state for two different frequencies.

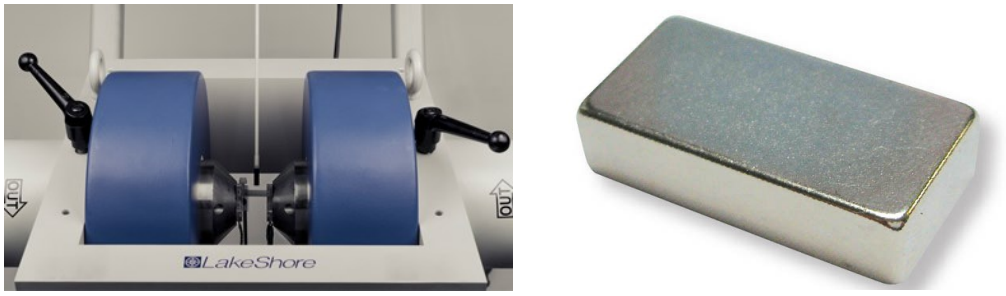

(a) (b)

Fig. 5.12 (a) Electromagnet and (b) Permanent magnet used for biasing of antenna [71], [72]

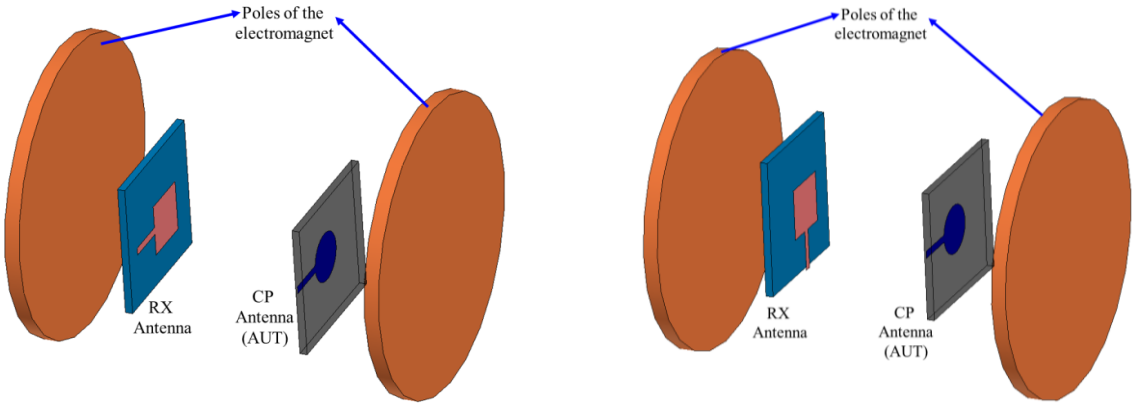

(a) (b)

Fig. 5.13 Test set up for AR measurement of the CP antenna (a) RX antenna with horizontal polarization (b) RX antenna with vertical polarization

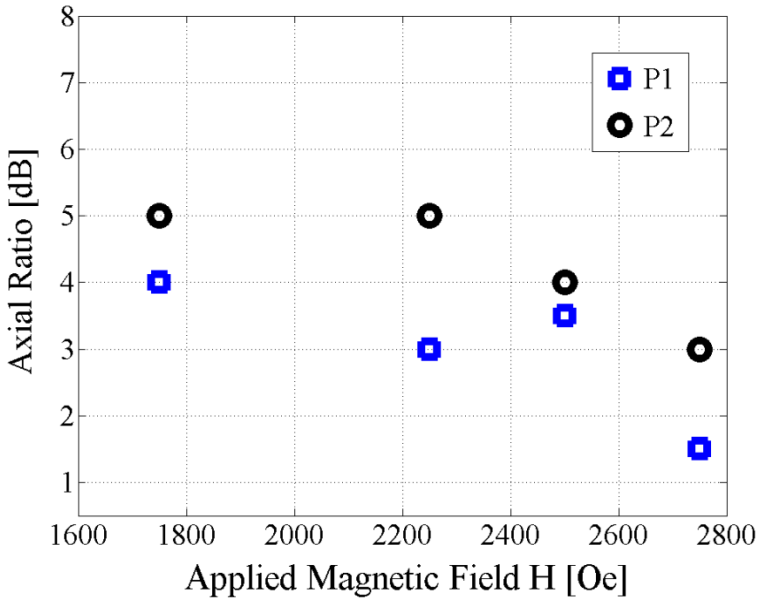

Fig. 5.14. Measured axial ratio vs. the applied magnetic field strength

Although the axial ratio measurements do verify the antenna to be circularly polarized, it does not verify the sense of polarization. To determine this, an RHCP and LHCP non-magnetic antennas were fabricated at 5.2 GHz and 6.3 GHz. These antennas are to be used as the receive antennas just as the linearly polarized antenna was used in the last measurements. Using the two antennas with opposite sense of polarization can help in deciding the sense of polarization of the antenna under test. At 5.2 GHz, it was observed that the value of S_{21} is 19 dB greater for the case when RHCP antenna is used as the receive antenna as compared to the scenario when LHCP antenna was used. This means that at 5.2 GHz the magnetic antenna shows an LHCP polarization. Similar measurements were performed at 6.3 GHz, where it was observed that the LHCP receive antenna shows a 14 dB greater S_{21} as compared to the RHCP receive antenna. These measurements prove that the magnetic antenna is RHCP at the measured frequency. Finally, it can be concluded that for a particular direction of bias the magnetic antenna shows

sense of polarizations which are opposite to each other at the two tuned frequency points which is consistent with the theory and simulations.

For the biased state radiation pattern measurement, a permanent magnet is used with the antenna inside the anechoic chamber. The radiation patterns are measured at 5.6 GHz and 6.1 GHz for the two frequency points. The measured radiation pattern results at the two frequencies are plotted in Fig. 5.15 (a) and Fig. 5.15 (b) respectively. These measurements again proved that the antenna is circularly polarized.

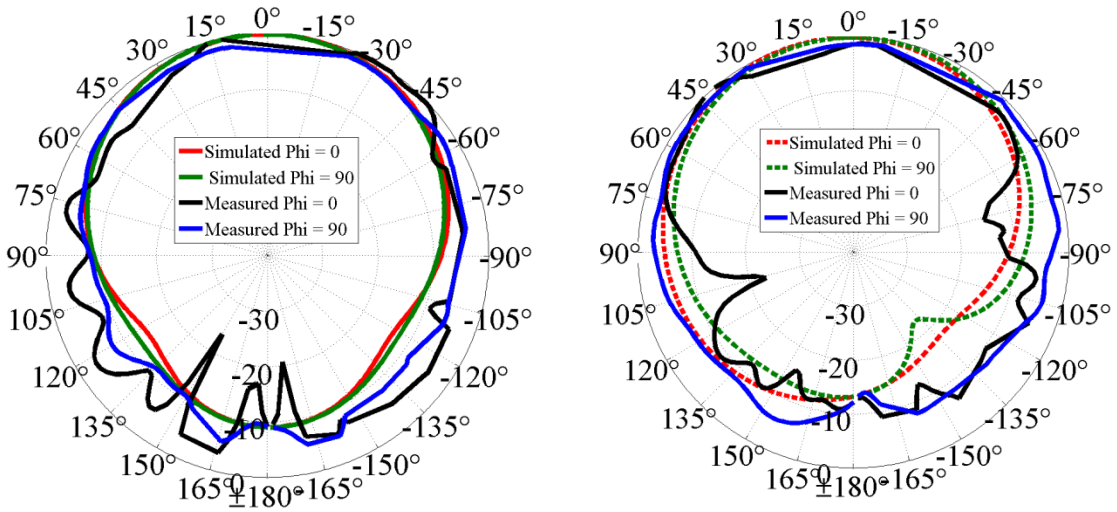

(a) (b)

Fig. 5.15. Measured radiation patterns in the presence of a magnet at (a) 5.6 GHz (b) 6.1 GHz

The final measurement for this design is for the gain of the antenna. The maximum measured gain of the antenna is found to be -1 dBi. This value is quite low as compared to the simulated value of 3.34 dBi. However, this low gain performance from the antenna is due to the surface roughness value measured in this device. It has already been discussed in the Ferrite LTCC based helical antenna and the patch antenna array that surface roughness can be a significant factor in

deteriorating the gain of the antenna. Therefore, due to roughness value of 4.5 μm and the S_{11} performance shown in Fig. 5.11, a poor gain from the antenna is obtained. In order to verify this effect, the measured surface roughness value is used in the simulator for post-measurement simulations. The post-measurement simulations show that the gain of the antenna drops from 3.34 dBi to -1.03 dBi due to this effect. This means that optimizing the fabrication process for better surface roughness value will improve the radiation performance considerably.

5.5 Conclusion

This chapter covers the theory, simulations and design of a circular patch antenna on an iron-oxide nano-particles based magnetic substrate. The substrate is realized using manual screen printing process (squeegee) while the conductor layers of SOC ink are printed using inkjet printing technique. The antenna is initially designed to operate as a linearly polarized antenna which on application of magnetic bias provides circular polarization at two different resonant frequencies. These frequencies can be tuned using the applied magnetic field strength. Although for this work, the substrate is magnetized using an external electromagnet, with better optimization of fabrication process, embedded bias windings can be realized in the same substrate as the antenna. For the proof-of-concept the antenna design is measured using external magnetic sources. The correlation between the theory, simulations and measurements is decent and therefore it can be said that the proposed theoretical model has been verified by simulations as well as measurements. The antenna shows a tuning range of 5 % and 16.7% for the two polarizations. Since the polarizations can be reversed with the direction of applied bias therefore it can be stated that both the polarizations can achieve the upper limit of the tuning. The concept thus shows that a polarization reconfigurable antenna can be designed on a partially magnetized

substrate which can be frequency tuned by changing the bias strength. A comparison between the tunability of the patch antenna on the magnetic ink with the ferrite LTCC design is shown in table below:

Table 5-2: Comparison of LTCC Patch Antenna with the Magnetic Ink Antenna

Substrate	Saturation Magnetization [G]	Center Frequency [GHz]	Tuning Range [%]	Applied Magnetic Field [Oe]
LTCC	4000	13.1	10	19
Magnetic Ink	1560	6	16.7	2750

From Table 5-2, it can be seen that the LTCC tape system has a higher saturation magnetization as compared to the Magnetic ink which is due to the different composition of ferromagnetic particles in the two substrates. Keeping in view, the saturation magnetization of the two mediums, the antennas are designed at different center frequencies to stay away from the low field losses by operating at frequencies above the magnetization frequency, ($f_m = \gamma 4\pi M_s$). Greater tuning range is achieved from the magnetic ink antenna due to the use of external electromagnets which do not have any limitations and can generate strong magnetostatic fields (in kOe) as compared to the bias windings which can be easily damaged by using higher values of current.

Chapter 6

Conclusion and Future Work

The ever increasing demand of the modern communication systems require added functionality in the RF and microwave components which includes, antennas, filters and phase shifters etc. One such requirement is the tunability of the antennas and filters while the other can be beam scanning capabilities from an antenna array. Magnetic mediums provide a suitable platform for the realization of such tunable and reconfigurable microwave components. In this thesis, tunable antennas, phase shifter, phased array and a polarization reconfigurable antenna has been presented. The issues of large size and inefficient performance of the previously reported ferrite based designs have been addressed by operating the designs in the partially magnetized state and using embedded bias windings. The multilayer ferrite LTCC technology is used for the realization of tunable antennas and phase shifter to provide proof-of-concept. Moreover, a custom in-house printing process using a novel magnetic ink is also studied. Using the new magnetic ink a polarization reconfigurable patch antenna has been demonstrated which shows the viability of this process for the implementation of tunable microwave components.

6.1 Ferrite LTCC based Tunable Antennas

Chapter 3 covers the theory and design of tunable antennas using multilayer ferrite LTCC technology. Two different antenna designs i.e. patch antenna and helical antenna are used as a proof-of-concept. Using the vertical integration technique of LTCC medium, embedded bias

windings are used for tuning the antennas instead of external electromagnets. Furthermore, the antennas are operated in the partially magnetized state as opposed to the conventional ferrite based designs that rely on saturated regime. The use of embedded windings in conjunction with the operation in the partially magnetized state provides a field reduction of almost 90 %. For the patch antenna, new theoretical models have also been proposed for different direction of bias. Both the antennas and the bias windings are modeled in the high frequency and magnetostatic simulators. Finally, prototypes of the antennas are realized using the multilayer LTCC fabrication technique. A good agreement is observed between the theory, simulations and measurements of the tunable antenna designs. A tuning range of almost 10 % is achieved from the two antenna designs. The absence of the electromagnets not only reduces the required magnetostatic fields but also helps in miniaturizing the antenna design. Finally, the proposed SoP concept for ferrites can allow its integration in the modern communication world where the demands for small size, low cost and high efficiency is consistently on the rise.

6.2 Ferrite LTCC based Half Mode SIW Phase Shifter for Phased Array Applications

In chapter 4, theory and design of a half mode SIW phase shifter is presented using the same multilayer technology that was used for the tunable antenna designs. This is the first time that half mode waveguide or SIW based phase shifter has been implemented in the ferrite technology. The added advantages of the embedded bias windings and operation in the partially magnetized state help in reducing the overall size of the system and the power requirements. The phase shifter provides a phase shift of 83.2° with an insertion loss of 1 dB. The general application of a

phase shifter is usually in the antenna arrays to provide beam steering capabilities. Therefore, to show the effectiveness of the proposed phase shifter design, it is integrated in a two element patch antenna array. The array is measured for its radiation performance whereby a measured steering of 30° is achieved from the designed array. The use of single phase shifter allows the steering in only in one direction of the H plane. However, if using the design concept shown in this work, the array can be integrated with two phase shifting elements that can cover both halves of the antenna plane. Nonetheless, the phase shifter and phased array design presented in this chapter prove that the ferrite LTCC technology is a viable option for realization of highly miniaturized and low weight reconfigurable microwave designs.

6.3 Polarization Reconfigurable Patch Antenna Realized Through Low Cost Additive Manufacturing

In chapter 5, a new fabrication technique has been studied for the realization of magnetically tunable antenna designs. For this purpose, a new iron oxide nano-particle based ink is presented that be screen printed using squeegee. In this way the substrate for the antenna itself is printed unlike the LTCC technology. Such an implementation can reduce the overall cost of the RF components manifolds. In addition to the substrate, the metallic layers for the antenna is also printed using inkjet technology. The novel magnetic ink based substrate is characterized for its microwave and magnetostatic properties. Eventually a circular patch antenna is implemented using the in-house prepared magnetic ink. On biasing the antenna perpendicular to its plane, frequency splitting is observed. In addition, the linear polarization of the antenna is reconfigured to circular polarization due to the application of magnetic bias. Both sense of rotation i.e. LHCP

and RHCP are obtained from the antenna at the same time but at different frequencies. Increasing the strength of the applied bias causes the frequencies to further tune away from each other. If the direction of the bias is reversed the two sense of polarizations interchange their operating frequencies. Like, the linear polarized patch antenna a theoretical model backed up by simulations and measurements has also been presented. The antenna provides a tuning range of almost 16 % of its center frequency. At this point, the antenna is biased using external electromagnets due to the immaturity of the fabrication process. However with the advancement in the fabrication techniques it can be expected that the same results can be obtained with an embedded bias winding and hence encompassing all the advantages of ferrite LTCC technology with an added advantage of cost-effectiveness.

6.4 Future Work

Although the magnetically tunable designs presented in this work provide promising results, there are number of directions which can be followed to further pursue this area of research. We will discuss these directions of research keeping in view the two different mediums used in this thesis.

Firstly, for ferrite LTCC there are two major issues which need to be investigated to improve the performance of the designed RF components. Among these issues one is related to the conductor surface roughness which is observed in two of the antenna designs reported in this thesis. The problem of the conductor surface roughness significantly affects the loss of the microwave design. A very crude technique to improve this roughness is to polish the metal layers after their deposition. However, this can be done only for the layers which are exposed externally. Ferrite LTCC is a multilayer fabrication process which uses vertical integration for

system realization. Therefore, some of the layers in the LTCC medium are embedded inside the module. These embedded layers are not exposed to the outside world and therefore they cannot be polished once the layers are fired together as a single module. Thus, it is important that new fabrication techniques and steps are examined which can help improve the conductor surface roughness. The other problem with the ferrite LTCC is the heating of the substrate due to the presence of the current in the bias windings. This heating of the substrate cannot only damage the windings themselves but can also alter the performance of the microwave design. This is because the saturation magnetization of a material is a temperature dependent property. Consequently, heating of the substrate can create serious issues in tunable microwave designs and needs to be investigated. One of the solutions to the problem of the substrate heating is the optimization of the bias windings. The heat generated due to the bias windings is because of the power dissipation through the bias windings conductors. This dissipated power is directly related to the resistance of the conductor and current flowing through it. The resistance of the conductor is inversely proportional to its cross-sectional area. Therefore, by using wider and thicker conductor lines, one can lower the resistance of the bias conductors hence reducing the power consumption. Similarly by using more number of turns in the windings the value of the current required to bias the substrate can be optimized for lower values. The combine effect of smaller current and lower resistance can significantly decrease the dissipated heat. The other solution for this problem can be the use of different cooling mechanisms with the ferrite substrates. This can be achieved by the utilization of heat sinks or fluidic channels inside the substrate. The presence of heat sinks or fluidic channels will allow the designers to control the temperature of the ferrite medium by dissipating heat through them. In this way the heat generated inside the ferrite

medium can be readily removed hence reducing its effect on the performance of the microwave component.

One more method to cater the problem of heating in ferrites is to exploit the remanent nature of the ferrite material. This technique of using remanent state of ferrites is more useful than the two techniques discussed above. It is well known that magnetic mediums usually show remanence which means that they can retain some portion of the applied magnetic field. Using this effect, the bias current can be applied in the windings in the form of square pulses whose time period can be controlled externally. The current can be applied for very short intervals of time, such that it does not increase the temperature of the material. After the removal of the applied current, the material will still hold some part of its magnetization due to its remanent nature. As a result, tuned response of the microwave component can be maintained to a certain degree. This use of remanence is a good solution to the problem of heating in ferrites. However, at present, the remanence performance of the ferrite LTCC designs is not up to the mark. The designs presented in this work show squareness of only 0.2 which means that only 20 % of the applied fields are retained in the medium. This value is quite low and is inefficient in its current state. This requires research in the materials domain. Ferrite LTCC is a mixture of ceramic and magnetic particles. Therefore, one direction of research can be towards the composition of this mixture. If squareness of the ferrite LTCC medium can be improved by investigating its magnetic composition, then this problem of heating can be significantly reduced.

For the magnetic ink proposed in this thesis the major problem is the printing of multiple conductor layers. As reported in chapter 5, that currently we were not able to print the isolation layer underneath the ground plane of the antenna due to which bias windings were not implemented in this design. This is the main concern in this new fabrication technique and it

needs to be resolved for the multilayer implementation of magnetically tunable components. For now, we have only tried one of the materials (i.e. Vero) to be used as the isolation layer. In future, different types of materials should be explored to evaluate their feasibility in such an application. If the realization of the bias windings can be achieved using the proposed multilayer printing process, then it will open doors for the design of various antennas, filters, phase shifters, phased arrays and other tunable microwave devices.

REFERENCES

[1] C. G. Christodoulou, Y. Tawk, S. A. Lane and S. R. Erwin, "Reconfigurable Antennas for Wireless and Space Applications," in *Proceedings of the IEEE*, vol. 100, no. 7, pp. 2250-2261, July 2012.

[2] J. Wernehag and H. Sjoland, "A 24-GHz Automotive Radar Transmitter with Digital Beam Steering in 130-nm CMOS," *Research in Microelectronics and Electronics, Ph. D.*, pp. 481-484, 2006.

[3] D. M. Pozar and V. Sanchez, "Magnetic tuning of a microstrip antenna on a ferrite substrate," *Electronics Letters*, vol. 24, no. 12, pp. 729-731, 1988.

[4] A. Petosa, E. K. Mongia, M. Cuhaci and J. S. Wight, "Magnetically tunable ferrite resonator antenna," *IEEE Electronic Letters*, vol. 30, no. 13, pp. 1021-1022, 1994.

[5] A. B. Ustinov and B. A. Kalinikos, "A microwave non-linear phase shifter," *Applied Physics Letters*, 93, 102504, 2008.

[6] R. K. Mishra, S. S. Pattnaik and N. Das, "Tuning of microstrip antenna on ferrite substrate," *IEEE Transactions on Antennas and Propagation*, vol. 41, no. 2, pp. 230–233, 1993.

[7] C. F. L. Vasconcelos, S. G. Silva, M. R. M. L. Albuquerque, A. G. d'Assuncao and J. R. S. Oliveeira, "Ferrite substrate in patch antennas for millimeter-wave applications," *IEEE Microwave and Optoelectronic Conference,* pp. 78-82, 2009.

[8] R. R. Tummala, "The SOP for miniaturized, mixed-signal computing, communication and consumer systems for the next decade," *IEEE Transactions on Advanced Packaging*, vol. 27, pp. 250-267, 2004.

[9] J. Bray and L. Roy, "Development of a Millimeter-Wave Ferrite-Filled Antisymmetrically Biased Rectangular Waveguide Phase Shifter Embedded in Low-Temperature Co-fired Ceramic," *IEEE Transactions on Microwave Theory and Techniques*, vol. 52, no. 7, 2004.

[10] D. M. Pozar, "Microwave Engineering," 3rd edition, chapter 9, 2005.

[11] J. J. Green and F. Sandy, "Microwave characterization of partially magnetized ferrites," *IEEE Transactions on Microwave Theory and Techniques,* vol. 22, no. 6. 1974.

[12] R. F. Sohoo, "Theory and applications of ferrites," Englewood Cliffs, NJ Prentice Hall, 1960.

[13] HyperPhysics website: Larmor Frequency [online] http://hyperphysics.phy-astr.gsu.edu/hbase/nuclear/larmor.html

[14] C. A. Balanis, “Advanced Engineering Electromagnetics,” chapter 2, John & Wiley Sons Inc, US, 1989.

[15] E. Schlomann, “Microwave behavior of partially magnetized ferrites,” Journal of Applied Physics, vol. 41, no. 1, pp. 204-214, 1970.

[16] G. T. Rado, “Theory of the microwave permeability tensor and Faraday Effect in non-saturated ferromagnetic materials,” *Physical Review,* vol. 89, no. 2, pp. 529, 1953.

[17] D. Bariou, P. Queffelec, P. Gelin and M. L. Flo’ch, “Extension of the effective medium approximation for determination of the permeability rensor of unsaturated polycrystalline ferrites,” *IEEE Transactions on Magnetics,* vol. 37, no. 6, pp. 3885-3891, 2001.

[18] D. M. Pozar, “Radiation and scattering characteristics of microstrip antennas on normally biased ferrite substrates,” *IEEE Transactions on Antennas and Propagation,* vol. 40, no. 9, pp. 1084-1092, 1992.

[19] P. J. Rainville and F. J. Harackiewicz, “Magnetic tuning of a microstrip patch antenna fabricated on a ferrite film,” *IEEE Microwave and Guided Wave Letters,* vol. 2, no. 12, pp. 483-485, 1992.

[20] G. M. Yang *et al*., "Tunable Miniaturized Patch Antennas With Self-Biased Multilayer Magnetic Films," *IEEE Transactions on Antennas and Propagation*, vol. 57, no. 7, pp. 2190-2193, 2009.

[21] G. M. Yang *et al*., "Electronically Tunable Miniaturized Antennas on Magnetoelectric Substrates With Enhanced Performance," *IEEE Transactions on Magnetics*, vol. 44, no. 11, pp. 3091-3094, 2008.

[22] L. R. Tan, R. X. Wu, C. Y. Wang and Y. Poo, "Magnetically Tunable Ferrite Loaded SIW Antenna," *IEEE Antennas and Wireless Propagation Letters*, vol. 12, pp. 273-275, 2013.

[23] L. R. Tan, R. X. Wu, C. Y. Wang and Y. Poo, "Ferrite-Loaded SIW Bowtie Slot Antenna With Broadband Frequency Tunability," in *IEEE Antennas and Wireless Propagation Letters*, vol. 13, no. , pp. 325-328, 2014.

[24] L. R. Tan, R. X. Wu and Y. Poo, "Magnetically Reconfigurable SIW Antenna with Tunable Frequencies and Polarizations," in *IEEE Transactions on Antennas and Propagation*, vol. 63, no. 6, pp. 2772-2776, 2015.

[25] M. A. Amiri, C. A. Balanis and C. R. Birtcher, "Gain and Bandwidth Enhancement of Ferrite-Loaded CBS Antenna Using Material Shaping and Positioning," in *IEEE Antennas and Wireless Propagation Letters*, vol. 12, no. , pp. 611-614, 2013.

[26] L. R. Tan, R. X. Wu and Y. Poo, "Magnetically Reconfigurable HMSIW Antenna with Broadband Frequency Tunability," in *IEEE Antennas and Wireless Propagation Letters*, vol. 15, pp. 1373-1376, 2016.

[27] J. R. Bray, “Millimeter-wave ferrite-loaded laminated waveguide phase shifters embedded in low temperature cofired ceramic,” Ph.D. Dissertation, Carleton University, 2003.

[28] W. E. Hord, “Microwave and millimeter-wave phase shifters,” *Microwave Journal*, vol. 32, pp. 81-94, 1989.

[29] E. Gimonet and B. C. S. Lint, “Optimization and design of millimeter wavelength phase shifters,” *IEEE International Microwave Symposium*, pp. 373-375, 1979.

[30] C. R. Boyd Jr., “A dual-mode latching reciprocal ferrite phase shifter,” *IEEE Transactions on Microwave Theory and Techniques*, vol. 18, pp. 1119-1124, 1970.

[31] L. R. Whichker and C. R. Boyd Jr., “A new reciprocal phaser for use at millimeter wavelengths,” *IEEE Transactions on Microwave Theory and Techniques*, vol. 19, pp. 944-945, 1971.

[32] C. R. Boyd Jr., “A 60 GHz dual-mode ferrite phase shifter,” *IEEE International Microwave Symposium*, pp. 257-259, 1982.

[33] X. Yansheng & J. Zhengchang, “Dual-mode latching ferrite devices,” *Microwave Journal*, vol.29, pp. 277-285, 1986.

[34] W. E. Hord, C. R. Boyd, and D. Diaz, “A new type of fast-switching dual-mode ferrite phase shifter,” *IEEE Transaction on Microwave Theory and Techniques*, vol. 35, pp. 1219-1225, 1987.

[35] R. W. Babbitt and R. A. Stern, “Non-reciporcal ferrite phase shifters for millimeter applications,” *IEEE International Microwave Symposium*, pp. 94-96, 1978.

[36] H. Luo, Y. Liang, J. Yuan, and Q. Qiu, “A Ka band compressed grooved waveguide ferrite phase shifter,” *International Conference on Millimeter-wave and Far Infrared Science and Technology*, pp. 150-153, 1996.

[37] R. W. Babbitt and R. A. Stern, “Fabrication and performance of ferrite phase shifters for millimeter-wave frequencies,” *IEEE Transactions on Magnetics*, vol. 15, pp. 1744-1746, 1979.

[38] J. F. McIlvenna, “Monolithic phased arrays for EHF communication terminals,” Microwave Journal, vol. 31, pp. 113-125, 1988.

[39] X. Zuo, H. How, P. Shi, S. A. Oliver, and C. Vittoria, “Development of high frequency ferrite phase shifter,” *IEEE Transactions on Magnetics*, vol. 37, pp. 2395-2397, 2001.

[40] X. Zuo, H. How, P. Shi, S. A. Oliver, and C. Vittoria, "Zn_2Y Hexaferrite ($Ba_2Zn_2Fe_{12}O_{22}$) single-crystal microstripline phase shifter," *IEEE Transactions on Magnetics*, vol. 38, pp. 3493-3497, 2002.

[41] X. Yang, *et. al.*, "Compact and low loss phase shifter with low bias fields using partially magnetized ferrite," *IEEE Transaction on Magnetics,* vol. 49, no. 7, pp. 3882-3885, 2013.

[42] A. L. Geiler, *et. al.*, "Multiferroic heterostructure fringe field tuning of meander line microstrip ferrite phase shifter," *Applied Physics Letter*, vol. 96, 053508, 2010.

[43] Y. J. Ban, "Tunable ferrite phase shifters using substrate integrated waveguide techniques," Ph.D. Dissertation, Ecole Polytechnique Montreal, 2010.

[44] S. Adhikari, A. Ghiotto, S. Hemour and K. Wu, "Tunable non-reciprocal ferrite loaded SIW phase shifter," *International Microwave Symposium*, pp. 1-3, 2013.

[45] H. How, Ta-Ming Fang, Wei Liu, C. Vittoria, M. H. Champion and H. L. Southall, "Antenna array of circular patches on ferrite substrate," in *IEEE Transactions on Magnetics*, vol. 33, no. 1, pp. 735-738, 1997.

[46] L. Dixit and P. K. S. Pourush, "Radiation characteristics of switchable ferrite microstrip array antenna," in *IEE Proceedings - Microwaves, Antennas and Propagation*, vol. 147, no. 2, pp. 151-155, 2000.

[47] R. Pourush, G. S. Tyagi, G. P. Srivastava and P. K. S. Pourush, "Radiation performance of switchable ferrite microstrip array antenna," in *IEEE Antennas and Wireless Propagation Letters*, vol. 5, no. 1, pp. 195-198, 2006.

[48] J. S. Roy, P. Vaudon, A. Reineix, F. Jecko and B. Jecko, "Axially magnetized circular ferrite microstrip antenna," *International Symposium on Antennas and Propagation, AP-S. Held in Conjunction with: IEEE URSI Radio Science Meeting and Nuclear EMP Meeting,* pp. 2212-2215 vol.4, 1992.

[49] A. Petosa, R. K. Mongia, M. Cuhaci and J. S. Wight, "Magnetically tunable ferrite resonator antenna," in *Electronics Letters*, vol. 30, no. 13, pp. 1021-1022, 1994.

[50] A. Petosa, R. K. Mongia, A. Ittipiboon and J. S. Wight, "Switchable LP/CP ferrite disk resonator antenna," in *Electronics Letters*, vol. 31, no. 3, pp. 148-149, 1995.

[51] K. K. Tsang and R. J. Langley, "Annular ring microstrip antennas on biased ferrite substrates," in *Electronics Letters*, vol. 30, no. 16, pp. 1257-1258, 1994.

[52] J. C. Batchelor, G. Classen and R. J. Langley, "Microstrip antennas on ferrites," *Tenth International Conference on Antennas and Propagation, (Conf. Publ. No. 436)*, pp. 30-33 vol.1, 1997.

[53] K. K. Tsang and R. J. Langley, "Design of circular patch antennas on ferrite substrates," *IEE Proceedings - Microwaves, Antennas and Propagation*, vol. 145, no. 1, pp. 49-55, 1998.

[54] G. Leon, R. R. Boix, M. J. Freire and F. Medina, "Characteristics of aperture coupled microstrip antennas on magnetized ferrite substrates," *IEEE Transactions on Antennas and Propagation*, vol. 53, no. 6, pp. 1957-1966, 2005.

[55] M. Sigalov, R. Shavit, R. Joffe and E. O. Kamenetskii, "Manipulation of the Radiation Characteristics of a Patch Antenna by Small Ferrite Disks Inserted in Its Cavity Domain," *IEEE Transactions on Antennas and Propagation*, vol. 61, no. 5, pp. 2371-2379, 2013.

[56] F. A. Ghaffar, M. U. Khalid, K. N. Salama, A. Shamim, "24 GHz LTCC Fractal Antenna Array SoP with Integrated Fresnel Lens", IEEE Antennas and Wireless Propagation Letter, vol. 10, no. 10, pp. 705- 708, 2011.

[57] R. V. Pucha, S. Hedge, M. Damani, K. J. Lee, K. Tunga, A. Perkins, S. Mahalingam, G. Lo, K. Klein, J. Ahmad, S. K. Sitaraman, "Design-for-Reliability Tools for Highly Integrated System on Package Technology", *IEEE International Conference on Thermal, Mechanical and Multi-Physics Simulation Experiments in Microelectronics and Micro-Systems, EUROSIME'07,* pp. 1-1, 2007.

[58] R. R. Tumala, "Packaging: Present, Past and Future", *IEEE 6th International Conference on Packaging Technology, ICEPT'05,* pp. 3-7, 2005.

[59] V. Sundaram, R. Tumala, G. White, K. Lim, L. Wan, D. Guidotti, F. Liu, S. Bhattacharya, R. M Pulugurtha, I. R Abuthu, R. Doraisuwami, R. V. Pucha, J. Laskar, M. Tenzteris, G. K. Chang, M. Swaminathan, "System on a Package (SoP) Substrate and Module with Digital, RF and Optical Integration", *IEEE Conference Proceedings on Electronic Components and Technology, ECTC'04,* Vol. 1, pp. 17-23, 2004.

[60] J. R. Bray, K. T. Kautio and L. Roy, "Characterization of an experimental ferrite LTCC tape system for microwave and millimeter-wave applications," in *IEEE Transactions on Advanced Packaging*, vol. 27, no. 3, pp. 558-565, 2004.

[61] ESL Electro-Science, "Magnetic Tape: Low fire tape for multilayer and high frequency applications",
*www.electroscience.com/pdf/**40012**.pdf*

[62] A. Shamim, J. Bray, N. Hojjat, L. Roy, "Microwave and magnetostatic characterization of ferrite LTCC for tunable and reconfigurable SiP Applications", *IEEE Symposium on Microwave Theory and Techniques,* pp. 691-694, 2007.

[63] A. Shamim, J. Bray, N. Hojjat, L. Roy, "Ferrite LTCC based antennas for tunable SoP applications," *IEEE Transactions on Components Packaging and Manufacturing Technology*, vol. 1, no. 7, pp. 999-1006, 2011.

[64] C. A. Balanis, “Antenna Theory: Analysis and Design,” chapter 14, John & Wiley Sons Inc, US, 2005.

[65] R. Hopkins and C. Free, “Equivalent circuit for the microstrip ring resonator suitable for broadband materials characterization”, *IET Microwaves Antennas and Propagation,* vol. 2, no. 1, pp. 66-73, 2008.

[66] R. K. Hoffmann, “Handbook of microwave integrated circuits”, Norwood, MA: Artech House, 1987.

[67] K. P. Latti, M. Kettunen, J. P. Stoem and P. Silventoinen, “A review of microstrip T resonator method in determining the dielectric properties of printed circuit board materials”, *IEEE Transactions on Instrumentation and Measurements,* vol. 56, pp. 1845-1850, 2007.

[68] D. Matkovic, B. Jokanovic, M. Marjanovic and M. Djordjevic, “Improved method for measurement of the dielectric properties of microwave substrate using microstrip T resonator”, *Proceedings of Instrumentation and Measurement Technology Conference,* pp. 1-3, 2007.

[69] J. G. Korvink, P. J. Smith and D. Y. Shin, “Inkjet-based micro manufacturing”, *Weinheim: Wiley-VCH*, 2012.

[70] M. Vaseem, G. McKerricher and A. Shamim "Robust Design of a Particle-Free SOC Ink with High Conductivity and Inkjet Stability for Flexible Electronics", *ACS Applied Materials Interface*s, vol. 8, no. 1 pp. 177-186, 2016.

[71] Lakeshore 7400 series electromagnet: http://www.lakeshore.com/products/Vibrating-Sample-Magnetometer/7400-Series-VSM/Pages/Overview.aspx

[72] Quader magnet: https://www.magno-sphere.de/quadermagnete-neodym-10-x-5-x-1mm/a-1025/